RÉPUBLIQUE ALGÉRIENNE DÉMOCRATIQUE ET POPULAIRE
MINISTÈRE DE L'ENSEIGNEMENT SUPÉRIEUR ET DE LA RECHERCHE SCIENTIFIQUE

ECOLE NATIONALE POLYTECHNIQUE

المدرسة الوطنية المتعددة التقنيات
Ecole Nationale Polytechnique

L G M D

Département du Génie Mécanique
Laboratory of Green and Mechanical Development LGMD

Final Year Project Thesis

In partial fulfillment of the requirements for the State Engineer Degree in Mechanical Engineering

---

Feasibility Study on the Use of Date Palm Fibers in 3D Printing : Application to Small Wind Turbine Blades

---

MENANI Fouad & DEHINA Mohamed Samy

Under the supervision of
Dr. BELOUADEH Zouheyr ENP
Dr. BOUHELAL Abdelhamid ENP
Pr.SMAILI Arezki ENP

Presented and publicly defended on (17/07/2025)

Committee Members :			
	President:	Dr.AMOURA Nasreddine	ENP
	Examiner :	Dr.SEDJAL Hamid	ENP

ENP 2025

RÉPUBLIQUE ALGÉRIENNE DÉMOCRATIQUE ET POPULAIRE
MINISTÈRE DE L'ENSEIGNEMENT SUPÉRIEUR ET DE LA RECHERCHE SCIENTIFIQUE

ECOLE NATIONALE POLYTECHNIQUE

المدرسة الوطنية المتعددة التقنيات
Ecole Nationale Polytechnique

L G M D

Département du Génie Mécanique
Laboratory of Green and Mechanical Development LGMD

Final Year Project Thesis

In partial fulfillment of the requirements for the State Engineer Degree in Mechanical Engineering

---

Feasibility Study on the Use of Date Palm Fibers in 3D Printing : Application to Small Wind Turbine Blades

---

MENANI Fouad & DEHINA Mohamed Samy

Under the supervision of
Dr. BELOUADEH Zouheyr ENP
Dr. BOUHELAL Abdelhamid ENP
Pr.SMAILI Arezki ENP

Presented and publicly defended on (17/07/2025)

Committee Members :	President:	Dr.AMOURA Nasreddine	ENP
	Examiner :	Dr.SEDJAL Hamid	ENP

ENP 2025

RÉPUBLIQUE ALGÉRIENNE DÉMOCRATIQUE ET POPULAIRE
MINISTÈRE DE L'ENSEIGNEMENT SUPÉRIEUR ET DE LA RECHERCHE SCIENTIFIQUE

ECOLE NATIONALE POLYTECHNIQUE

المدرسة الوطنية المتعددة التقنيات
Ecole Nationale Polytechnique

L G M D

Département du Génie Mécanique
Laboratoire de Développement Vert et Mécanique

Mémoire de projet de fin d'études

Pour l'obtention du diplôme d'ingénieur d'état en génie mécanique

---

Étude de faisabilité sur l'utilisation de fibres de palmier dattier en impression 3D : application aux pales de petites éolienness

---

MENANI Fouad & DEHINA Mohamed Samy

Sous la supervision de
Dr. BELOUADEH Zouheyr ENP
Dr. BOUHELAL Abdelhamid ENP
Pr.SMAILI Arezki ENP

Présenté et défendu publiquement le (17/07/2025)

Membres du jurée :

President:	Dr.AMOURA Nasreddine	ENP
Examinateur :	Dr.SEDJAL Hamid	ENP

ENP 2025

ملخص

تستكشف هذه الدراسة تطوير مواد مركبة قابلة للتحلل الحيوي لاستخدامها في شفرات توربينات الرياح صغيرة الحجم المصنّعة بالطباعة ثلاثية الأبعاد، مع التركيز على الاستدامة والأداء الميكانيكي. تم تصميم مركب مكوَّن من حمض البولِلاكتيك (PLA) مدعَّم بألياف أوراق النخيل، وتصنيعه باستخدام مكبس هيدروليكي، وتوصيفه ميكانيكياً من خلال اختبارات الشد وتجارب بثق الفتيل للطباعة. وتدعم مراجعة أدبية مفصلة اختيار ومعالجة المواد. تُستخدم الخصائص التي تم الحصول عليها في عمليات محاكاة هوائية ومرنة باستخدام برنامج QBlade، وتشمل تحليل الشكل الهوائي، وتوليد هندسة الشفرة، ونمذجة التشوّه البنيوي. يُقارن المركب نخيل–PLA بالمواد التقليدية مثل CFRP وGFRP. وتُظهر النتائج أداءً واعداً، مما يشير إلى أن هذا المركب الحيوي يمكن أن يكون بديلاً صديقاً للبيئة وجديراً بالتطبيق في مجال طاقة الرياح.

الكلمات المفتاحية: المركبات القابلة للتحلل الحيوي، حمض البولياكتيك (PLA)، ألياف أوراق النخيل، التوصيف الميكانيكي، محاكاة QBlade.

Résumé

Ce projet explore le développement de matériaux composites biodégradables pour des pales d'éoliennes à petite échelle imprimées en 3D, en mettant l'accent sur la durabilité et la performance mécanique. Un composite à base d'acide polylactique (PLA) renforcé par des fibres de feuilles de palmier est conçu, fabriqué à l'aide d'une presse hydraulique, et caractérisé mécaniquement par des essais de traction et des tests d'extrusion de filament. Une revue de littérature détaillée soutient le choix et le traitement des matériaux. Les propriétés obtenues sont utilisées dans des simulations aéroélastiques et aérodynamiques via QBlade, couvrant l'analyse des profils, la géométrie des pales et la modélisation de la déformation structurelle. Le composite PLA–palmier est comparé aux matériaux conventionnels tels que le CFRP et le GFRP. Les résultats montrent des performances prometteuses, suggérant que ce biocomposite est une alternative écologique et viable pour les applications dans l'énergie éolienne.

Mots-clés : Composites biodégradables, Acide polylactique (PLA), Fibres de feuilles de palmier, Caractérisation mécanique, Simulation QBlade.

Abstract

This project explores the development of biodegradable composite materials for 3D-printed small-scale wind turbine blades, emphasizing sustainability and mechanical performance. A composite of polylactic acid (PLA) reinforced with palm leaf fibers is designed, fabricated using a hydraulic press, and mechanically characterized through tensile testing and filament extrusion trials. A detailed literature review supports material selection and processing. The obtained properties are used in aeroelastic and aerodynamic simulations via QBlade, covering airfoil analysis, blade geometry, and structural deformation. The PLA–palm composite is compared with conventional materials like CFRP and GFRP. Results demonstrate promising performance, suggesting this bio-composite as a viable, eco-friendly alternative for wind energy applications.

Keywords: Biodegradable Composites, Polylactic Acid (PLA), Palm Leaf Fibers, Mechanical Characterization, QBlade Simulation.

Dedication

To my Mother, Father , Grand-Mother and little brother: *All of this is for you , you are my inspiration, my daily source of strength and motivation, the reason I wake up each morning with purpose. Without your endless support, love, and belief in me, I would have never reached this point. There is nothing i could do that could ever repay even 1% of what you have given me, but I carry your sacrifices and love with me in everything I do. To my brother, I wish nothing but the very best in life , may your path be bright and fulfilling.*

To my dear friends: Yanis and Yanis ,Abd El-Wahab , Anis: *Words simply can not explain how much i appreciate every one of you . It would be unfair*

To my incredible mechanical engineers friends: *You are the best classmates i could ever ask for , Thank you for existing ,Thank you for choosing this college and for choosing Mechanical Engineering . I never thought i would make such good friends when i first stepped in this school . Thank you for allowing me to enjoy the three years together.*

To my partner and friend : Fouad *You are the best partner i have ever had and the best i will ever have , Thank you for turning the struggles we have been through this year into beautiful , cherished memories that i will never forget .*

Lastly , I wish nothing but success and happiness to all of you in life and after it .

Dehina Mohamed Samy.

Dedication

To my beloved father, mother and little brother: *From the bottom of my heart, thank you for being the anchor in my life. Mom and Dad, your love, sacrifices, and quiet strength have shaped who I am you taught me resilience without ever needing to say the word. Your belief in me, even when I struggled to believe in myself, has carried me through the most difficult moments of this journey. You gave me the freedom to grow, while always making sure I never felt alone. To my little brother thank you for being my constant source of joy and motivation. Your innocence, your curiosity, and the way you always found a way to make me smile reminded me why it's all worth it. This achievement is not mine alone; it's a reflection of the home you've built around me one filled with love, patience, and the quiet kind of strength that never wavers. I owe you more than words can say.*

To my dear friends: Oussama, Ubay, Imad, Smail *Your friendship has been one of the most precious gifts throughout my journey. Thank you for walking beside me, for the deep conversations, the endless support, and the moments of laughter that offered light in times of stress. You've been my sounding boards, my cheerleaders, and sometimes my much needed escape from the weight of deadlines. Whether near or far, your presence made a difference. You reminded me that even in the most solitary moments, I was never truly alone. I will always remember your patience, your encouragement, and your ability to lift my spirits. This work carries the traces of your kindness and your belief in me, and for that, I am truly grateful.*

To my incredible mechanical engineers friends: Yanis, Touati, Riyad, Ismail, Adem, El Mondhir, Hilel, Nazim and Chakib *Thank you for being the constant light through the fog of deadlines, doubts, and long nights. Your presence whether in laughter, silence, distraction, or encouragement made this journey bearable and often beautiful. You reminded me to breathe when things felt heavy, to smile when I was too tired to speak, and to keep going when giving up felt easier. You never asked for anything in return, yet you gave me so much your time, your energy, your warmth. Whether through late-night calls, spontaneous coffee breaks, or just being there without needing to say a word, you reminded me of the value of true friendship. I carry this achievement not only for myself, but also in honor of the care, loyalty, and strength you've shown me along the way. I'm beyond lucky to have you.*

To my partner, my duo, my GOAT: Samy *Thank you for being more than just a teammate for being my greatest support, my sounding board, and the steady presence I could always count on. Through every late night, every setback, and every small victory, you were there committed, driven, and always ready to push forward, even when things got tough. Your dedication, intelligence, and sense of humor made this project not just possible, but truly meaningful. We built this together,* ***brick by brick****, and I couldn't have asked for a better person to share this journey with. You turned a challenging experience into one of growth, trust, and shared pride. Whatever comes next, know that I am incredibly proud of what we've accomplished side by side.*

Menani Fouad.

Acknowledgment

First and foremost, we would like to express our sincere gratitude to the National Polytechnic School for providing a rich and challenging environment throughout our engineering studies. From the very first day of our specialty to our final end of study project.

We are deeply thankful to all the professors and academic staff who guided us with dedication, shared their expertise with passion and constantly encouraged us to go beyond our limits, especially our dear teacher and head of department ***Mr Yacine Belkacemi****. Their commitment played a vital role in our academic and personal growth. We also would like to appreciate the administrative and technical staff of ENP for their behind-the-scenes efforts.*

We are particularly gratefull to the Laboratory of Green and Mechanical Development for their collaboration and support. Their assistance and professionalism greatly enriched the quality and relevance of our work.

We would especially like to thank our project supervisors, ***Mr Zouheyr Belouadeh, Pr Arezki Smaili and Mr Abdelhamid Bouhelal****, for their valuable guidance, constant availability and constructive feedback throughout this work.*

We would like to thank the commitee members, ***Mr Naserddine Amoura and Mr Sedjal Hamid*** *for giving us their time and accepting to evaluate our work.*

We would like to express our sincere thanks to ***Mr Wahab Ait-kaci*** *for his valuable support and always being present for us, throughout the whole project, his expertise and availability were of great help to us.*

Dehina Mohamed Samy and Menani Fouad.

Contents

List of Tables

List of Figures

List of abbresviations

Abbreviation	Definition
ABS	Acrylonitrile Butadiene Styrene
ASTM	American Society for Testing and Materials
BEM	Blade Element Momentum
Cd	Drag Coefficient
CFRP	Carbon Fiber Reinforced Polymer
Cl	Lift Coefficient
Cl/Cd	Lift-to-Drag Ratio
Cp	Power Coefficient
DMA	Dynamic Mechanical Analysis
FDM	Fused Deposition Modeling
GFRP	Glass Fiber Reinforced Polymer
HSE	Health, Safety, and Environment
ISO	International Organization for Standardization
LLFVW	Lifting Line Free Vortex Wake
MATLAB	Matrix Laboratory (numerical computing environment)
NaOH	Sodium Hydroxide
OOP	Out of Plane
PBAT	Polybutylene Adipate Terephthalate
PBS	Polybutylene Succinate
PCL	Polycaprolactone
PETG	Polyethylene Terephthalate Glycol
PHA	Polyhydroxyalkanoates
PLA	Polylactic Acid
PLA 4043D	Grade of Polylactic Acid used (NatureWorks Ingeo™ 4043D)
QBlade	Open-source wind turbine simulation software
RPM	Revolutions Per Minute
SEM	Scanning Electron Microscope
TSR	Tip Speed Ratio
UD	Unidirectional
VM Stress	Von Mises Stress

List of symboles

Symbol	Meaning	Unit
A	Cross-sectional area	m^2
C_d	Drag coefficient	–
C_l	Lift coefficient	–
C_p	Power coefficient	–
δ	Blade deflection	m
ΔL	Elongation	m
E	Young's modulus	Pa (or GPa)
F	Force	N
G	Shear modulus	Pa (or GPa)
L	Length of specimen or blade	m
P	Power	W
R	Rotor radius	m
TSR	Tip Speed Ratio	–
v	Wind speed	m/s
γ	Shear strain	–
ρ	Density	kg/m^3
σ	Stress	Pa
σ_v	Von Mises stress	Pa
τ	Shear stress	Pa
θ	Angle of attack	degrees (°)
ε	Strain	–
ω	Angular velocity	rad/s

General introduction

General context

Over the past few decades, rising environmental concerns and the steady depletion of fossil fuel resources have accelerated the global shift toward greener, more sustainable materials. While petroleum-based plastics remain widely used due to their versatility and low cost, their non-biodegradable nature contributes significantly to long-term pollution. In today's world, continued reliance on such materials—especially in engineering and mechanical design—is neither realistic nor environmentally responsible. This has prompted researchers and industries to seek out bio-based, biodegradable alternatives that reduce ecological impact across sectors such as packaging, construction, automotive, and renewable energy.

Among the most promising materials is polylactic acid (PLA), a biodegradable thermoplastic derived from renewable sources like corn starch or sugarcane. PLA is highly favored in 3D printing, particularly fused deposition modeling (FDM), due to its excellent processability and low environmental footprint. However, its limited mechanical strength and thermal resistance restrict its use in more demanding applications. To overcome these limitations, PLA is increasingly being reinforced with natural fibers to improve its performance and extend its range of functional uses.

Not all natural fibers are equally effective, which makes fiber selection a critical step. Date palm fibers (Phoenix dactylifera), abundant in arid regions and typically treated as agricultural waste, represent a strong candidate. They are biodegradable, lightweight, and possess a surprisingly robust structure. In this study, we aim to valorize this underutilized biomass by developing a PLA-based composite specifically adapted for 3D printing, reinforced with treated date palm fibers. This approach not only enhances the mechanical properties of PLA for engineering applications—such as small wind turbine blades—but also contributes to a circular economy by transforming low-value agricultural residues into high-performance, sustainable materials.

Problem Statement

The transition toward sustainable materials in engineering applications is gaining global momentum, particularly in sectors like renewable energy. Biocomposites such as those combining biodegradable polymers with natural fibers are emerging as promising alternatives to conventional synthetic materials. However, their development remains technically challenging. In this project, we explore the use of date palm leaf fibers, an abundant agricultural byproduct in Algeria, reinforced with PLA to create an eco-friendly composite suitable for wind turbine blades. The success of such a material depends not only on its formulation but also on its compatibility

with manufacturing techniques and its mechanical performance in real world conditions.

This study seeks to address the following questions:

- What is the most effective chemical treatment method to prepare palm leaf fibers for reinforcement use?
- How can PLA and palm fibers be combined into a homogeneous composite matrix that maintains strong mechanical integrity?
- Is this material suitable in filament extrusion for 3D printing using the available equipment and technologies?
- Do the mechanical properties of the resulting composite meet the requirements for wind turbine blade applications?

Objectives

This aims to investigate the potential of using date palm leaf fibers as reinforcement for polylactic acid (PLA) to develop a sustainable, biodegradable composite suitable for mechanical applications—particularly in small wind turbine blades. The project is built around both experimental fabrication and digital simulation to evaluate the technical feasibility of the material.

The main objectives of this work are:

- To identify and apply an effective chemical treatment method to improve the surface quality and adhesion properties of palm leaf fibers.
- To develop and process a PLA–palm fiber composite material adapted for 3D printing using available laboratory equipment.
- To characterize the mechanical properties of the resulting composite (Young's modulus, tensile strength, stiffness) through experimental testing.
- To evaluate the feasibility of extruding the developed composite into filament form for 3D printing applications.
- To simulate a wind turbine blade made from the developed composite using QBlade software, and compare its structural and aerodynamic behavior to that of conventional materials like carbon and glass fiber-reinforced composites.
- To assess the viability of using PLA–palm fiber composites as an alternative to synthetic materials for environmentally responsible engineering applications.

Structure

This thesis is structured into four main chapters that follow the logical progression of the study.

- **Chapter 1: State of the Art**
  Introduces key concepts related to biodegradable polymers, PLA, natural fibers especially palm fibers and composite materials. It also outlines common treatment and integration methods along with challenges reported in previous research.

- **Chapter 2: Processing and Development of PLA Composites**
  Describes the experimental process of preparing and treating palm fibers, integrating them into PLA, and fabricating composite plates.

- **Chapter 3: Mechanical Characterization**
  Focuses on evaluating the mechanical properties of the composites, including tensile testing and shear modulus calculation. It compares different fiber contents and provides insight into their mechanical behavior.It also highlights challenges encountered, particularly with filament extrusion.

- **Chapter 4: Wind Turbine Simulation**
  Applies the developed composites in a simulation context using QBlade software, exploring their potential for use in small wind turbine blades through aerodynamic and structural analysis.

Chapter 1

State of the art

1.1 Introduction

The growing demand for materials that are both high-performing and environmentally friendly has driven major progress in the field of biodegradable polymers and natural fiber composites. As concerns about pollution and resource depletion continue to rise, the need for materials that strike a balance between functionality and sustainability is becoming increasingly important across many industries.

Polylactic acid (PLA) is a leading example of such materials. Made from renewable resources like corn or sugarcane, PLA has gained attention for its versatility, biodegradability, and ease of use in various manufacturing processes. At the same time, incorporating natural fibers into polymer matrices has proven to be a promising way to boost mechanical strength while keeping the environmental impact low.

This chapter introduces the key concepts behind biodegradable polymers, with a focus on PLA how it's made, where it's used, and what makes it special. It also explores the role of natural fibers as reinforcements and the fundamental principles of composite material design. Together, these topics provide a solid foundation for understanding both the potential and the challenges of using PLA-based natural fiber composites in today's materials science landscape.

1.2 Biodegradable Polymers

1.2.1 Definition and Classification

Biodegradable polymers are materials that can naturally break down into harmless substances like water, carbon dioxide, and biomass, thanks to the action of microorganisms, enzymes, and environmental conditions. Unlike traditional plastics, this breakdown process doesn't leave behind any toxic residue, which makes biodegradable polymers a strong choice for sustainable development and environmentally conscious applications.

These polymers can be categorized based on their source and how they are synthesized. The main categories include:

- **Natural biodegradable polymers**: These are directly extracted from natural sources. Examples include:
  - *Polysaccharides* such as starch and cellulose.
  - *Proteins* like casein and collagen.
  - *Chitosan*, which is obtained from crustacean shells.
- **Synthetic biodegradable polymers from renewable resources**: These are created through the polymerization of monomers derived from biomass. Examples include:
  - Polylactic acid (PLA)
  - Polyhydroxyalkanoates (PHA)
- **Synthetic biodegradable polymers from fossil resources**: These are made from petrochemical monomers but are engineered to degrade after use. Examples include:
  - Polycaprolactone (PCL)
  - Polybutylene succinate (PBS)
  - Polybutylene adipate terephthalate (PBAT)

PLA falls under the category of synthetic biodegradable polymers made from renewable resources. It is usually produced by fermenting plant based sugars like those from corn starch or sugarcane into lactic acid, which is then polymerized through a ring opening process of lactide.[19]

1.2.2 Environmental Importance

As the world grows more aware of the environmental damage caused by plastic waste and the limited availability of fossil fuels, there is increasing demand for sustainable alternatives to traditional plastics. Conventional petroleum based polymers like polyethylene (PE), polypropylene (PP), and polystyrene (PS) are not biodegradable they can linger in the environment for hundreds of years, causing long term harm, especially to marine life and soil health.

Biodegradable polymers offer a promising way forward. Thanks to their ability to break down naturally into water, carbon dioxide, and biomass with the help of microorganisms, they leave behind a much smaller environmental footprint. Unlike standard plastics that require

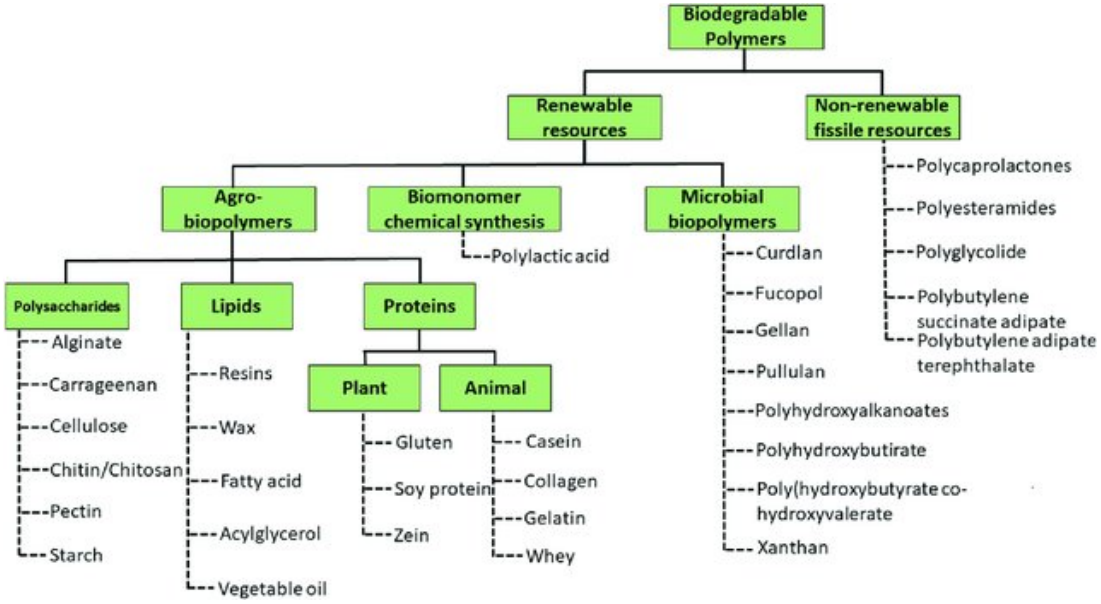

Figure 1.1: General classification of biodegradable polymers by origin and type[5]

complex waste management systems, many biodegradable polymers can be broken down in industrial composting facilities and in some cases, even in natural conditions, depending on the material and its environment.

Another important advantage is that many of these biodegradable polymers are made from renewable resources, like corn starch, sugarcane, or even agricultural waste. This shift away from petroleum-based sources helps lower greenhouse gas emissions and reduces the carbon footprint of plastic production. In fact, by using agricultural byproducts such as palm leaf fibers, as explored in this study we can support circular economy practices, reduce waste, and make better use of local natural resources.

The environmental value of biodegradable polymers can be summed up in three main points:

- **They help reduce plastic pollution**, thanks to their ability to decompose naturally.
- **They have a smaller environmental impact**, especially when made from renewable feedstocks.
- **They encourage sustainable material design**, particularly when combined with natural fiber reinforcements.

1.2.3 Polymers Selection for Our Work

Polylactic acid (PLA) was selected as the polymer matrix for this study due to its unique combination of properties that make it particularly well-suited for additive manufacturing and sustainable engineering applications. Among all biodegradable polymers, PLA stands out as the most widely used material in 3D printing, especially in fused deposition modeling (FDM), owing to its low melting point, minimal warping, and excellent printability without the need for a heated chamber. Beyond its printability, PLA is derived from renewable resources such as corn starch or sugarcane, offering a lower environmental impact compared to petroleum-based polymers. It also exhibits good mechanical rigidity, dimensional stability, and a relatively high modulus, making it a viable candidate for structural applications like small-scale wind turbine

blades. Furthermore, PLA is thermoplastic, compostable under industrial conditions, and generally safer to process due to its low emission of toxic fumes—an advantage not commonly found in alternatives . These combined factors—ease of processing, environmental friendliness, and mechanical adequacy—make PLA an ideal baseline material for developing a reinforced, eco-efficient composite for 3D-printed wind energy components.

1.3 Overview on Polylactic Acid

1.3.1 Common Uses of PLA

Polylactic acid (PLA) is widely used across various industries due to its biodegradability, renewability, and ease of processing. Its popularity has grown significantly in recent years as a sustainable alternative to traditional petroleum-based plastics. Below are some of the most common applications of PLA:

Table 1.1: Common Applications of Polylactic Acid (PLA)[1].

Sector	Applications	Key Benefits
1. Packaging	- Food containers - Disposable cups and plates - Cling films and blister packs	Transparency, compostability, ideal for single-use, eco-friendly
2. 3D Printing	- FDM 3D printing filament	Low melting point, minimal warping, biocompatibility, low odor
3. Medical Applications	- Sutures - Stents - Drug delivery systems - Tissue scaffolds	Biocompatible, biodegradable, safe for temporary implants
4. Agriculture	- Compostable mulch films - Seedling pots - Fertilizer capsules	Soil-degradable, reduces agricultural waste, no need for removal
5. Textiles & Consumer Goods	- Non-woven fabrics - Disposable hygiene products - Clothing blends - Stationery, toys, electronic casings	Sustainable alternative to ABS or polystyrene, suitable for everyday products

1.3.2 Raw Materials

In this study, the main raw material used for the polymer matrix is **polylactic acid (PLA)**—a biodegradable thermoplastic polyester made from renewable resources. Specifically, the PLA selected is the **4043D grade** produced by *Ingeo*^{TM}*, NatureWorks LLC*, supplied in pellet form. This grade is commonly used in extrusion and 3D printing due to its reliable processing properties and performance.

PLA is typically produced through the fermentation of sugars extracted from plants such as

corn (maize), *sugarcane*, or *cassava*. During this process, microorganisms convert the plant-based sugars into lactic acid. This lactic acid is then transformed into lactide, a cyclic compound, which undergoes ring opening polymerization to form long chains of high molecular weight PLA. The result is a material that not only supports environmentally friendly manufacturing but also fits well within modern fabrication technologies like additive manufacturing.

Globally, *corn* is the most common source of feedstock for PLA production, especially in the **United States**, which is also home to *NatureWorks LLC*, one of the world's leading producers of commercial PLA. In addition to the U.S., **China**, **Thailand**, and parts of **Europe** (notably the **Netherlands** and **Germany**) are key contributors to global PLA production, either through large-scale corn processing or sugarcane-based systems .

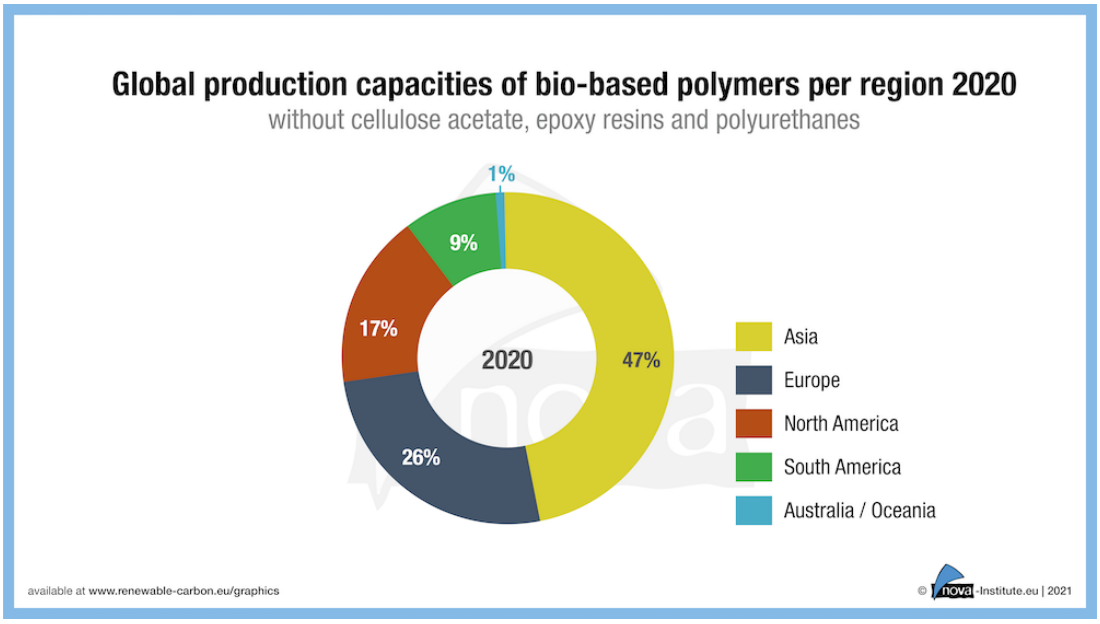

Figure 1.2: PLA Global production and supply [6]

The diagram above illustrates the global distribution of PLA and other bio based polymer production capacities. As shown, the **Asia Pacific region dominates** the market, accounting for nearly 47% of global production capacity. This leadership is largely attributed to China, which has rapidly expanded its bio-based plastics infrastructure in recent years.

North America, primarily represented by the United States, contributes around 17% to global capacity. The U.S. is home to *NatureWorks LLC*, one of the largest PLA producers worldwide, with a major facility in Blair, Nebraska.

Europe follows with approximately 26% of the global PLA capacity. Notable European players include *Total Corbion PLA* in the Netherlands and *Futerro* in Belgium, both of which focus on sustainable PLA production from renewable resources.

This distribution highlights the increasing global demand for biodegradable materials and the strategic role of industrialized regions in scaling up PLA production.[20]

1.3.3 Production Process of PLA

The production of polylactic acid (PLA) involves a series of steps that convert renewable, plant-based resources mainly crops rich in starch or sugar into a biodegradable thermoplastic. This

transformation can be broken down into three main stages: **fermentation**, **purification and polymerization**, and **pelletization**.

1. **Fermentation of Biomass to Lactic Acid**
   The process starts by extracting fermentable sugars from agricultural crops such as corn, sugarcane, or cassava. These sugars serve as a food source for beneficial microorganisms, typically lactic acid bacteria like *Lactobacillus* species. Through fermentation, these microbes convert the sugars into lactic acid a key building block for PLA. This stage is both ef

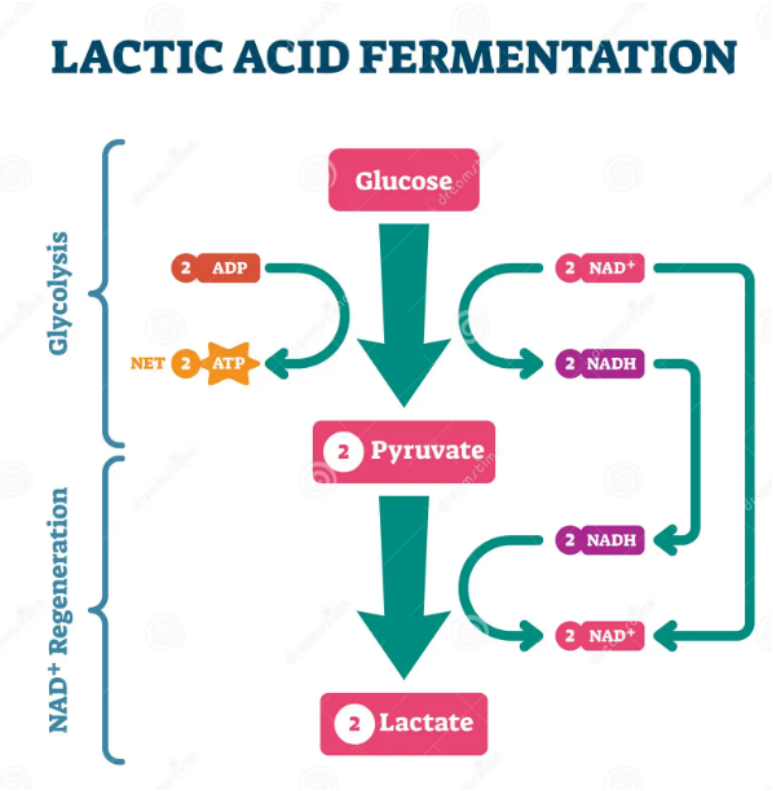

Figure 1.3: Lactic acid fermentation[7]

2. **Purification and Polymerization**
   After fermentation, the lactic acid is carefully purified and then transformed into a compound called lactide a cyclic dimer formed through dehydration and condensation reactions. This lactide is the key intermediate for making PLA. It undergoes a process known as *ring-opening polymerization (ROP)*, typically in the presence of a metal based catalyst such as tin(II) octoate. This step results in the formation of high molecular weight PLA, with precise control over its molecular structure and mechanical properties. This control is crucial for tailoring PLA to meet the requirements of different industrial applications.

3. **Pelletization and Processing**
   Once the polymerization is complete, the PLA is cooled and solidified, then cut into small granules or pellets. These pellets are the standard form in which PLA is distributed for industrial use. They can be processed through various methods, including extrusion, injection molding, film casting, and most notably, converted into filament for 3D printing applications.

The entire production chain is designed to be efficient and environmentally responsible. It makes use of renewable raw materials and relies on low-emission technologies. The final product

PLA resin is a thermoplastic that is biodegradable under industrial composting conditions. Its versatility and sustainable profile make it well suited for a wide range of applications, from eco-friendly packaging and medical devices to innovative uses in additive manufacturing.[21]

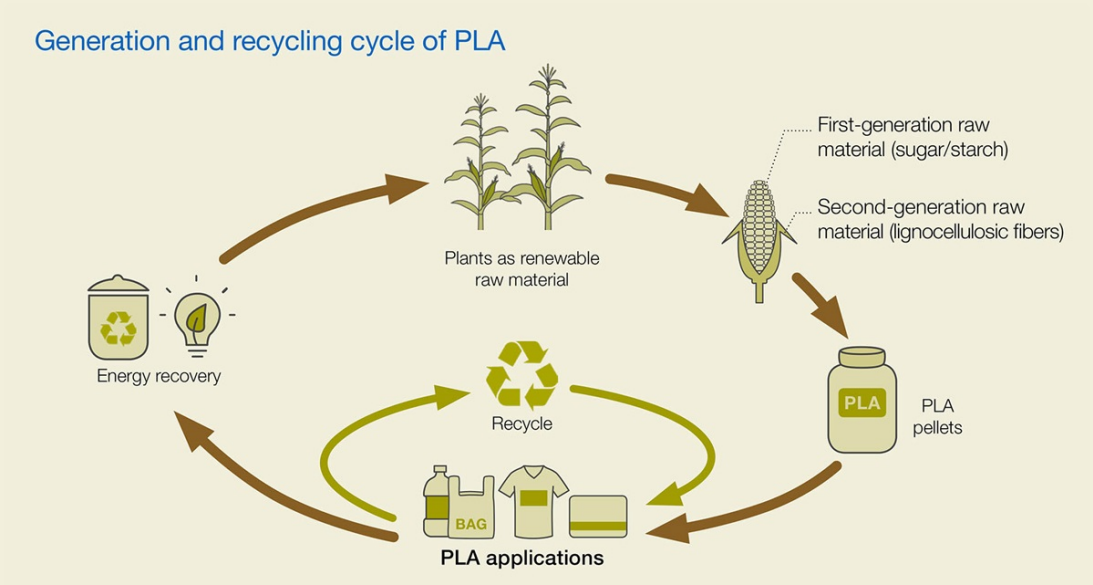

Figure 1.4: Generation and recycling of PLA[8]

1.3.4 Overview of Commercial PLA Grades

Polylactic acid (PLA) is commercially available in a range of specialized grades also referred to as references each tailored for specific industrial applications. These grades are optimized by adjusting factors such as molecular weight and stereochemistry, allowing manufacturers to fine-tune the material's flow behavior, strength, clarity, and thermal performance. This adaptability makes PLA a versatile choice across various processing methods and product requirements.

The most commonly used PLA grades include:

Table 1.2: PLA Grades [2]

PLA Grade	**Notes**
PLA 2003D	Balanced properties, suitable for general-purpose injection molding applications.
PLA 4032D	Higher toughness and strength, commonly used for sheet extrusion and semi-rigid packaging.
PLA 4043D	Versatile and easy to process, ideal for 3D printing and composite applications; stable under thermal processing.
PLA 3052D	Flexible and transparent, suitable for film production and biodegradable packaging.
PLA 7001D	Heat-resistant PLA grade, often used in applications requiring thermal stability such as hot beverage containers.

While the PLA grades listed in Table 1.3 are provided by NatureWorks, one of the leading global producers of polylactic acid under the brand name Ingeo, it is important to note

that many other commercial PLA grades are available on the market from various suppliers. For example, TotalEnergies Corbion offers PLA under the Luminy® brand like (LUMINY LX175,LUMINY LX930, LUMINY L130 [22]), which includes high heat and standard PLA grades suited for a wide range of industrial and packaging applications. Another key producer is Futerro, which also manufactures PLA for diverse applications, particularly with a focus on sustainability and closed-loop bioplastics systems. These alternative sources highlight the growing market and availability of PLA grades tailored to specific processing and performance needs.

Table 1.3: Comparison of Commercial PLA Suppliers

Supplier	**Main PLA Grades**	**Key Applications**	**Sustainability Focus**
NatureWorks (USA)	PLA 2003D , 4032D , 4043D , 3052D	Packaging, 3D printing, textiles, durable goods	Biobased, compostable, large-scale supply chain sustainability
TotalEnergies Corbion (Netherlands)	Luminy® L105, L130, LX175, LX930	High-heat packaging, thermoforming, injection molding, 3D printing	Certified cradle-to-gate LCA, circular production ambitions
Futerro (Belgium)	LUX Line (customized grades for packaging, films, and fibers)	Films, injection molding, compostables, flexible packaging	Closed-loop PLA recycling, biorefinery model, zero-waste focus

1.4 Natural Fibers as Reinforcement

1.4.1 Overview of Natural Fibers

Natural fibers sourced from plants, animals, or minerals have been used by humans for centuries, mostly in textiles and construction. In more recent years, as the push for greener and more sustainable materials has grown stronger, these fibers have gained renewed interest particularly as reinforcements in composite materials. Thanks to their low cost, light weight, biodegradability, and renewable nature, along with decent mechanical performance, natural fibers offer a compelling alternative to synthetic options like glass or carbon fibers—especially in applications that don't require extreme strength or stiffness.

Among the various types, plant-based fibers are by far the most commonly used in composites. These fibers are made up primarily of cellulose, hemicellulose, and lignin, along with smaller amounts of pectin and waxes. The exact makeup varies depending on the type of plant, how old it is, and the conditions in which it was grown all of which can affect the fiber's mechanical properties.

Table 1.4: Classification of Natural Fibers

Origin	**Examples**
Plant-Based (Lignocellulosic)	Flax, Hemp, Jute, Kenaf, Sisal, Abaca, Cotton, Coir, Bamboo
Animal-Based (Protein)	Wool, Silk, Alpaca
Mineral-Based	Asbestos (limited use due to toxicity)

Figure 1.5: Different-types-of-natural-fibers [9]

Plant fibers generally possess low density (about 1.2 to 1.5 g/cm^3), giving them a high specific strength and stiffness. Their tensile strength ranges from 200 MPa to over 1000 MPa, depending on the type of fiber and its treatment.

Table 1.5: Main Chemical Components of Plant-Based Natural Fibers

Component	**Typical Content (%)**	**Function**
Cellulose	40–80	Provides mechanical strength and stiffness
Hemicellulose	10–50	Influences flexibility and water absorption
Lignin	5–25	Adds rigidity and biodegradation resistance
Pectin and Waxes	<5	Affects surface properties and matrix adhesion

That said, natural fibers aren't without their drawbacks. Because they're hydrophilic by nature, they tend to absorb moisture from the environment. This can cause issues like swelling, reduced mechanical strength, and weak bonding with hydrophobic polymers. On top of that, the properties of natural fibers can vary significantly depending on the source, and they generally have lower thermal resistance compared to synthetic fibers. These factors can limit their suitability for high-performance structural applications, where consistent properties and heat resistance are crucial. [23]

1.4.2 Palm Tree Composition and Its Types of Fibers

The date palm tree (*Phoenix dactylifera*) is a monocotyledonous plant widely cultivated in arid and semi-arid regions. In addition to fruit production, the palm tree generates significant agricultural byproducts including leaves, rachis, and trunk components that are potential sources of natural lignocellulosic fibers.

Types of Fibers Extracted from the Palm Tree

Different parts of the palm tree yield various types of fibers, each with distinct characteristics:

1. **Leaf Fibers**: Extracted from palm fronds or leaflets, these fibers are long and flexible, with high cellulose content. They are commonly used for reinforcement in polymer composites.
2. **Rachis Fibers**: Obtained from the central stalk of the palm leaf. These fibers are more rigid and shorter, making them suitable as structural fillers.
3. **Trunk Fibers**: Collected during pruning or from aging trees, trunk fibers contain more lignin and are coarser. They offer good thermal resistance and dimensional stability, though they are more challenging to extract and treat.
4. **Coir or Root Fibers**: Less commonly used, these fibers are extracted from the root zone or basal sheath. They may offer reinforcing properties but require more processing.[10]

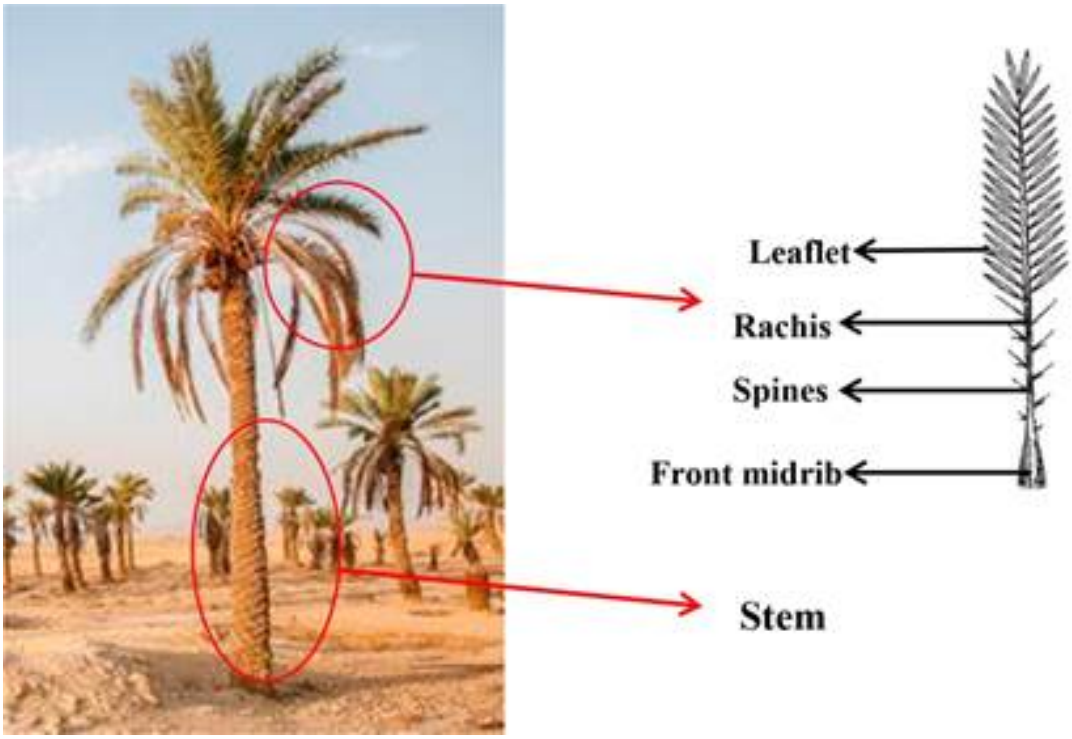

Figure 1.6: Palm-tree-composition [10]

1.5 Composite Materials

1.5.1 Definition and Classification of Composite Materials

Composite materials are engineered systems made by combining two or more constituent materials with significantly different physical or chemical properties. When combined, they produce a material with characteristics superior to those of the individual components. In a typical composite, the constituents remain separate and distinct within the final structure, but work together synergistically to offer enhanced performance.

A composite material consists primarily of two phases:

- **Matrix**: The continuous phase that holds everything together. It serves to bind the reinforcement, transfer stress, and protect it from environmental damage. The matrix also defines the overall shape and structural integrity of the composite.
- **Reinforcement**: The discontinuous phase embedded in the matrix. It provides the mechanical strength, stiffness, and resistance to deformation. Reinforcements can be fibers, particles, or flakes, and are often selected for their high strength-to-weight ratio.

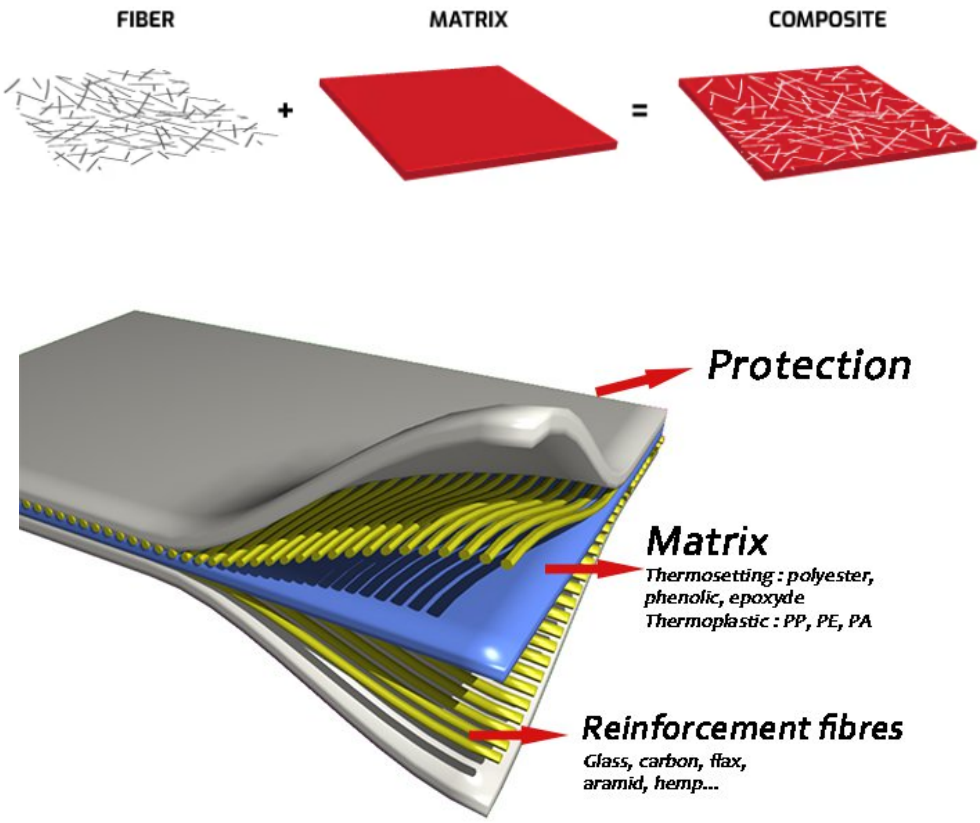

Figure 1.7: Composite Materials [11]

1. Classification Based on Matrix Type

Composites can be classified according to the type of matrix material:

- **Polymer Matrix Composites (PMCs)**: The most commonly used class, based on thermoplastics or thermosets. Examples include fiberglass-reinforced polyester or PLA reinforced with natural fibers. These are widely used due to low cost and ease of processing.
- **Metal Matrix Composites (MMCs)**: Use metals like aluminum or titanium as the matrix. They offer higher thermal resistance and strength, suitable for aerospace and automotive components.
- **Ceramic Matrix Composites (CMCs)**: Composed of ceramic matrices (e.g., alumina, silicon carbide) reinforced with ceramic fibers. These materials are extremely heat-resistant and are used in high-temperature applications like turbine blades.[24]

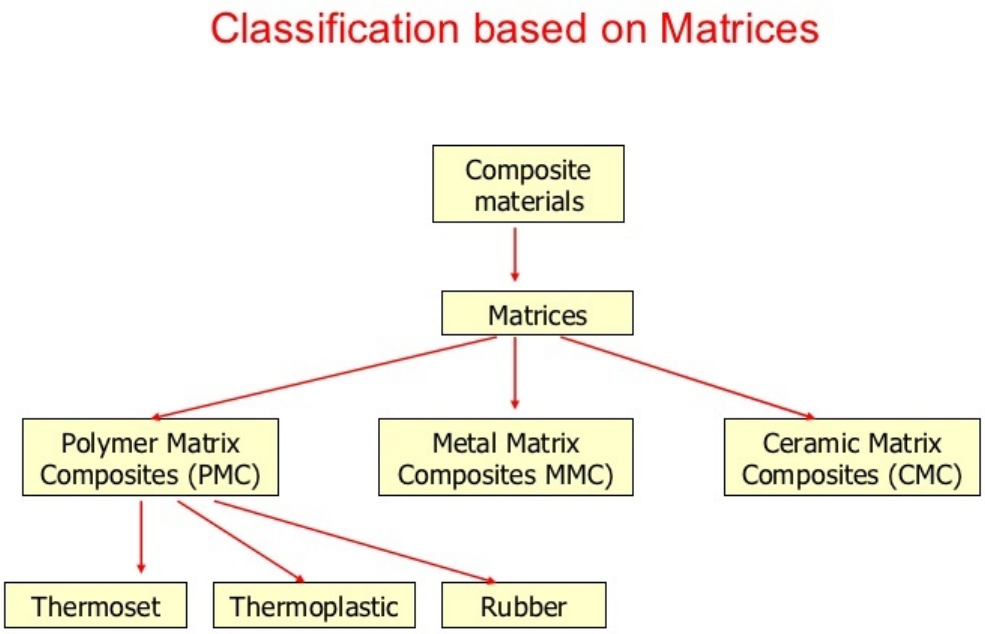

Figure 1.8: Classification-of-composites-based-on-matrices [12]

1.5.2 Role of the Matrix in Composite Performance

Regardless of the material class, the matrix plays several critical roles in the behavior and reliability of a composite system:

- **Load Transfer**: The matrix ensures mechanical stress is effectively transferred from one fiber to another, enabling the composite to behave as a unified structure under load.
- **Encapsulation and Protection**: It surrounds the reinforcement, shielding it from physical damage, moisture, UV radiation, and chemical degradation.
- **Shape Maintenance**: The matrix maintains the geometric integrity of the composite, giving it form and dimensional stability throughout its service life.
- **Toughness and Ductility**: While reinforcements are typically brittle and stiff, the matrix provides energy absorption capacity and helps delay or prevent catastrophic failure.

A well selected matrix is essential for achieving good interfacial adhesion, optimizing mechanical performance, and enhancing the long-term durability of the composite material.[25]

1.6 PLA/Natural Fiber Composites

The reinforcement of PLA with natural fibers has been the subject of extensive research over the past two decades. These studies aimed to overcome the limitations of PLA's mechanical

performance and brittleness by incorporating bio sourced reinforcements, such as flax, hemp, jute, kenaf, and bamboo fibers.

1.6.1 Types of Chemical Treatment For Natural Fibers

Chemical treatment of natural fibers is a crucial step in improving their compatibility with polymer matrices. Natural fibers, as extracted from biomass, contain not only cellulose but also non cellulosic components such as lignin, hemicellulose, waxes, and oils that interfere with bonding to the polymer. These impurities lead to poor interfacial adhesion, high moisture absorption, and weak mechanical performance of the resulting composite.

To overcome these issues, fibers are often subjected to chemical surface treatments, which aim to:

- Remove undesirable components
- Increase surface roughness
- Introduce functional groups that improve bonding with the polymer

Several types of chemical treatments are commonly applied:

- **Alkaline treatment (Mercerization):** Uses NaOH to remove hemicellulose, lignin, and surface waxes. It increases surface roughness and exposes more cellulose, enhancing matrix adhesion.
- **Silane treatment:** A coupling agent that forms a chemical bridge between fiber and matrix, often used in high-performance composites.
- **Acetylation:** Replaces hydroxyl groups with acetyl groups to reduce moisture sensitivity.
- **Other treatments:** Such as benzoylation, maleated coupling, and peroxide treatment, are used in specialized applications to improve compatibility or modify fiber properties.

Among these, alkaline treatment is widely recognized as the most effective and accessible method for leaf fibers such as palm leaves. It not only improves fiber matrix adhesion but also enhances thermal stability and mechanical strength without requiring expensive or complex chemicals. For this reason, it was selected as the most appropriate chemical treatment method for this study. [26]

1.6.2 Integration of Fibers into PLA Methods

Integrating natural fibers into a PLA matrix is a key step in the development of bio composites, and it plays a major role in determining the final material's performance. The goal is to ensure that the fibers are evenly dispersed and well bonded within the polymer, so that the composite benefits from both the strength of the fibers and the flexibility of the matrix. To achieve this, several processing methods can be used each with its own advantages, challenges, and suitability depending on the application and scale of production.

1-Chloroform Dissolution Method

The chloroform dissolution method is a solvent based composite fabrication technique that involves dissolving the PLA polymer in chloroform to create a viscous solution into which reinforcing fibers can be uniformly dispersed.

Chloroform, also known as trichloromethane ($CHCl_3$), is a colorless, dense liquid commonly used in laboratories as a solvent for organic materials. It has a sweet smell and evaporates quickly at room temperature. Despite its effectiveness as a solvent, it is considered hazardous and must be handled with proper ventilation and personal protective equipment.

In terms of cost, laboratory grade chloroform typically ranges from €60 to €100 per liter, depending on purity and supplier. Although relatively affordable for small scale laboratory work, its health risks and environmental concerns must be carefully considered.

The chloroform dissolution process starts by gradually dissolving PLA granules in chloroform under magnetic stirring at ambient conditions. Once fully dissolved, treated natural fibers (such as sieved palm leaf fibers) are added to the solution and mixed until a homogeneous dispersion is achieved. The resulting mixture is then cast into molds and left to dry under a fume hood or in a well-ventilated space. The slow evaporation of chloroform allows the composite to solidify into a thin film, ready for trimming and shaping.

This method is often used in research settings due to its simplicity and the good dispersion it provides, although it has clear limitations in safety and scalability. [27]

2-PLA Grinding Method

After exploring the solvent based chloroform dissolution method, this section focuses on a more practical and scalable approach: the mechanical mixing of ground PLA with palm leaf fibers. In this method, commercial PLA pellets are first ground into a fine powder to improve surface contact and facilitate uniform mixing with the treated fibers. This dry blending technique helps ensure a more even distribution of the fibers throughout the polymer matrix before the composite is processed through molding or extrusion. Compared to solvent-based methods, solid-state mixing avoids the use of chemicals, reduces environmental impact, and is more suitable for larger-scale production. However, the quality of the final blend largely depends on the fiber size, moisture content, and the homogeneity achieved during the mixing stage.

Table 1.6: Comparison Between Chloroform Dissolution and Solid-State Mixing Methods

Criteria	**Chloroform Dissolution Method**	**Solid-State Mixing (Dry Blending)**
Process Type	Solvent based	Mechanical (solvent-free)
PLA Form	Dissolved in chloroform	Ground into powder
Environmental Impact	Involves use of hazardous solvent (chloroform)	Environmentally friendlier (no solvent use)
Health & Safety	Requires fume hood and strict safety protocols	Safer; standard lab precautions suffice
Fiber Dispersion	Generally good at micro-scale dispersion	Depends on thorough mixing; risk of uneven dispersion
Scalability	Limited (lab-scale only)	More scalable for industrial use
Processing Time	Longer (includes dissolution, mixing, and solvent evaporation)	Faster (direct mixing and processing)
Final Composite Quality	Good bonding but potential residual solvent issues	Cleaner interface but may need thermal processing optimization
Equipment Required	Magnetic stirrer, solvent-safe containers, drying oven	Grinder, mixer, and compression/extrusion tools

1.6.3 Challenges in Composite Matrix Fabrication

During the development of composite materials, particularly those involving natural fiber reinforcements and polymer matrices, several challenges may arise. These issues can be grouped into material related, process related, and performance-related problems.

1. Material Compatibility Issues :

- **Poor adhesion between matrix and fibers**: Natural fibers are hydrophilic, while most polymers (including PLA) are hydrophobic, leading to weak interfacial bonding and poor stress transfer.
- **Moisture content in natural fibers**: High moisture can lead to void formation during processing, degrade mechanical properties, and reduce dimensional stability.
- **Thermal degradation of fibers**: If processing temperatures exceed the thermal stability of the natural fibers, decomposition can occur, releasing gases and weakening the structure.[25]

2. Dispersion and Distribution Problems :

- **Poor fiber dispersion**: Non-uniform distribution of fibers may lead to clustering and localized weaknesses in the composite.
- **Fiber sedimentation**: Heavier fibers may settle during the mixing or extrusion process, resulting in uneven reinforcement throughout the material. [13]

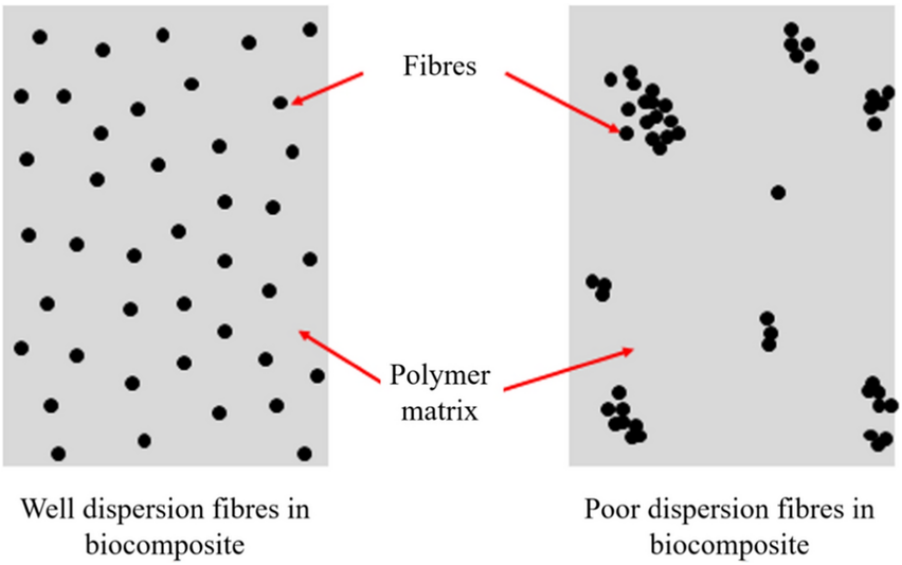

Figure 1.9: Fibers Destribution[13]

3. Processing Challenges :

- **Equipment incompatibility**: Natural fiber composites may clog extruder nozzles or react poorly in standard processing conditions if not properly dried.
- **Increased viscosity**: High fiber content can make the molten matrix too viscous, complicating mixing and extrusion, particularly during filament fabrication.
- **Air entrapment and voids**: Insufficient mixing or degassing can lead to trapped air pockets, which compromise the structural integrity of the final product.

4. Failure Mechanisms :

Composite materials exhibit complex failure modes due to the interaction between the matrix and the reinforcement. Understanding these mechanisms is essential for designing durable and efficient composite structures. Common failure mechanisms include:

- **Fiber Pull Out**: Occurs when the bond between the fiber and the matrix is too weak, causing the fiber to slide out under stress instead of breaking.
- **Matrix Cracking**: Initiated when the matrix alone cannot withstand the applied load, resulting in microcracks that may propagate through the material.[28]

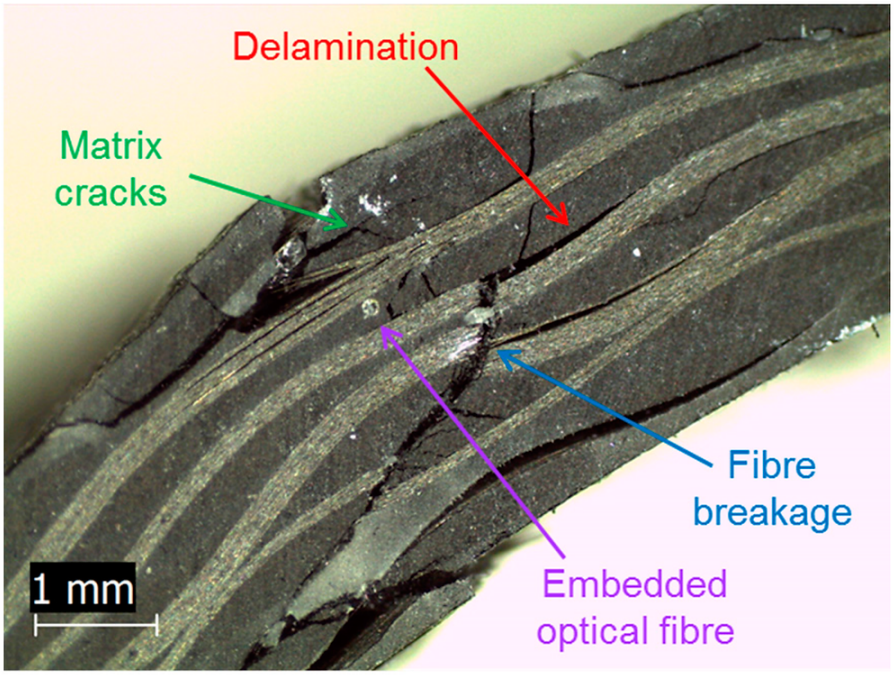

Figure 1.10: Demonstration of multiple matrix problems [14]

- **Debonding at the Interface**: Caused by insufficient interfacial adhesion, this leads to a loss of stress transfer efficiency between the fiber and matrix.
- **Delamination**: In layered or laminated composites, delamination refers to the separation of layers due to out-of-plane stresses or weak bonding between layers.

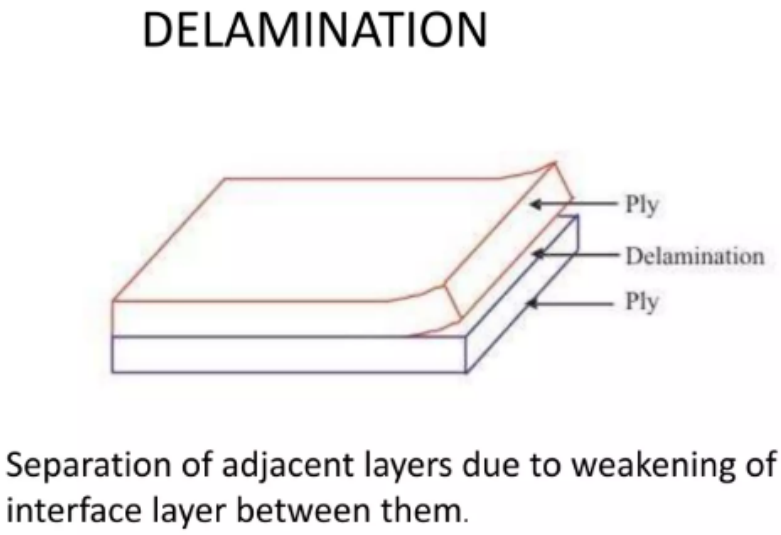

Figure 1.11: Delamination [15]

1.6.4 Summary of Notable Studies

- **Flax/PLA:** A study by Bax and Müssig (2008) showed that alkali treated flax fibers at 30% weight fraction significantly increased Young's modulus without compromising ductility.

- **Hemp/PLA:** John and Anandjiwala (2009) demonstrated improved impact strength with silane treated hemp fibers via injection molding.

- **Kenaf/PLA:** Huda et al. (2006) showed that the addition of MAH-g-PLA as a compatibilizer enhanced tensile properties and moisture resistance.

- **Jute/PLA:** Islam et al. (2010) found that composites with treated jute fibers exhibited better thermal stability and fiber dispersion.

1.6.5 Challenges Reported in Previous Studies

Despite the environmental and mechanical advantages of natural fiber-reinforced PLA composites, several challenges have been consistently reported in the literature:

- **Printability and Processability Issues:** The incorporation of natural fibers often results in processing difficulties. Common issues include nozzle clogging during 3D printing due to long or poorly dispersed fibers, increased melt viscosity that hinders uniform flow, and limited flowability during extrusion and molding—especially at higher fiber loadings.

- **Fiber Degradation During Processing:** Many natural fibers degrade thermally at temperatures around or above 200 C. Since PLA is typically processed between 180–200 C, this narrow processing window often leads to fiber degradation, discoloration, and odor emissions during melt blending or extrusion.

- **Poor Interfacial Adhesion:** Untreated natural fibers are hydrophilic, whereas PLA is hydrophobic, leading to weak interfacial bonding. This mismatch results in fiber pull-out, matrix cracking, and suboptimal mechanical performance. To address this, researchers have used treatments such as alkali (NaOH), silane coupling agents, and maleic anhydride grafted PLA (MAH-g-PLA) as compatibilizers.

- **Moisture Sensitivity:** Both PLA and natural fibers are sensitive to moisture absorption. Residual water during processing may lead to porosity, gas formation, and poor surface finish in final parts. Therefore, strict drying protocols are often required before compounding.

These challenges highlight the importance of fiber treatment, controlled processing conditions, and the use of compatibilizers in producing high-quality PLA/natural fiber composites.

1.7 Conclusion

This chapter has provided a comprehensive overview of the fundamental concepts and materials relevant to the development of biodegradable composites reinforced with natural fibers. The classification and properties of biodegradable polymers were discussed in detail, with a particular focus on polylactic acid (PLA), highlighting its advantages such as renewability, printability, and commercial availability, as well as its limitations in terms of brittleness and thermal resistance.

An in-depth review of PLA's origin, manufacturing process, and mechanical behavior set the stage for understanding its suitability as a matrix in fiber-reinforced composites. In parallel, we

examined the structure and composition of the date palm tree, identifying various fiber types and justifying the specific selection of palm leaf fibers for this work based on their abundance, light weight, and limited exploration in the literature.

A review of composite material fundamentals was also presented, including the role of the matrix, key failure mechanisms, and the main challenges encountered during composite formation. Finally, previous studies involving PLA reinforced with other natural fibers were analyzed to identify technical difficulties such as poor interfacial bonding, moisture sensitivity, and processing limitations.

Together, these insights underline both the potential and the technical complexity of developing PLA–palm leaf fiber composites. The next chapter will focus on the experimental approach used to extract, treat, and integrate these fibers into a functional composite matrix for use in additive manufacturing applications.

Chapter 2

Processing and Development of PLA Reinforced with Palm Leaf Fibers Composites

2.1 Introduction :

The development of fiber-reinforced composites relies heavily on careful material selection, preparation, and processing techniques to ensure both compatibility and performance. When working with natural fibers and biodegradable polymers, such as polylactic acid (PLA), several critical steps must be followed to overcome inherent challenges related to interfacial bonding, dispersion, and mechanical integration. This chapter provides a detailed overview of the processes involved in preparing natural fibers for composite use, with particular attention to the physical and chemical treatments required to enhance their adhesion and stability within a polymer matrix. It also addresses key considerations in polymer preparation, material mixing, and composite fabrication methods, all of which play a crucial role in determining the final properties of the resulting biocomposite. Through this comprehensive framework, the chapter lays the foundation for understanding how raw, bio-based materials can be transformed into engineered composites suitable for structural and functional applications

2.1.1 Selection of Palm Leaf Fibers over Other Palm-Based Fibers

In this study, we selected palm leaf fibers as reinforcement for our composite because they offer the lowest diameter and density and for their availability, and limited prior research. Widely found in regions with date palm plantations, these leaves are often treated as waste, making them a sustainable and cost-effective raw material. Their low density also suits lightweight applications such as 3D printing and small structural parts. Unlike better-known palm components like kenaf or coir, palm leaf fibers remain underexplored in polymer composites. By focusing on this abundant yet little-studied fiber, our work offers original insights into sustainable material development.

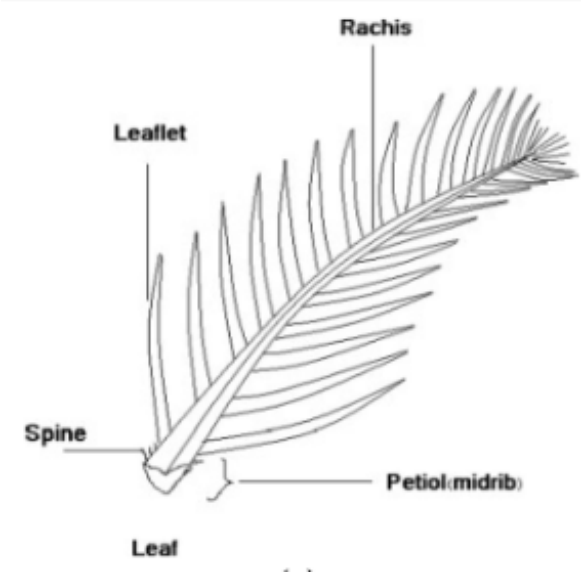

Figure 2.1: Palm Tree Composition [16]

2.2 Collection of Date Palm Leaves

The initial step of any natural fiber extraction process relies on the careful selection of raw material. In this project, date palm leaves were chosen due to their local availability, fibrous structure, and potential as reinforcement in composite materials. This section details the conditions under which the palm trees were identified, the methods used to harvest their leaves, and the manual sorting performed to prepare the leaves for the next stage.

Location of Palm Fibers

The date palms used in this study were identified within the grounds of our university. These trees are typical of the region's semi arid climate and are often planted in institutional green spaces. The choice of these specimens was based not only on their accessibility but also on the maturity of their leaves an essential criterion to ensure good fiber quality. Indeed, very young leaves contain more moisture and soluble matter, while overly old leaves may be too rigid or degraded.

A visual inspection was carried out to identify the most suitable trees. The goal was to select palms with long, strong leaves in good health and accessible without the need for specialized equipment.

Figure 2.2: Palm Tree

Palm leaves were manually collected using pruning tools, targeting healthy branches and minimizing environmental impact. Cut at the base and carefully transported, they arrived intact at the lab, where they were cleaned of dust and organic matter. The leaflets were then manually separated and cut into manageable fragments, with hard or non-fibrous parts removed. This step ensured that only fiber-rich portions were retained, aiding the efficiency of drying, treatment, and extraction. The selected segments were stored dry, awaiting thermal pretreatment.

2.3 Physical Pretreatment of the Leaves

2.3.1 Leaf Cutting

Once the leaflets are separated from the trunk, they are manually cut using scissors or cutters into small segments of appropriate size (generally between 5 and 15 cm in length). This cutting step facilitates their arrangement in the drying oven and optimizes the drying process by increasing the heat exchange surface area.

This step is carried out carefully to avoid damaging the internal fibrous structures. The resulting pieces are then placed on mesh racks or perforated trays to allow good circulation of hot air during the drying phase.

Figure 2.3: Leaves

2.3.2 Oven Drying

Drying is a crucial step in preparing plant fibers, as it reduces residual moisture, prevents mold growth, and stabilizes the material for further treatment. The cut leaf segments were dried in a forced convection oven at 70°C for 48 hours—hot enough for effective dehydration but mild enough to avoid damaging lignocellulosic components. To ensure uniform drying, the leaves were arranged in a single layer, and periodic checks were made to monitor temperature and humidity conditions.

Figure 2.4: Oven at 70C

Visual Inspection of the Condition of the Dried Leaves

After the 48-hour drying period, a visual inspection was conducted to assess the final condition of the leaves. The evaluation criteria included:

- **Color**: Properly dried leaves display a uniform light brown hue, with no black spots or signs of burning.
- **Rigidity**: The leaves become brittle, indicating that internal moisture has been effectively removed.
- **Odor**: The absence of any fermentation or mold smell confirms the success of the process.
- **Fiber integrity**: A slight peeling between the leaf layers suggests that the fibrous structure remains intact and ready for extraction.

Figure 2.5: Dried Leaves

2.3.3 Grinding of the Fibers

After drying and visual inspection, the date palm leaves undergo a grinding step. This operation aims to transform the rigid and brittle leaves into fine fibrous fragments or powder, facilitating their integration into the polymer matrix during the fabrication of the bio-composite.

The grinding was carried out using a mechanical grinder available at Mechanical Department which was designed for processing dry plant materials. The leaves were gradually fed into the grinding chamber, where they underwent mechanical reduction by rotating blades.

Grinder Description :

Figure 2.6: Ktchef Grinder

Table 2.1: Technical Specifications of KTchef KT-1000Y Grinder

Attribute	**Value**
Model Number	KT-1000Y
Brand	KTchef
Voltage	220 V
Rated Power	3000 W
Rotation Speed	28 000 rpm
Capacity	1000 g
Fineness Range	30–300 mesh
Recommended Working Time	0–5 minutes per batch
Country of Manufacture	People's Republic of China

–Power (3kW) and high rotational speed (28000rpm) make it suitable for grinding palm leaf fibers efficiently.

–Fineness range (30–300 mesh) gives a particle size control you can relate to downstream processing like extrusion or mixing.

The goal is to obtain particles of uniform size while preserving the structural integrity of the fibers. This controlled particle size distribution allows for better dispersion in PLA which improves the matrix reinforcement adhesion.

Precautions were taken to prevent excessive heating of the fibers during grinding, which could alter their mechanical properties. At the end of the process, the ground fibers were sieved to remove overly fine dust and stored in airtight bags, awaiting chemical treatment . the final result after grinding :

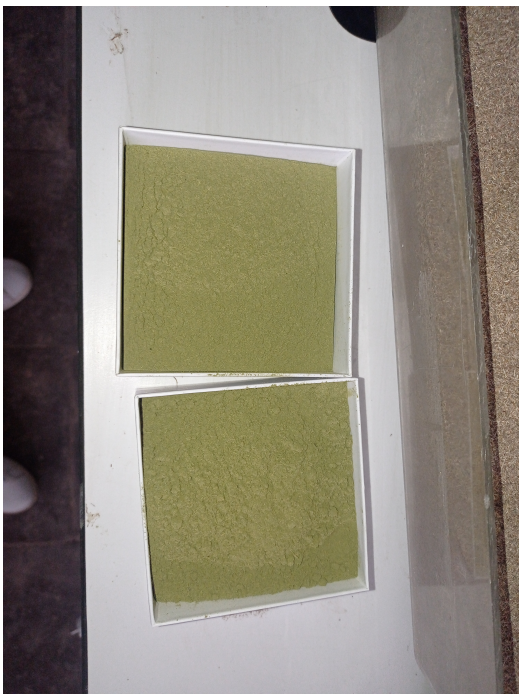

Figure 2.7: Grinded Fibers

2.4 Chemical Treatment of the Fibers

Chemical treatment of natural fibers is a crucial step in enhancing their compatibility with polymer matrices. Due to their hydrophilic nature, untreated fibers often exhibit poor interfacial bonding with hydrophobic polymers such as PLA. Chemical modifications—most commonly alkali (NaOH) treatment—help remove surface impurities like waxes, lignin, and hemicellulose, while also increasing surface roughness. This improves fiber–matrix adhesion, mechanical interlocking, and overall composite performance. The choice of treatment method depends on the fiber type, the desired surface properties, and the specific application of the composite.[29]

2.4.1 Preparation and Application of the Alkaline Treatment

Before starting the chemical treatment , Strict safety practices must be followed when working with NaOH and treated fibers, including proper PPE, ventilation, and neutralization of chemical waste. Handling errors or improper disposal can lead to severe chemical reactions, health risks, and environmental harm.

To carry out the chemical treatment of the palm leaf fibers, an alkaline solution was prepared using sodium hydroxide (NaOH). If lignin and hemicellulose are not properly removed during the fiber treatment process, they can negatively affect the quality of the final composite material:

- **Lignin** can hinder the adhesion between the fiber and the polymer matrix because of its hydrophobic and chemically inactive nature. This poor interfacial bonding leads to lower mechanical strength and a higher risk of delamination or cracking under stress.

- **Hemicellulose** is highly hydrophilic, meaning it absorbs moisture easily. If not removed,

it can cause the composite to swell or degrade in humid environments, reducing its dimensional stability and long-term durability.

In summary, the presence of lignin and hemicellulose in untreated fibers weakens the fiber-matrix interface, increases moisture sensitivity, and compromises both the mechanical and thermal performance of the composite.[30]

So a 3% NaOH solution was required, using NaOH pellets of 99% purity, and distilled water, with a final volume of 1000 mL (1 L).

Figure 2.8: NAOH Bottle

Figure 2.9: Distilled Water

Table 2.2: Technical Specifications of Sodium Hydroxide (NaOH)

Property	**Value**
Form	Solid pellets (99% purity)
CAS Number	1310-73-2
Appearance	White solid pellets
Purity	99%
pH (1 N solution)	14
Melting Point	323 °C
Boiling Point	1,388 °C
Solubility in Water (20 °C)	Miscible
Vapor Pressure (20 °C)	< 0.1 hPa
Vapor Density	2.5 (AIR = 1)

Calculation (accounting for 99% purity)

A 3% NaOH solution was chosen because it is the most commonly used concentration in fiber treatment research, offering effective removal of lignin and hemicellulose. It provides a good balance between surface modification and preserving the structural integrity of the fibers.[31]

A 3% w/v solution means 3 grams of pure NaOH per 100 mL of water.

For 1000 mL:

$$\frac{3\,\text{g}}{100\,\text{mL}} \times 1000\,\text{mL} = 30\,\text{g (pure NaOH)}$$

Since the NaOH pellets are only 99% pure, the actual mass needed is:

$$\text{Required mass of pellets} = \frac{30\,\text{g}}{0.99} \approx 30.30\,\text{g}$$

Approximately 30.30 grams of NaOH pellets (99% purity) were accurately weighed and gradually dissolved in 1000 mL of distilled water while stirring continuously.

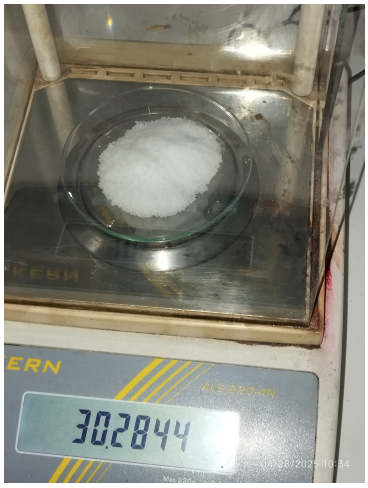

Figure 2.10: 30grams of NAOH

Figure 2.11: Solution preparation

Note: The addition of NaOH pellets to water is exothermic so we pour water first, then slowly add NaOH pellets while stirring. Appropriate personal protective equipment ; gloves, goggles, and a lab coat were used, and the dissolution was carried out slowly to avoid splashing and overheating.

Once fully dissolved and cooled, the solution was stored in a tightly sealed container and used immediately for the fiber treatment process.

The ground fibers are then immersed in the NaOH solution for a duration of two hours. During this step, gentle stirring can be carried out to ensure uniform contact between the fibers and the solution.

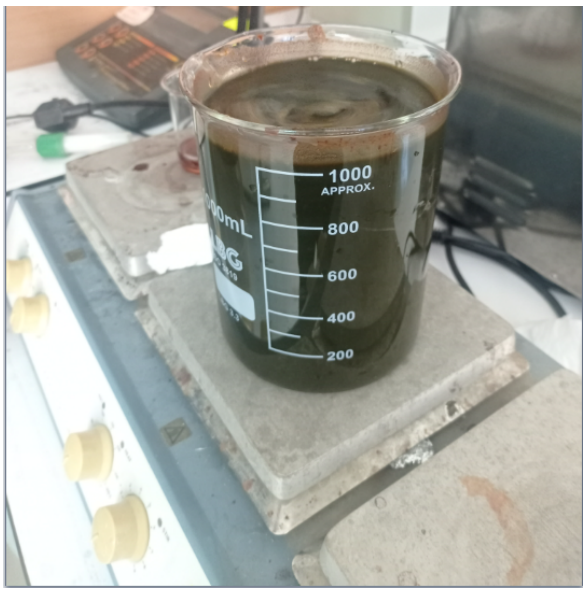

Figure 2.12: Fibers in the Alkaline Solution

2.4.2 Rinsing of the Fibers with Distilled Water and pH Stabilization

After the alkaline treatment, the fibers are thoroughly rinsed with distilled water. This rinsing is carried out multiple times to completely remove any residual sodium hydroxide from the fibers.

Successive rinses are continued until the pH of the fibers stabilizes between 6.5 and 7.5 , indicating relative neutrality. To monitor this, a pH meter is used after each rinse.

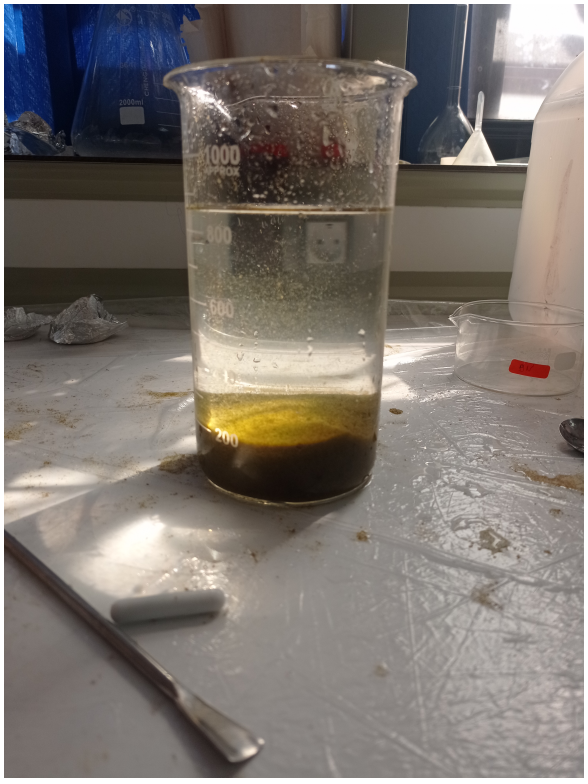

Figure 2.13: Rinsed fibers

After 20 to 30 rinces that took a day we finally stabilized the pH at 7.31 which means the fibers are neutral and no longer contain any Sodium Hydroxide. After that the fibers are separated from the distilled water and are spread out on racks and dried in a moderately heated oven at 60C and left for at least 24 hours to make sure they get dried of all the moisture without getting burnt .

Figure 2.14: Neutralized PH

Figure 2.15: Fibers in the Oven

2.4.3 Sieving of the Fibers

After chemical treatment and drying, palm leaf fibers undergo a sieving process to achieve a uniform particle size below 0.2 mm, using the finest mesh available in the laboratory. This step ensures consistency in fiber dimensions, which is essential for achieving homogeneity in the composite material. Controlled fiber size significantly improves dispersion within the PLA matrix, enhances interfacial adhesion, and facilitates better stress transfer across the fiber–matrix interface. These factors contribute to improved mechanical performance, reduced void content, and minimized stress concentrations within the composite. The chosen size also reflects a practical balance between fiber refinement and preservation of reinforcement capacity, ensuring that the fibers retain sufficient length to contribute meaningfully to the composite's structural integrity. Therefore, sieving is not a mere preparatory step but a critical process that directly influences the composite's quality, repeatability, and performance during mechanical testing and application

2.4.3.1 Impact of Using Fibers Larger than 0.2 mm

Using palm leaf fibers larger than 0.2 mm in the PLA composite can lead to several processing and material-related issues, particularly during extrusion and in the final performance of the composite.

In the Composite Material

- **Poor dispersion:** Larger fibers are more likely to agglomerate or distribute unevenly in the PLA matrix, creating weak zones in the material.

- **Reduced interfacial adhesion:** Fibers with larger diameters have a lower surface-area-to-volume ratio, which limits their ability to bond effectively with the matrix and reduces stress transfer efficiency.
- **Void formation:** Irregular or coarse particles may cause internal gaps or voids, which can act as stress concentrators and degrade mechanical properties.
- **Lower printability:** In additive manufacturing applications, poor dispersion and voids may result in poor surface finish, warping, or delamination during 3D printing.

Overall, exceeding the 0.2 mm threshold compromises the homogeneity and processability of the composite, which negatively affects both the manufacturing workflow and the final material quality. [32]

2.4.3.2 Sieving Procedure and Results

Sieving was carried out using a calibrated mesh sieve with a mesh size smaller than 200 microns. The treated and dried fibers were gradually poured onto the sieve and then subjected to manual movements (vibration, gentle shaking) to effectively separate the particles by size.

Only fibers with a diameter smaller than 200 microns are retained for the next stage of the process. These fibers have a fine, uniform texture and are now perfectly ready to be mixed with PLA for the formulation of the biocomposite material.

This particle size control is an essential quality step to ensure the performance of the final composite material as well as the reliability of the additive manufacturing process.

Figure 2.16: Dried Fibers

Figure 2.17: Sieve

Figure 2.18: Sieved Fibers

Challenges Faced During the Extraction and Treatment Process

Throughout the various stages of extracting and treating date palm leaf fibers, several practical challenges were encountered. These challenges had a direct impact on the efficiency, time management, and quality of the resulting fibers intended for composite fabrication.

- **Extended Rinsing Time for pH Stabilization:** One of the most challenging parts of the process was rinsing the chemically treated fibers to bring their pH back to a neutral level. Even though the 3% NaOH alkaline solution was prepared with care, rinsing the fibers thoroughly took multiple wash cycles—and in some cases, it ended up taking an entire workday just to get the pH close to neutral. This step turned out to be both time-consuming and resource-intensive, requiring a significant amount of distilled water and adding to the overall cost and complexity of the procedure.

  .

- **Uneven Drying:** After the chemical treatment, getting the fibers to dry evenly turned out to be another tricky step. Moisture often got trapped inside thicker bundles of fibers, leading to uneven drying—especially when using an oven. This inconsistency wasn't just inconvenient; it posed real risks. If some areas stayed damp, it could compromise the quality of the fibers or even lead to microbial growth over time.

- **Loss of Fiber Material During Chemical Treatment and Sieving:** During the grinding process, a portion of the fine fibers ended up sticking to the internal surfaces of the grinder, leading to some unavoidable material loss. On top of that, sieving the fibers to a fine 0.2 mm size turned out to be time-consuming, as clumped particles had to be cleared repeatedly. This added extra steps to the process, causing delays and a small amount of material waste along the way.

- **Clogging of the Sieve Mesh:** Because of the small mesh size used for sieving (0.2 mm), the sieve often became clogged—either from fibers sticking together or from leftover traces of moisture. As a result, the process had to be stopped frequently for manual cleaning, which slowed things down and reduced overall efficiency.

- **Time Intensive Manual Operations:** Manual separation, grinding, and rinsing of the fibers were labor-intensive and time-consuming steps. These operations required significant attention to detail to maintain consistency and avoid contamination or fiber damage.

2.5 Fibers Integration Into PLA

In order to ensure proper matrix formation during the composite fabrication using the hydraulic press, it was essential to reduce the size of the PLA pellets. The raw PLA pellets typically have a diameter of approximately 3 mm, which makes them unsuitable for direct use in the matrix due to poor compactability and non-uniform dispersion. For optimal processing and homogeneity within the composite, the PLA must be transformed into a fine powder form.

This section addresses the grinding process implemented to convert the PLA pellets into powder. This step is crucial for improving the efficiency of the molding process and ensuring consistent quality in the final composite material.

2.5.1 PLA Grade Selection

For this project, we chose PLA grade 4043D because it strikes a good balance between being eco friendly and mechanically strong—two qualities that were central to our goals. This particular grade is known for its solid tensile strength and stiffness, which makes it suitable for

structural applications like small wind turbine blades. Another key reason behind this choice is its compatibility with 3D printing. On top of that, 4043D processes well when combined with natural fibers like palm, ensuring good bonding and overall composite quality. And since it remains fully biodegradable, it fits perfectly with the sustainability aspect of the project. It's also important to note that access to PLA in Algeria is currently very limited, and there is no local supplier of PLA grades. As a result, the selection was constrained, and 4043D was chosen not only for its technical properties but also for its relative availability in our context.

PLA 4043D Properties

Table 2.3: Summary of Technical Properties of PLA 4043D[2]

Property	**Value**
Density	1.24 g/cm^3
Melt Flow Rate	6 g/10 min (210°C / 2.16 kg)
Tensile Modulus	∼3GPa
Tensile Strength (Break)	∼53 MPa
Elongation at Break	∼6%
Flexural Modulus	∼3.8 GPa
Flexural Strength	∼83 MPa
Notched Izod Impact	∼16 J/m

Table 2.4: Thermal and Rheological Properties of PLA 4043D

Property	**Value**
Glass Transition Temperature (Tg)	55–60°C
Melting Temperature	145–160°C
Heat Distortion Temperature at 0.45 MPa	∼66°C

Table 2.5: Processing Recommendations for PLA 4043D

Parameter	**Value**
Drying Conditions	80°C for 4 hours, ≤0.025% moisture
Extrusion Temperature Range	190–230°C (start at 210°C)
3D Print Bed Heating	50–70°C may improve adhesion

Figure 2.19: PLA 4043D Pellets

2.5.2 PLA Grinding Process

Freezing and Intermittent Grinding

To convert PLA pellets into a powder form suitable for composite matrix fabrication. This method, based on freezing and intermittent grinding, was chosen for its accessibility, safety, and adaptability to the laboratory's available resources.

Grinding Procedure

The method involved freezing the PLA pellets in a conventional household freezer to make them brittle enough for grinding. Once chilled, the pellets were ground using an electric grinder for a controlled duration of 15 to 20 seconds. This short interval was critical: any longer would cause the PLA to soften or partially melt due to frictional heat, which would not only reduce grinding efficiency but also risk damaging the grinder or altering the polymer's structure.

After each grinding cycle, the material was immediately returned to the freezer for approximately 15 minutes, allowing it to regain brittleness before repeating the grinding process. This cycle of freezing, grinding, and refreezing was repeated multiple times until the desired particle size and texture were obtained.

Figure 2.20: Grinded PLA

On average, producing 300 grams of adequately ground PLA powder required nearly a full working day. The time investment was due to the repeated freezing cycles and the need to avoid overheating. However, this method ensured that the structural and thermal properties of the PLA were preserved while producing a particle size suitable for homogeneous blending with the sieved palm fibers.

Although labor-intensive and time consuming , the freezing and intermittent grinding approach proved to be a reliable and effective method for transforming PLA pellets into a form compatible with solid state composite processing. It demonstrated that, with careful thermal control and equipment selection, high-quality PLA powder can be produced even under limited laboratory conditions. This step was critical in achieving uniform fiber dispersion and consistent matrix behavior in the subsequent pressing and molding stages.

2.5.3 Mold Preparation and Material Mixture

In this section, we describe the molds used during the fabrication process and outline the procedure followed to prepare the PLA-fiber mixture, from component mixing and drying to mold filling. Each step was carefully controlled to optimize the consolidation of the matrix and reduce the likelihood of voids, defects, or inconsistent reinforcement distribution in the final composite.

The objective is to achieve uniform shaping and consistent mechanical structure of the composite.

2.5.3.1 Molds Description

In the composite fabrication process, the molds played a fundamental role in shaping and containing the PLA-fiber mixture during compression. Two different mold sizes were used in this study to accommodate varying material quantities and to serve different testing and prototyping purposes.

Two molds were used during the composite fabrication process:

- **Mold 1**: 13 × 9 cm
  - Maximum capacity: approximately 50 grams
  - Used for small test samples and process trials
  - Ideal for checking fiber distribution and validating process parameters
- **Mold 2**: 23 × 23 cm
  - Maximum capacity: approximately 300 grams
  - Used for full-scale composite plate fabrication
  - Enabled cutting of standardized specimens for mechanical testing

Both molds were fabricated from robust steel to withstand the high pressure and temperature conditions applied during the hydraulic pressing process.

Figure 2.21: Molds

2.5.3.2 Mixture Preparation

To determine the most effective fiber content for reinforcing the PLA matrix, a gradual and systematic approach was adopted. Instead of selecting a single fixed ratio, different composite mixtures were prepared by incrementally increasing the proportion of palm leaf fibers. This method allowed for a clearer understanding of how fiber content influences the mechanical behavior of the material. At low fiber ratios, the composite maintained good processability but showed limited reinforcement. As the fiber content increased, improvements in stiffness and strength were observed—up to a point. Beyond a certain threshold, however, excessive fiber loading led to poor dispersion, reduced interfacial adhesion, and processing difficulties, which negatively impacted the material's performance. This step-by-step approach enabled us to identify the most balanced formulation—one that offers enhanced mechanical properties without compromising the structural integrity or workability of the composite.

For each mold we calculated the fibers mass that needs to be added :

Fiber Volume Percentage	**Fibers Mass in 50g Mixture (g)**	**Fibers Mass in 300g Mixture**
5%	2.5	15
15%	7.5	45
30%	15	90

Table 2.6: Calculated fiber masses required to achieve selected weight percentages in 50g and 300g composite mixtures

After calculating and weighing the appropriate proportions of PLA and palm leaf fibers, the two components were manually pre-mixed and then thoroughly blended using a laboratory mixer for approximately 3 to 5 minutes. This mixing step was essential to ensure a homogeneous dispersion of the fibers within the PLA matrix, promoting consistency in the final composite structure. Once mixed, the blend was placed in a drying oven at a controlled temperature and left for a minimum of 1 hour and 30 minutes. This drying process was critical to eliminate any residual moisture in both the PLA and the natural fibers, as the presence of humidity could significantly affect the interfacial bonding and processing quality during the subsequent molding or pressing steps .

After completing the drying process, the mixture was carefully removed from the oven and immediately transferred into a metallic mold. This step had to be done swiftly to avoid moisture absorption from the surrounding air. The mold had been previously prepared and cleaned to ensure uniform compaction and to prevent any contamination. The mixture was spread evenly within the mold to allow for consistent thickness and distribution before the pressing phase.

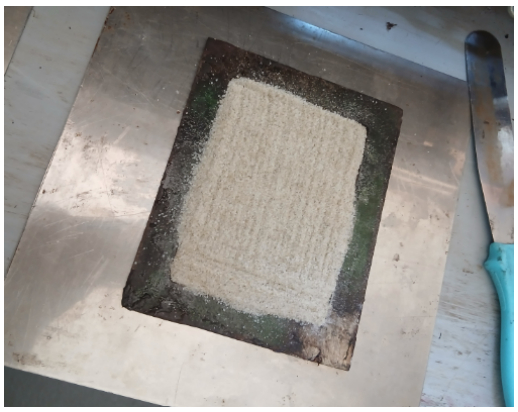

Figure 2.22: 50g Mixture

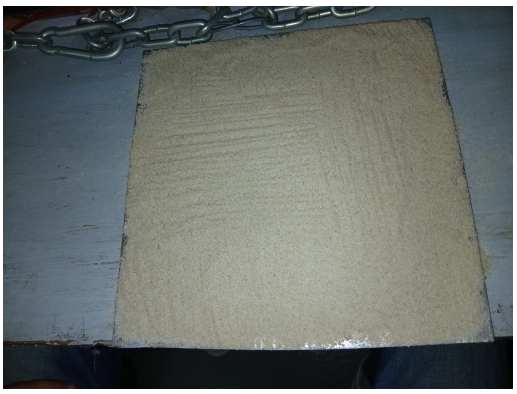

Figure 2.23: 300g Mixture

2.6 Composite Material Fabrication

2.6.1 Hydraulic Press Procedure

The hydraulic press used in this study was developed by Dr. Belouadah as part of the laboratory's specialized equipment for materials engineering applications. This robust and efficient device played a crucial role in the fabrication of composite material matrices by enabling the controlled compaction and molding of the PLA-fiber mixture. The press has a maximum capacity of 12 tons, and both the upper and lower platens have surface dimensions of 25×25cm, providing sufficient area for uniform pressure distribution during composite molding.

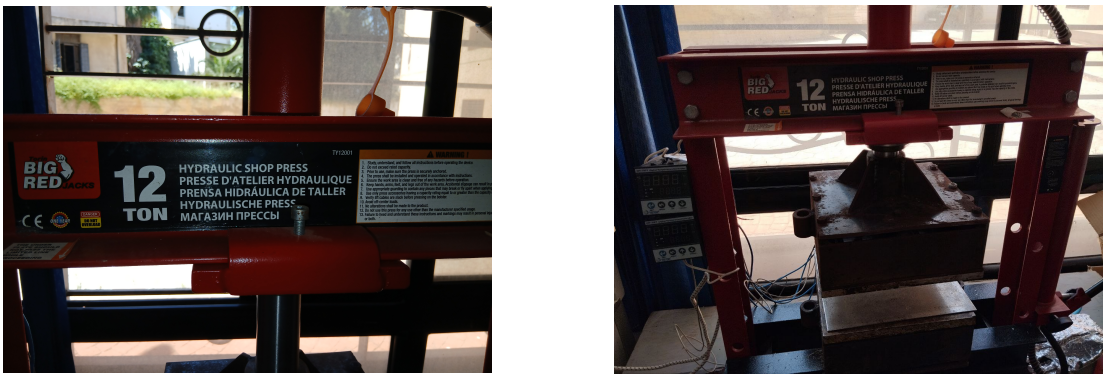

Figure 2.24: Hydraulic Press Setup

Working with a hydraulic press requires strict adherence to safety guidelines to prevent accidents and ensure smooth operation.

Before each use, the hydraulic press was carefully inspected for wear, leaks, and stability, and the molds were securely positioned to ensure safe and precise operation under a controlled load of up to 12 tons. After pressing, the system was slowly depressurized and the mold was left to cool before removal to prevent burns or deformation. Finally, the equipment and workspace were cleaned and reset to maintain safety and readiness for the next operation.

The process began by closing the upper and lower platens of the press and initiating the preheating cycle. The temperature was set to reach at least 200 °C, which is slightly higher than the melting point of PLA (approximately 170–180 °C). This ensured complete softening of the PLA, allowing it to flow properly and infiltrate the palm fibers during compression.

Figure 2.25: Hydraulic Press at 200C

Once the target temperature of 200 °C was reached, a flat steel plate was placed on the lower platen. This plate served as the base surface to support the mold and ensure even heat distribution. The mold, pre-filled with a homogenous mixture of PLA pellets and palm fibers, was carefully positioned on the steel plate. To avoid injury or contamination, gloves were worn when handling the hot components.

A second steel plate was then placed over the top of the mold to close the assembly and ensure uniform compression during pressing. The mold setup was then carefully inserted into the hydraulic press. It was observed that upon placing the cold steel plates and mold inside the press, the temperature of the platens temporarily dropped to around 175–180 °C. This was expected due to heat absorption by the colder materials.

Compression was applied immediately after the setup was in place. We gradually increased the pressure until maximum value was reached (1.8MPa) . The system was held under 180 °C for 2 to 3 minutes to ensure proper melting, flow, and bonding of the PLA matrix with the natural fibers. . After this , the heating elements were turned off and the press was left to cool naturally, with the plates still compressed. This natural cooling process lasted approximately 2 hours, until the temperature reached around 50 °C.

Figure 2.26: Hydraulic Press at 50C

Once cooled, the press was opened and the composite plate was carefully removed. The final samples exhibited good structural integrity and were ready for further cutting or mechanical testing.

Key Steps Summary

1. **Preheat the press:** Set the platens to reach 200 °C.
2. **Place base steel plate:** On the lower platen.
3. **Add and position mold:** Fill with PLA/palm fiber mix.
4. **Use gloves:** Carefully handle all hot components.
5. **Place top steel plate:** Over the mold to complete the assembly.
6. **Insert setup into press:** Noting temperature drop to 175–180 °C.
7. **Apply compression:** Hold pressure for 2–3 minutes.
8. **Natural cooling:** Let cool under pressure to 50 °C over 2 hours.
9. **Remove final plate:** Open press and extract the composite.

And the final plates results are shown in the next figures :

Figure 2.27: 300g Composite Material Plate

Figure 2.28: 50g Composite Material Plate

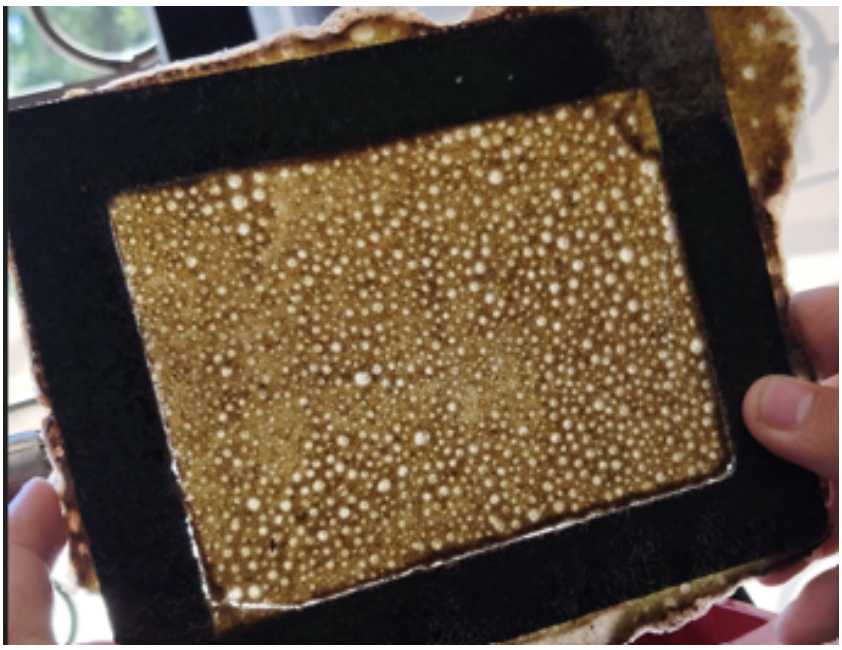

Figure 2.29: 50g Failed Composite Material Plate

Different Fiber Rates Results

Figure 2.30: 5% Fibers Rate

Figure 2.31: 15% Fibers Rate

Figure 2.32: 30% Fibers Rate

Figure 2.33: 40% Fibers Rate

Results Discussion

The 300 g composite plates displayed a compact, dense, and uniform surface finish, indicating efficient material distribution and consistent fiber integration during the molding process. Minor texture variations or faint surface marks were noticed, which may have been caused by slight inconsistencies in pressure or localized fiber orientation during pressing. However, no visible porosity was observed, which suggests that the degassing and compression conditions were effective. The larger quantity of material likely helped fill the mold cavity more completely, improving pressure transmission and heat transfer across the plate. This contributed to more uniform cooling and minimized the risk of internal voids. The resulting composite showed favorable structural integrity and a matrix–fiber interface that appears strong and continuous,

which is essential for achieving reliable mechanical performance.

On the other hand, the 50 g composite plate exhibited partial transparency and visible signs of irregular dispersion, particularly in regions with lighter coloration. These areas may point to uneven fiber distribution or local compaction issues during the molding process. The plate's edges and corners were less well-formed, likely due to premature cooling or a lack of material flow to the outermost parts of the mold. Some light transmission through the plate was also observed, which may indicate lower fiber concentration or microvoids within the matrix. These signs reflect a thinner and less densely packed composite, possibly affecting its mechanical consistency and overall performance.

The failed composite plate showed clear signs of porosity and void formation, which appeared as small trapped bubbles or gaps within the material. These defects are mainly caused by moisture or air becoming trapped during pressing—often due to insufficient drying of the PLA and fibers or poor temperature control. In some cases, rapid heating or inadequate mold venting can also prevent gases from escaping properly. As a result, issues like blistering, foaming, or uneven consolidation can occur. These defects not only weaken the mechanical strength of the material but also lead to reduced density, poor fiber–matrix adhesion, and a lower-quality surface finish. To avoid such problems, it's essential to ensure proper drying, controlled heating, and an effective mold design that allows gases to escape.

For the different fiber content results , the visual comparison of composite plates with increasing palm fiber content (5%, 15%, and 30%) reveals a clear degradation in material integrity as the fiber rate increases.

At **5% fiber content**, the composite plate presents a relatively homogeneous surface with minimal visible defects. The fibers appear well dispersed and adequately bonded with the PLA matrix, resulting in a compact and mechanically stable material. This composition maintains good cohesion, likely due to sufficient polymer matrix coverage around the limited amount of reinforcement.

In contrast, the plate with **15% fiber content** shows signs of irregular surface texture and increased roughness. This suggests that the higher fiber content begins to exceed the matrix's ability to fully encapsulate and bond with each fiber, leading to early signs of poor fiber–matrix interaction. While still usable, the structural quality begins to decline.

At **30% fiber content**, the deterioration becomes significantly pronounced. The plate exhibits surface porosity, weak edge cohesion, and possible signs of fiber clustering. These defects indicate *poor matrix wetting*, *fiber agglomeration*, and *interfacial debonding*. The excess fiber volume reduces the matrix's ability to effectively transfer stress, which can lead to *brittleness*, *cracking*, and premature failure under mechanical load.

Overall, the results demonstrate that increasing the fiber content beyond a certain threshold compromises the structural integrity of the composite. While natural fiber reinforcement can enhance sustainability and stiffness at low concentrations, excessive loading reduces processing quality and mechanical performance due to poor dispersion and weak fiber–matrix adhesion.

2.7 Conclusion

In this chapter, we have laid the essential groundwork for the development of a natural fiber-reinforced biocomposite by detailing the entire processing pathway of PLA reinforced with date

palm fibers. The successful performance of any composite material depends not only on the quality of its constituents but also on the precision and care with which they are prepared and combined. The physical pretreatment of the date palm leaves, including cutting, drying, and grinding, ensured the fibers were processed into a suitable form for further treatment. The subsequent chemical treatment—particularly the alkaline process—was crucial for enhancing the surface properties of the fibers, improving their compatibility with the PLA matrix, and promoting better interfacial adhesion.

Moreover, the sieving process allowed us to control the fiber size distribution, which is a key factor in ensuring uniform dispersion and mechanical consistency in the composite. On the polymer side, the selection and preparation of PLA, including grinding and thermal softening, were essential to creating a homogeneous mixture when combined with the treated fibers. The mold preparation and final composite fabrication using hydraulic pressing completed the manufacturing stage, resulting in test-ready samples designed to simulate practical application conditions.

With the composite material now fully processed, the study is positioned to move into its next critical phase. The upcoming chapters will focus on the mechanical characterization of the material through a series of standardized tests to evaluate properties such as tensile strength, stiffness, and elasticity. These tests are vital to understanding how the material might perform in real-world structural applications. Additionally, part of this phase includes assessing the feasibility of filament extrusion using the developed composite. If successful, this would open the door to 3D printing possibilities, offering a flexible, low-waste, and sustainable manufacturing method for components such as small wind turbine blades.

Ultimately, this chapter marks a turning point in the research—from material development to performance evaluation—and establishes the necessary technical foundation to judge the practical viability of PLA–palm fiber composites in both conventional and additive manufacturing contexts.

Chapter 3

Evaluation of Mechanical Properties of the Reinforced PLA Composite

3.1 Introduction

Following the successful development and fabrication of the PLA–palm fiber composite, the next logical step is to evaluate its mechanical performance in order to determine its suitability for real-world applications . In material science and engineering, the assessment of mechanical properties is essential to understanding how a newly developed material will behave under various loads and conditions. This is particularly important for composites, where the interaction between the matrix and the reinforcement phase plays a critical role in determining overall performance.

Mechanical characterization not only provides quantitative data on key parameters such as tensile strength, stiffness, and modulus, but also reveals insights into the quality of bonding, fiber dispersion, and structural homogeneity of the composite. These properties must be thoroughly examined to assess the reliability and potential functionality of the material in practical applications, such as small wind turbine blades or additive manufacturing.

In this chapter, emphasis is placed on identifying the mechanical strengths and limitations of the developed biocomposite. Additionally, extrusion trials are discussed to explore the potential for adapting the material to 3D printing technologies. Together, these evaluations provide a comprehensive understanding of the composite's behavior and help determine whether it meets the performance standards required for sustainable, engineering-grade applications.

3.2 Mechanical Characterization of the Composite Material

This section presents the mechanical characterization of the PLA–palm fiber composite developed in this project. The goal is to experimentally determine key material properties needed for structural simulations—specifically for modeling a wind turbine rotor blade. These properties include the composite's density, Young's modulus, and shear modulus. The results from these tests will be used as input data for the simulation software QBlade, enabling a realistic assessment of how the composite behaves under aerodynamic loading. All tests were conducted using standardized procedures to ensure the results accurately reflect the material's performance in structural applications.

3.2.1 Common Characterization Techniques for Composites

To accurately characterize the mechanical properties of composite materials, it's important to use well-defined experimental methods that follow standardized procedures. These methods ensure consistency across studies and allow the resulting data to be confidently applied in design and simulation work. The following subsections describe the most commonly used experimental techniques for evaluating the mechanical behavior of fiber-reinforced composites like PLA reinforced with palm fibers.

1-Tensile Testing

Tensile testing is one of the most essential methods for evaluating the stiffness and strength of composite materials. It measures how a material behaves when stretched along a single axis, providing key information such as **Young's modulus**, **tensile strength**, and **strain at break**.

The tensile testing procedure typically follows standards like *ASTM D638*, which specify the specimen shape, gripping method, and testing speed.

Proper sample preparation is essential for accurate results. This includes ensuring uniform thickness, precisely machining the specimen edges, and conditioning the samples under controlled temperature and humidity before testing. To improve the accuracy of strain measurements, extensometers or strain gauges may also be used during the test.

2-Shear Modulus Calculation Methods

The shear modulus (also known as modulus of rigidity) is a fundamental mechanical property that describes how a material responds to shear stress. It reflects the material's ability to resist deformation when forces are applied parallel to its surface. It can be determined using several experimental and analytical methods. Below are three common approaches:

From Tensile Test Data :
When Young's modulus (E) and Poisson's ratio (ν) are known, the shear modulus can be

estimated using the following relation:

$$G = \frac{E}{2(1+\nu)}$$

This method is convenient for materials where direct shear testing is impractical, though it relies on accurate knowledge of ν.

Torsion Test :
For cylindrical specimens subjected to torque, the shear modulus can be calculated using:

$$G = \frac{TL}{J\theta}$$

where T is the applied torque, L is the gauge length, J is the polar moment of inertia of the cross-section, and θ is the angle of twist in radians.

ASTM D5379 (V-Notched Beam Method):
This standard method uses a V-notched Iosipescu specimen, where shear load is applied at 45° through a special fixture. The shear modulus is derived from measured stress and strain in the gauge section. This method is especially useful for composite materials.

Table 3.1: Comparison of Shear Modulus Determination Methods.[3]

Method	**Advantages (Pros)**	**Disadvantages (Cons)**
From Tensile Test Data	Simple and indirect; does not require additional testing	Requires a known or estimated Poisson's ratio.
Torsion Test	Direct measurement; ideal for isotropic and metallic materials.	Requires cylindrical specimens and specific fixtures; not suitable for all geometries.
ASTM D5379	Suitable for composite materials; standardized and well-accepted for shear characterization.	Needs a special fixture; specimen preparation is more complex and sensitive to alignment.

3-Density Measurement

Density (ρ) is a key physical property in dynamic simulations, as it directly affects mass distribution and inertia. It can be determined through basic geometric measurements or, for greater accuracy, using fluid displacement methods..

Experimental Density (Archimedes Method)

Based on Archimedes' principle, the density is calculated as:

$$\rho_c = \frac{m_{\text{dry}}}{m_{\text{dry}} - m_{\text{immersed}}} \cdot \rho_{\text{liquid}} \tag{3.1}$$

Where:

- m_{dry} = mass of the dry sample in air

- m_{immersed} = mass of the sample when immersed in a fluid
- ρ_{liquid} = density of the immersion fluid (usually water = 1.00 g/cm^3)

Geometrical Density (Volume-Measured Method)

If the composite has a regular shape, the density can be calculated by:

$$\rho_c = \frac{m}{V} \tag{3.2}$$

Where:

- m = mass of the composite sample
- V = volume of the sample, calculated based on shape (e.g., $V = L \cdot W \cdot H$ for a rectangular prism)

For our Composite material :

Figure 3.1: Composite Material Weight

In this case, the sample had a measured mass of $m = 40$ g and dimensions of 13 cm × 9 cm × 3 mm. The thickness was converted to centimeters: 3 mm = 0.3 cm. Thus, the volume is:

$$V = 13 \times 9 \times 0.3 = 35.1 \text{ cm}^3$$

Substituting into the formula:

$$\rho = \frac{43}{35.1} \approx 1.22 \text{ g/cm}^3$$

Therefore, the density of the composite is approximately $\boxed{1.22\ \text{g/cm}^3}$, which is equivalent to 1220 kg/m^3.

3.2.2 Sample Preparation

For mechanical characterization, the composite specimens were prepared using the Type V geometry specified by the ASTM D638 standard for tensile testing. This specimen type is specifically designed for materials available in limited quantities, such as those produced by injection molding or pressed composite plates.

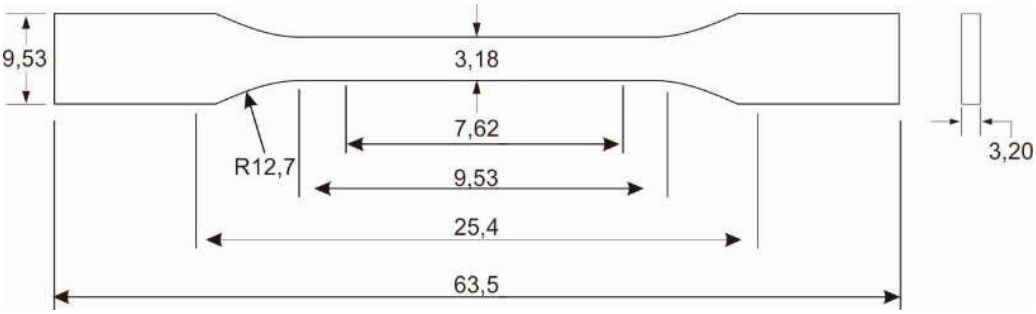

Figure 3.2: Type 5 traction sample [17]

The specimens were cut from the molded PLA–palm fiber composite plates using a CNC (Computer Numerical Control) milling machine. For the cutting process, a 3 mm diameter solid carbide single-flute end mill was used, as it's well suited for machining thermoplastic composites reinforced with natural fibers. This method provided high dimensional accuracy, clean edges, and consistent geometry across all specimens—helping to minimize variability during mechanical testing.

Figure 3.3: CNC Speciment Cutting

All specimens were inspected visually to verify uniformity in thickness, absence of visible defects, and proper fiber distribution.

Tensile Test Specimens

Figure 3.4: Tensile Specimens of 5% Fibers

Figure 3.5: Tensile Specimens of 15% Fibers

Figure 3.6: Tensile Specimens of 30% Fibers

Unfortunately it was not possible to extract tensile specimens from the composite plate containing 40% palm fiber reinforcement. The plate proved too fragile and repeatedly cracked during CNC cutting, making it unsuitable for preparing test specimens. As a result, no mechanical tests were carried out on this particular composition.

3.2.3 Tensile Testing

The tests were performed using a universal testing machine (UTM), following the ASTM D638 standard for Type V specimens. The machine applied a steadily increasing uniaxial tensile force until each specimen failed. Throughout the test, both **load** (force) and **displacement** were continuously recorded. These raw data were then used to calculate the **engineering stress** and **engineering strain** for each sample.

- **Load–displacement curves** The raw output from the testing machine is directly represented in force–elongation curves, where the vertical axis shows the applied force (in newtons) and the horizontal axis shows the specimen's elongation (in millimeters). These curves visually illustrate how the material responds under load, capturing the entire process—from elastic deformation to eventual failure.

- To analyze the material properties independently of specimen dimensions, the data was converted into **stress–strain curves**:
    - *Stress* (measured in MPa) is calculated by dividing the applied load by the specimen's initial cross-sectional area. This gives a normalized value that reflects how much force the material experiences per unit area.
    - *Strain* (dimensionless) is calculated as the ratio of the specimen's elongation to its initial gauge length. This expresses how much the material stretches relative to its original size.

The initial straight-line portion of the stress–strain curve represents the **elastic region**, where any deformation is fully reversible once the load is removed. The slope of this region corresponds to **Young's modulus**, which indicates the material's stiffness. The **maximum stress** reached before failure is reported as the **tensile strength**, and the **strain at break** indicates the material's ductility.

Figure 3.7: Tensile Testing Machine

Tensile Testing Parameters

- Crosshead speed: **2 mm/min**
- Data acquisition: The stress–strain data were recorded directly from the machine's output.

- Cross-sectional area: $A = 9.52\ \text{mm}^2$
- Ambient temperature: $T = 20\,^{\circ}\text{C}$
- Gauge length: $L = 22$ mm
- Thickness : e = 2.8 mm

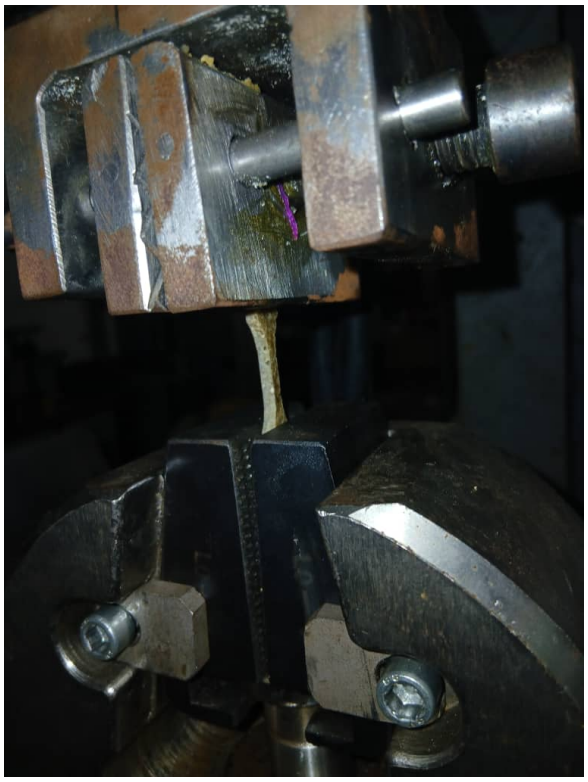

Figure 3.8: Tensile Test

3.2.4 Tensile Test Results :

The experimental results obtained from the mechanical characterization of the PLA–palm fiber composite are presented in the figures below. The measured properties were determined using standardized testing procedures. These results are essential for evaluating the structural performance of the composite material and will be used as input data in the wind turbine blade simulation conducted in QBlade. The tests provided stress–strain curves, from which Young's modulus was extracted.

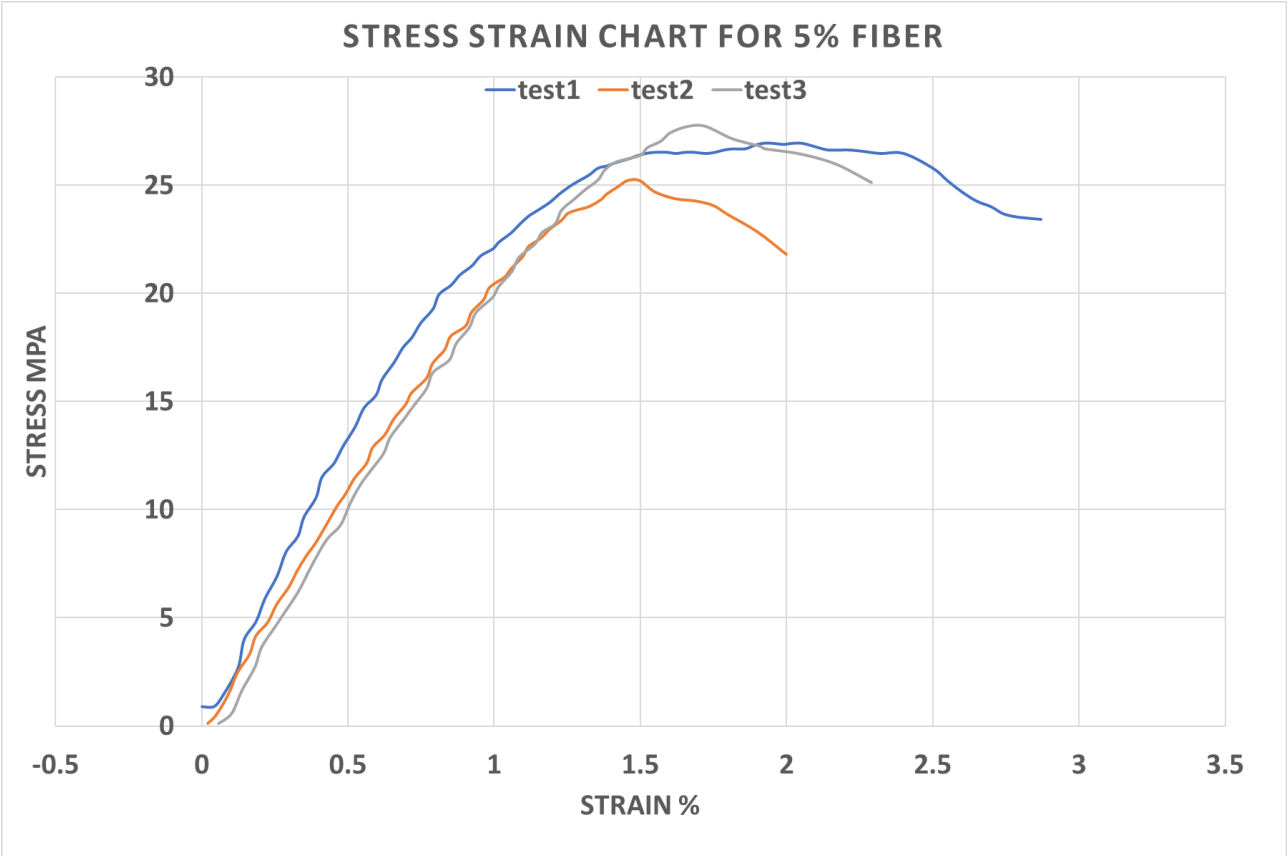

Figure 3.9: Stress-Strain Chart for 5% Fibers rate

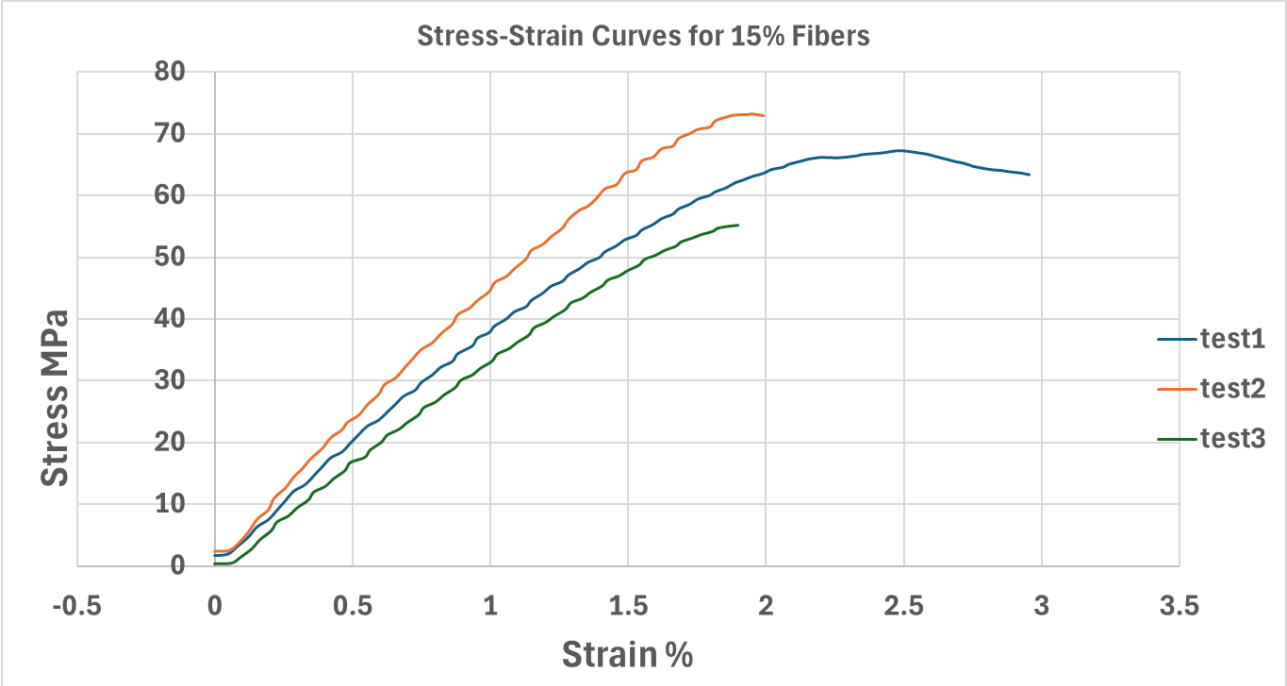

Figure 3.10: Stress-Strain Chart for 15% Fibers rate

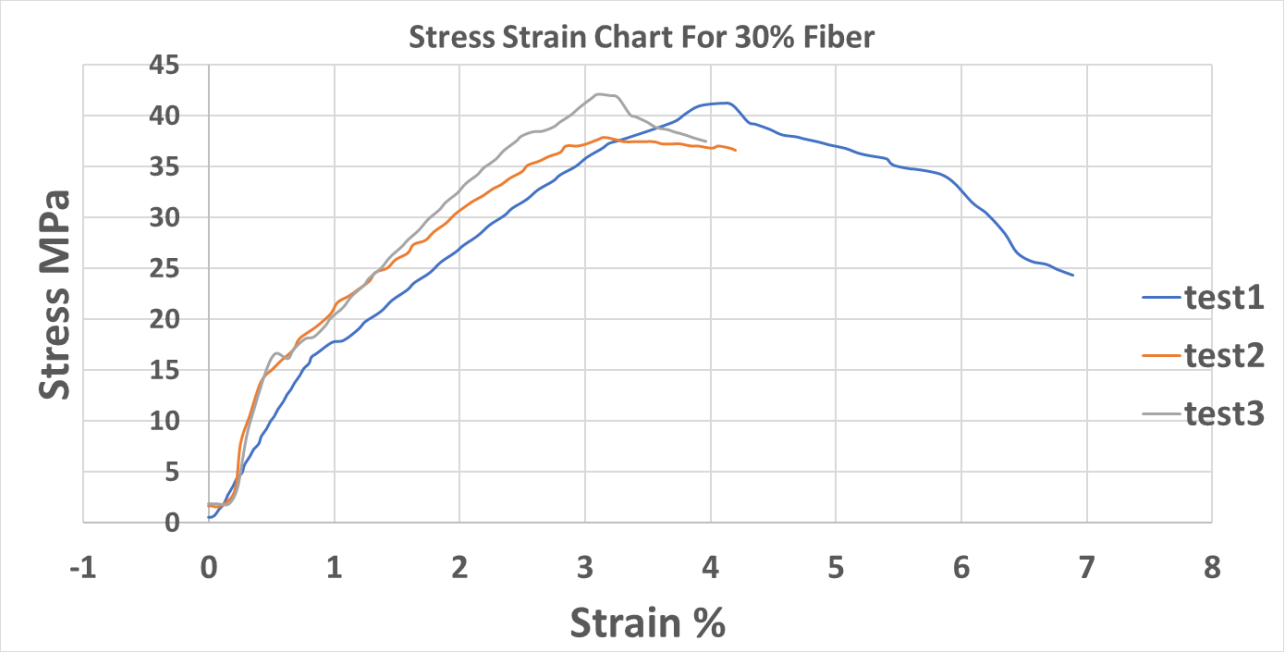

Figure 3.11: Stress-Strain Chart for 30% Fibers rate

Based on the stress–strain curves obtained from the tensile tests of PLA reinforced with different percentages of palm leaf fibers (5%, 15%, and 30%), the following observations and interpretations can be made: The mechanical evaluation of the PLA composites reinforced with palm leaf fibers provided valuable insight into the role of fiber content in determining structural behavior and load response. At a lower fiber content, such as 5%, the composite material exhibited a stable and predictable stress–strain response, with moderate tensile strength and noticeable elongation before failure. This behavior suggests that the fibers were well distributed within the PLA matrix, allowing for effective stress transfer and maintaining a good degree of flexibility. No signs of premature delamination or brittle fracture were observed, indicating that the interface bonding was sufficient for the applied loads and the processing conditions used.

When the fiber content was increased to 15%, the composite displayed a clear enhancement in mechanical performance. The material demonstrated a consistent elastic region under tensile loading and supported significantly higher stress levels. This outcome reflects a successful reinforcement effect, where the additional fibers contributed to the stiffness and load-bearing capacity of the composite. The structure remained coherent, with no evident internal defects or processing inconsistencies, pointing to effective fiber-matrix interaction and optimized dispersion during mixing and molding.

At higher reinforcement levels, such as 30%, the behavior shifted notably. Despite the increased fiber presence, the material began to exhibit reduced tensile capacity and early signs of structural failure. This can be attributed to the saturation of the PLA matrix, which may no longer adequately encapsulate and bind the excess fibers. Poor wetting, fiber agglomeration, or insufficient interfacial adhesion could result in stress concentrations that initiate early cracking or pull-out under load. Furthermore, over-reinforcement may compromise the homogeneity of the mix, leading to local weaknesses and irregular mechanical responses.

Extracted Data

Young's modulus (E) was calculated from the linear elastic portion of the stress–strain curve obtained during tensile testing. This modulus corresponds to the slope of the initial straight segment of the curve, where the material undergoes elastic deformation. For each specimen, stress (σ) was found by dividing the applied force by the cross-sectional area, and strain (ε) was determined as the elongation divided by the original gauge length. Young's modulus was then computed using the formula:

$$E = \frac{\Delta\sigma}{\Delta\varepsilon}$$

The slope was determined by performing a linear regression on the most linear section of the curve.

According to standard testing norm ASTM 638, the elastic modulus (E) was determined from the linear portion of the stress–strain curve, specifically between 0.05 and 0.25 strain. This range ensures consistency across materials and accurately reflects their elastic behavior. This method ensures accurate estimation while avoiding the influence of noise or early nonlinear effects. The final reported value of E for each material is the average of three individual tests, with standard deviation used to assess measurement consistency.

The average elastic modulus, the standard deviation, and the coefficient of variation (CV) for each material were calculated. The standard deviation shows how much the values vary from the average, while CV, shows how large this variation is compared to the average. These values help us compare the mechanical behavior of the different composites.

Table 3.2: Results of the tensile tests for different fiber contents

Material	**Sample**	**E (GPa)**	**Max Stress (MPa)**	**Max Strain (%)**
5% Fibers Rate	1	1.36	26.94	1.46
	2	1.49	27.73	1.54
	3	1.25	24.94	1.68
	Mean	1.37	26.40	1.54
	Std. Dev.	0.12	1.42	0.11
	CV	0.0588	0.0519	0.0536
15% Fibers Rate	1	2.91	67.27	2.48
	2	3.65	73.10	1.92
	3	3.17	54.72	1.82
	Mean	3.24	64.77	2.03
	Std. Dev.	0.38	9.61	0.28
	CV	0.1169	0.1299	0.1516
30% Fibers Rate	1	1.053	41.17	4.09
	2	1.01	37.80	3.15
	3	1.18	42.12	3.10
	Mean	1.08	37.84	3.085
	Std. Dev.	0.09	2.39	0.54
	CV	0.0815	0.0586	0.1419

Comparison Charts between the fibers rate

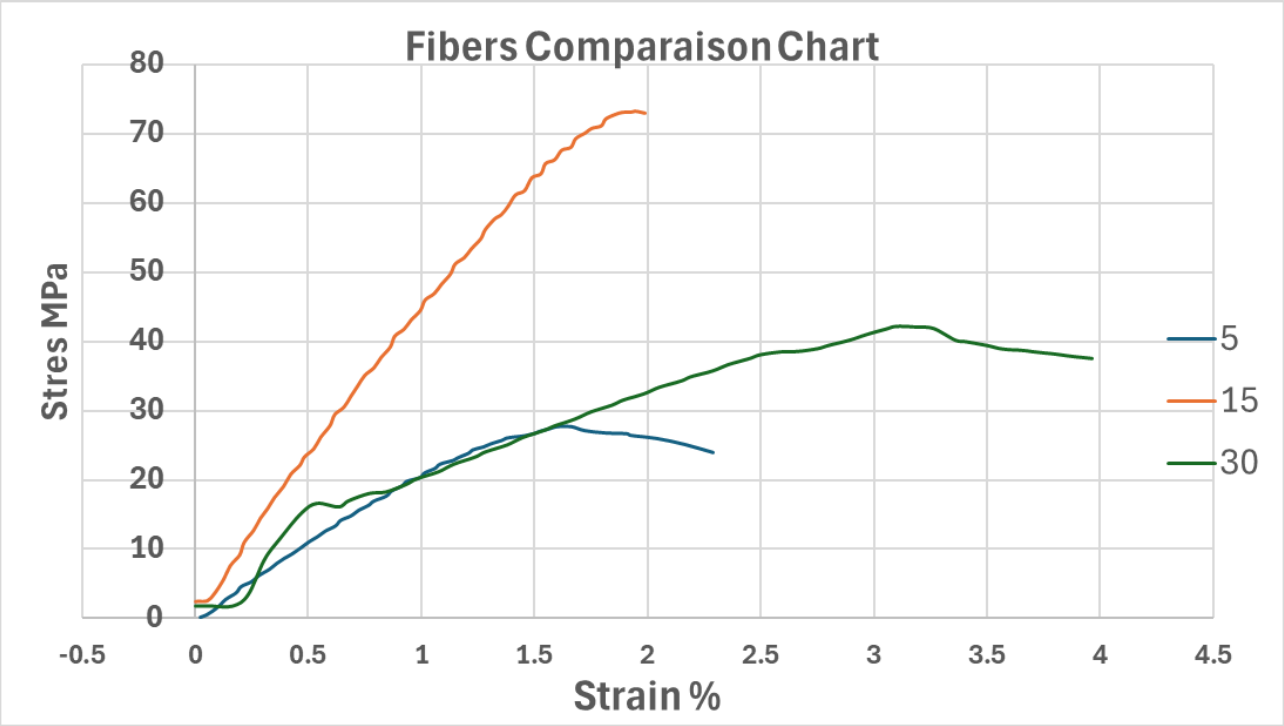

Figure 3.12: Stress-Strain Comparison Between Fibers Rate

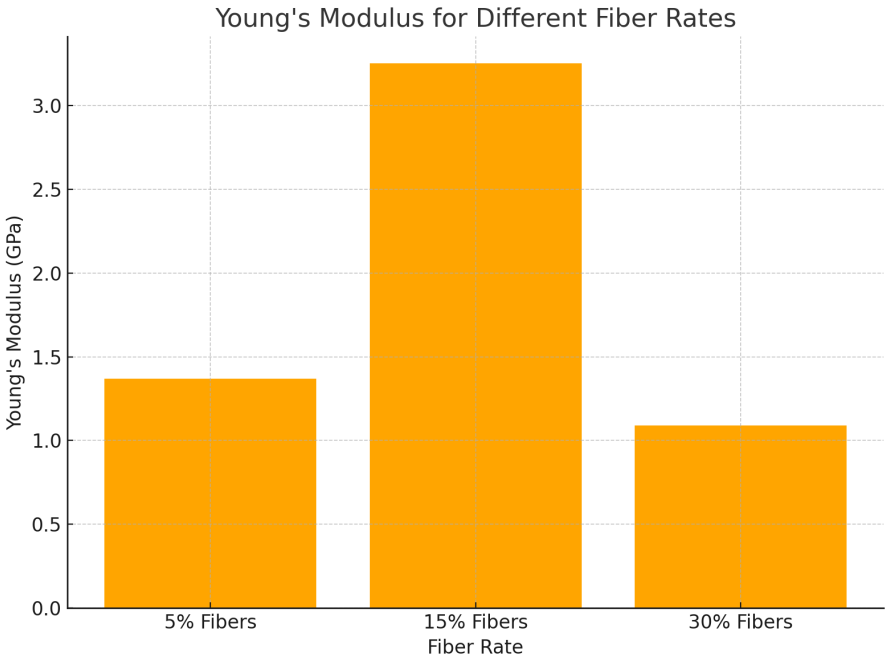

Figure 3.13: Young Modulus Comparison Histogram

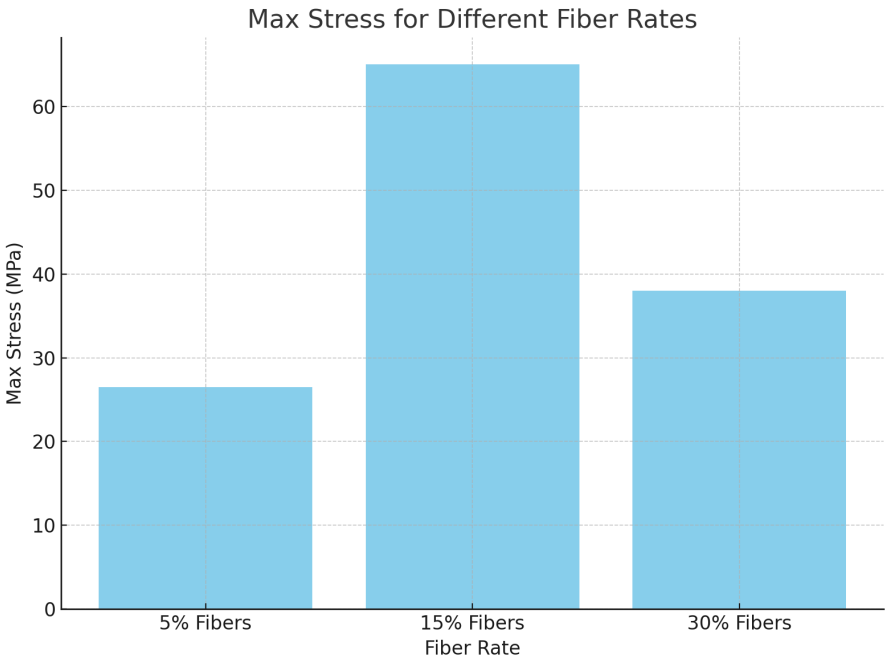

Figure 3.14: Maximum Stress Comparison Histogram

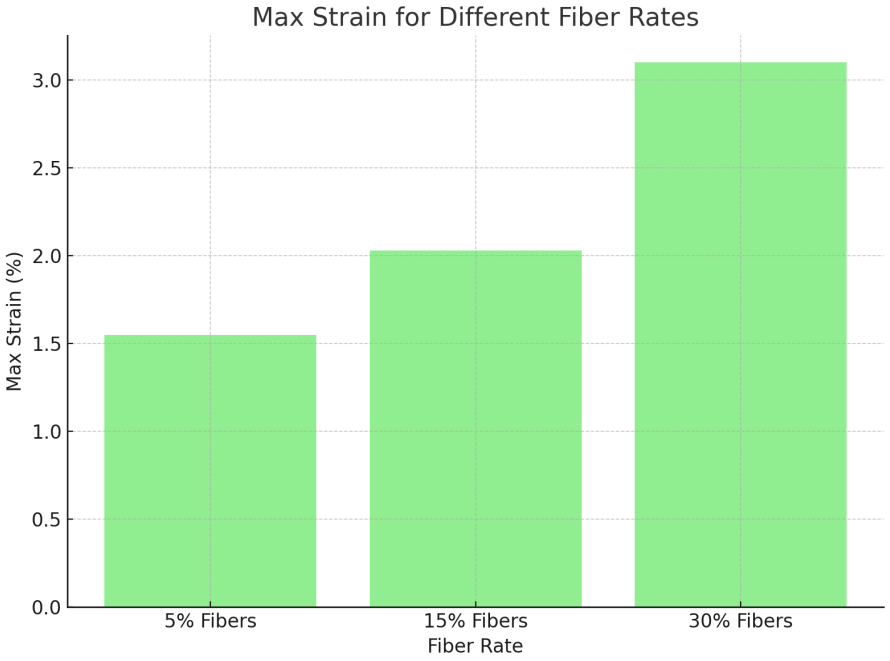

Figure 3.15: Maximum Strain Comparison Histogram

The tensile test results demonstrate the influence of fiber content on the mechanical performance of PLA-based composites, particularly in terms of stiffness (Young's modulus), strength, and ductility.

At a 5% fiber content, the composite showed only limited reinforcement. The average Young's modulus was relatively low—around 1.37 GPa—indicating only a small increase in stiffness. The maximum tensile stress reached 26.4 MPa, reflecting moderate strength. With a strain at break of 1.57%, the material retained decent ductility but still had limited stiffness. Overall, this fiber content offered modest improvement compared to pure PLA but did not provide a significant mechanical advantage.

In contrast, the composite with 15% fiber content showed the best mechanical performance among all the tested formulations. It achieved a high Young's modulus of 3.24 GPa and a maximum tensile stress of 64.77 MPa, demonstrating significant improvements in both stiffness and strength. The strain at break was 2.03%, indicating the material maintained good ductility. These results suggest effective stress transfer and strong interfacial bonding between the palm fibers and the PLA matrix.

At the 30% fiber content, a decline in mechanical properties was observed. The Young's modulus decreased to 1.08 GPa, and the maximum tensile stress dropped to 37.84 MPa. However, the strain at break increased to 3.08%, showing greater ductility. This reduction in stiffness and strength is likely caused by fiber clumping, poor dispersion, and inadequate fiber wetting at higher concentrations, all of which can reduce the efficiency of load transfer.

The stress–strain analysis of the PLA composites reinforced with varying fiber contents reveals distinct mechanical behaviors depending on the reinforcement level. At 15% fiber content, the composite exhibits the highest stiffness and peak tensile strength, suggesting optimal load transfer between the fibers and the PLA matrix. This indicates a well-balanced composition with strong interfacial bonding, allowing it to withstand greater mechanical stress and perform reliably under load. In contrast, the 5% fiber content results in moderate performance, with lower strength values but improved ductility, suggesting that the matrix still dominates the mechanical response. Meanwhile, the composite containing 30% fibers shows a noticeable decline in performance, characterized by a more brittle response and lower tensile strength. This is likely due to poor fiber dispersion, clumping, or insufficient matrix coverage, which compromise structural integrity. Overall, the results highlight the existence of an optimal fiber content—around 15%—where mechanical performance peaks before deteriorating due to processing and structural limitations.

3.2.5 Comparison with Pla/Other Natural Fibers

Fibers such as kenaf, flax, bamboo, and sisal have been widely studied for their ability to improve the mechanical performance of PLA-based composites. This section compares the Young's modulus and the maximum tensile stress of PLA reinforced with palm leaf fibers against those reinforced with other natural fibers. The goal is to assess how much palm leaf fibers contribute to the overall stiffness and strength of the composite compared to other, more commonly used natural reinforcements.

Table 3.3: Mechanical Properties of Pure PLA and PLA Reinforced with Natural Fibers

Material	**Fiber Content**	**Young's Modulus (GPa)**	**Max Stress (MPa)**	**Source**
Pure PLA (Neat)	–	3.0	53	Oksman *et al.* [33]
PLA + Kenaf fibers	15%	3.2	62	Graupner *et al.* [34]
PLA + Flax fibers	20%	6	66	Denis [35]
PLA + Bamboo fibers	5%	4.5	50	Tokoro *et al.* [36]
PLA + Sisal fibers	5%	3.4	75	Samouh [37]
PLA + Palm Fibers	15%	3.2	65	Present Work

The mechanical performance of PLA reinforced with palm leaf fibers was compared to that of PLA composites made with other well known natural fibers such as kenaf, flax, bamboo, and sisal. The comparison focused on two key indicators: Young's modulus, which measures

the stiffness of the material, and maximum tensile stress, which shows how much stress the material can handle before breaking.

When it came to stiffness, the palm fiber composite reached a Young's modulus of about 3.1 GPa, which is very close to that of pure PLA (3.0 GPa). This suggests that while palm fibers do not significantly increase the stiffness, they manage to maintain it offering reinforcement without compromising the material's rigidity. When compared to other reinforced PLA composites, this value is slightly lower than those of flax (3.8 GPa), bamboo (4.5 GPa), and sisal (3.4 GPa), and nearly equivalent to that of kenaf (3.2 GPa). However, it is important to emphasize that the palm fiber composite achieved this stiffness at a very low fiber content of only 5 wt%, whereas the other natural fiber composites typically involved fiber contents ranging from 30 to 40 wt%. The relatively modest increase in stiffness observed is consistent with the low fiber loading used in this study and points to opportunities for further optimization. By increasing the fiber content, aligning the fibers, or enhancing the treatment process, it may be possible to significantly improve stiffness without sacrificing other important properties.

When looking at maximum tensile stress, the composite reinforced with palm leaf fibers showed an average strength of about **64.78 MPa** a clear improvement over neat PLA, which typically reaches around **53 MPa**. This result is also stronger than PLA composites reinforced with kenaf (**62 MPa**), flax (**55 MPa**), and bamboo (**50 MPa**). Only the sisal fiber composite performed better, with a tensile strength of **75 MPa**, but it's important to note that this was achieved using a much higher fiber loading (**30 wt%**) compared to just **5 wt%** in the palm fiber system. This is a key finding, as it shows that palm leaf fibers can significantly strengthen the PLA matrix even at low concentrations.

Several factors likely contribute to this strong performance. First, the chemical treatment of the palm fibers seems to have improved adhesion with the PLA matrix, leading to more efficient stress transfer. Second, the palm fibers themselves may have favorable mechanical properties like good tensile strength and aspect ratio that help resist deformation under load. Finally, the hydraulic pressing process used during fabrication likely promoted good fiber dispersion, reducing weak points and stress concentrations in the composite.

Taken together, these findings suggest that palm leaf fibers are a promising natural reinforcement for PLA composites. While their stiffness may still fall short of that offered by bamboo or flax, the tensile strength is already quite competitive especially given the low fiber content used. This opens the door to further research into optimizing fiber loading, alignment, and treatment techniques to boost both stiffness and strength.

From a sustainability standpoint, using palm leaf waste a readily available and often underutilized agricultural byproduct offers both environmental and economic benefits. Its strong performance under tensile stress makes it a viable, eco-friendly option for applications that demand strength without compromising biodegradability, aligning well with circular economy principles.

3.2.6 Shear Modulus Calculation

The shear modulus G, also known as the modulus of rigidity, describes a material's response to shear stress. It is a fundamental mechanical property that complements Young's modulus in fully characterizing elastic behavior. In the absence of direct shear testing, G can be estimated using the following relationship:

$$G = \frac{E}{2(1+\nu)}$$

where:

- G is the shear modulus (in GPa),
- E is Young's modulus (in GPa),
- ν is Poisson's ratio.

In this work, the Poisson's ratio was taken to be **0.35**, a value taken from literature on PLA reinforced with natural fibers. This approximation is commonly used for similar biocomposites and offers a reasonable basis for estimating shear behavior. Using this formula, the shear modulus was computed for the most optimal fiber rate 15% using the previously obtained values of Young's modulus from tensile testing.[38][39]

For our work we picked the mean Young modulus for the 15% to calculate Shear's modulus

Given:

- Young's modulus $E = 3.2\,\text{GPa}$
- Poisson's ratio $\nu = 0.35$

Substituting into the formula:

$$G = \frac{3.2}{2(1+0.35)} = \frac{3.2}{2 \times 1.35} = \frac{3.2}{2.7} = 1.18\,\text{GPa}$$

Therefore, the shear modulus is **1.18 GPa**.

The calculated shear modulus of 1.18 GPa indicates that the PLA composite reinforced with palm leaf fibers has a moderate resistance to shear deformation. This value aligns well with expected ranges for natural fiber-reinforced PLA, confirming that the material has gained additional rigidity compared to pure PLA. The result also suggests good internal cohesion and fiber–matrix bonding, making the composite suitable for applications where moderate shear loads may be encountered.

Table 3.4: Summary of Maximum Mechanical Properties for Different Fiber Contents

Material	Max Stress (MPa)	Young's Modulus (GPa)	Max Strain (%)	Shear Modulus G (GPa)
5% Fibers Rate	27.73	1.494	1.682	0.5533
15% Fibers Rate	73.109	3.6	2.483	1.18
30% Fibers Rate	42.1218	1.188	4.09	0.44

At a 5% fiber rate, the shear modulus was calculated to be approximately 0.5533 GPa, which corresponds to the low Young's modulus observed at this concentration. The results suggest that at low fiber content, the reinforcement effect is minimal—offering only a slight

improvement in internal rigidity and resistance to shear. This confirms that at this loading level, the mechanical enhancement remains relatively weak.

In contrast, the composite with **15% fiber content** showed a **much higher shear modulus of 1.18 GPa**, the highest among all tested samples. This notable increase reflects better stiffness and strong bonding between the PLA matrix and the palm leaf fibers. The improved shear resistance at this concentration suggests more efficient load transfer when the material is subjected to shear stress, which aligns well with the excellent tensile performance previously observed for this same composition.

However, when the fiber content was increased to **30%**, the shear modulus dropped significantly to **0.44 GPa**—despite the higher amount of reinforcement. This decrease is likely due to fiber agglomeration and poor dispersion at high loading levels, which reduce the material's stiffness and disrupt effective matrix–fiber bonding. These defects weaken the composite's ability to resist shear forces and ultimately reduce its structural integrity under more complex loading conditions.

Altogether, the variation in shear modulus across the different fiber loadings reinforces the conclusion that **15% fiber content** offers the best balance. At this level, the composite benefits from improved tensile strength, stiffness, and shear resistance without the drawbacks introduced by excessive fiber concentration rigidity.

3.3 Filament Extrusion

After Finishing the mechanical characterization of our composite material , we passed to the next step of tyring the extrusion of our PLA–palm fiber composite filament, first we cut the plates developed in the previous chapter into small composite pellets of maximum 3mm diameter which is the best for the single screw extruder, but unfortunately we encountered a recurring mechanical issue that significantly hindered the process. The extruder was unable to generate sufficient torque to ensure a continuous material flow, leading to frequent stoppages and inconsistent output. In an effort to resolve this, we replaced the original gear reducer with a more robust one and designed a custom coupling shaft to connect it securely to the extruder. To maintain proper alignment and structural stability, we also reinforced the machine's frame by welding square steel tubes, creating a solid support for the new configuration.

Despite all our efforts—mechanical adjustments, structural reinforcements, and countless fine-tunings—the problem persisted. The extrusion process remained unpredictable, and the filament continued to break almost immediately after exiting the nozzle. After several failed attempts and careful consideration, we had to face the reality: producing reliable filament with our composite material wasn't achievable at this stage. Rather than letting this setback halt our progress, we shifted our focus to the next step of the study. Using the mechanical characterization results we had obtained, we proceeded to simulate the behavior of a wind turbine blade made from our composite. This allowed us to explore the material's potential and evaluate whether, if extrusion challenges are overcome in the future, the composite could still be a viable and effective option.

Figure 3.16: Pla/Palm Leaf Composite Pellets

Figure 3.17: Failed Composite Filament Extrusion

3.3.1 Causes of Extrusion Failure and Recommendations for Future Work

The extrusion difficulties encountered during this project highlighted several critical challenges associated with processing natural fiber-reinforced PLA composites. Despite mechanical modifications to the extrusion system—including upgrading the gear reducer and stabilizing the

structure—the process remained unstable and ultimately unsuccessful. Several potential factors may explain this outcome.

Firstly, the PLA grade (4043D) used in this work may not have been fully compatible with palm fibers in terms of melt viscosity and bonding behavior. This incompatibility can result in poor dispersion, inconsistent flow, and uneven filament formation. It is also possible that this PLA grade was not ideally suited to the extruder design itself. Additionally, a potential mechanical dysfunction in the extruder—such as irregular torque delivery or inconsistent heating—could have contributed to the failure . Furthermore, the extrusion system may not have been optimized for filled or abrasive materials, such as fiber-reinforced polymers, which typically require specific screw profiles and higher pressure tolerances.

Another major constraint was the limited quantity of PLA pellets available for testing. Since there are currently no domestic suppliers of PLA in Algeria, sourcing the material involved importation, which limited both availability and the opportunity to experiment with different grades. This lack of access made it difficult to carry out a full parameter optimization study or to trial alternative .

Recommendations for Future Work

To overcome the limitations encountered during this project and to enable successful extrusion of PLA–natural fiber composite filaments in future studies, several improvements and directions are recommended:

- **Select Alternative PLA Grades:** Experiment with PLA grades that offer better thermal stability, higher melt flow index, or known compatibility with fiber reinforcements. Grades designed specifically for compounding or filament extrusion (such as high-viscosity or impact-modified PLA) may yield better results.
- **Use Compatibilizers and Plasticizers:** Incorporate additives such as maleic anhydride (MA-g-PLA), polyethylene glycol (PEG), or citrate-based plasticizers to enhance dispersion and reduce melt viscosity. These can significantly improve the flow behavior and homogeneity of the composite. [40]
- **Pre-compounding Step:** Adopt a two-step process by using a *twin-screw extruder* to pre-mix and compound the PLA–fiber material before filament extrusion. This allows for better fiber distribution and melt consistency.
- **Upgrade Extrusion Equipment:** Use an extruder with higher torque capacity, enhanced heating control, and screw geometries designed for filled or abrasive materials. Ideally, dedicated equipment for biocomposites should be used.
- **Optimize Process Parameters:** Conduct a systematic study of extrusion parameters including screw speed, barrel temperature profile, die diameter, and cooling method. This helps identify the processing window that ensures stable filament formation.
- **Secure Material Supply:** Establish collaboration with international PLA suppliers or local importers to ensure access to sufficient quantities of PLA resin. Exploring multiple sources will also allow testing of various grades and formulations.

By implementing these recommendations, future researchers and engineers can better address the challenges of biocomposite filament extrusion and contribute to the development of accessible, eco-friendly materials for additive manufacturing and mechanical applications.

3.4 Conclusion

This chapter has presented a comprehensive evaluation of the mechanical behavior of the PLA–palm fiber composite developed in the previous stage of the study. Through standardized testing procedures, key properties such as tensile strength, stiffness, and shear modulus were determined, offering critical insights into the internal structure and performance potential of the material. These mechanical parameters not only reflect the success of the fiber reinforcement and processing strategy, but also serve as the basis for assessing the composite's ability to perform under realistic mechanical loads.

Despite these promising results, the extrusion process—originally intended to transform the composite into filament suitable for 3D printing—did not yield the expected outcome. The filament consistently failed at the nozzle exit, likely due to a combination of material incompatibility, fiber dispersion issues, and limitations of the extrusion equipment. While this outcome was a setback in terms of exploring additive manufacturing capabilities, it does not diminish the importance or usability of the mechanical characterization data obtained.

On the contrary, these results provide a solid foundation for further analysis. One of the core strengths of engineering research lies in adaptability: when physical prototyping reaches its limits, simulation becomes a powerful alternative. In this context, the validated mechanical properties of the composite can still be effectively used in numerical simulations to assess the behavior of wind turbine blades manufactured from this material. Using software such as QBlade, we are able to evaluate both structural deformation and aerodynamic performance under operational conditions.

Therefore, even though the filament extrusion trials were inconclusive, the chapter successfully fulfills its goal of characterizing the material's mechanical profile and opens a new path forward through digital validation. This transition from experimental data to computational modeling ensures that the material's potential is thoroughly assessed and that the project continues to move toward its central objective: evaluating the technical feasibility of using PLA–palm fiber composites in sustainable small-scale wind energy systems.

Chapter 4

Wind Turbine Simulation

4.1 Introduction

Simulation plays a vital role in modern engineering, allowing designers and researchers to model complex systems, predict behavior, and optimize performance before physical prototypes are built. In the context of wind energy, simulations help evaluate aerodynamic efficiency, structural integrity, and overall turbine performance under various operating conditions. Among the tools available, QBlade stands out as a powerful open-source software specifically developed for the design and simulation of wind turbines. It integrates both aerodynamic and aeroelastic analysis using advanced methods such as Blade Element Momentum (BEM) theory and dynamic structural modeling. QBlade enables users to perform detailed simulations of airfoil behavior, blade loading, rotor performance, and structural deflection with high accuracy. By combining user-friendly visualization tools and robust numerical solvers, QBlade offers an efficient and cost-effective solution for optimizing wind turbine designs especially crucial in the development of small-scale, sustainable, and high-performance systems like those using bio-composite materials.

4.2 Theory Guide of QBlade and Its Simulation Methods

4.2.1 Introduction to QBlade

QBlade is an open-source software tool developed at the Technical University of Berlin for the design and simulation of wind turbine blades. It offers a powerful suite for airfoil design, rotor blade definition, and aerodynamic performance analysis under various flow conditions. QBlade is particularly useful for horizontal-axis wind turbine (HAWT) simulations and supports multiple aerodynamic modeling methods.

Two primary methods are integrated in QBlade:

- **Blade Element Momentum (BEM)** theory – a steady, axisymmetric method suitable for fast and accurate performance prediction under uniform flow conditions.
- **Lifting-Line Free Vortex Wake (LLFVW)** method – an advanced unsteady 3D aerodynamic model that accounts for wake dynamics, yawed flow, and radial flow effects.

In this chapter, both methods will be presented, followed by their application to a small wind turbine using the SG6041 airfoil.

4.2.2 Aerodynamic Simulation in QBlade

At the core of QBlade's aerodynamic analysis is the Blade Element Momentum (BEM) theory and its enhanced variations. Additionally, QBlade offers advanced lifting-line vortex wake models to better capture unsteady and three-dimensional aerodynamic effects.

4.2.2.1 Blade Element Momentum Theory (BEM)

In QBlade the aerodynamic forces acting on a rotor can be modeled either using a steady Blade Element Momentum (BEM) or a with a more advanced, time resolved unsteady BEM (UBEM) which is enhanced by several correctional models. The theory interlinks the actuator disc theory and the blade element theory and it was first introduced by Glauert. Despite its simplicity, the BEM method allows for an accurate representation of the steady aerodynamic loads that act on the rotor of a wind turbine, provided certain model assumptions are not violated.[18]

This method accounts for:

- Tip and root losses using Prandtl's correction.
- Unsteady aerodynamic phenomena such as dynamic stall via semi-empirical models (e.g., Beddoes-Leishman).
- Empirical correction factors for skewed inflow and yawed wind conditions.

4.2.2.2 Momentum Theory

Under the assumptions of a steady, incompressible and axisymmetric inflow of an inviscid fluid the actuator disc theory may be applied. The rotor plane is treated as an actuator disk that causes a uniform pressure drop over the rotor area while the flow velocity varies continuously through the disk. In its simplest form, the actuator disc theory assumes that the velocity through the rotor plane does not contain a tangential component and the pressures far up- and downstream of the rotor are equal to the ambient pressure. These assumptions allow for the calculation of the rotor performance (power and thrust) and the velocity in the rotor plane by invoking the conservation of mass and momentum (see Branlard [41]. The introduction of the induction factor a allows for the expression of the velocity in the rotor plane as function of the incoming velocity u_0:

$$u = (1 - a)u_\infty. \tag{4.1}$$

The rotor performance coefficients for power and thrust may also be expressed as a function of the axial induction factor a:

$$C_T = 4a(1 - a), \tag{4.2}$$
$$C_P = 4a(1 - a)^2. \tag{4.3}$$

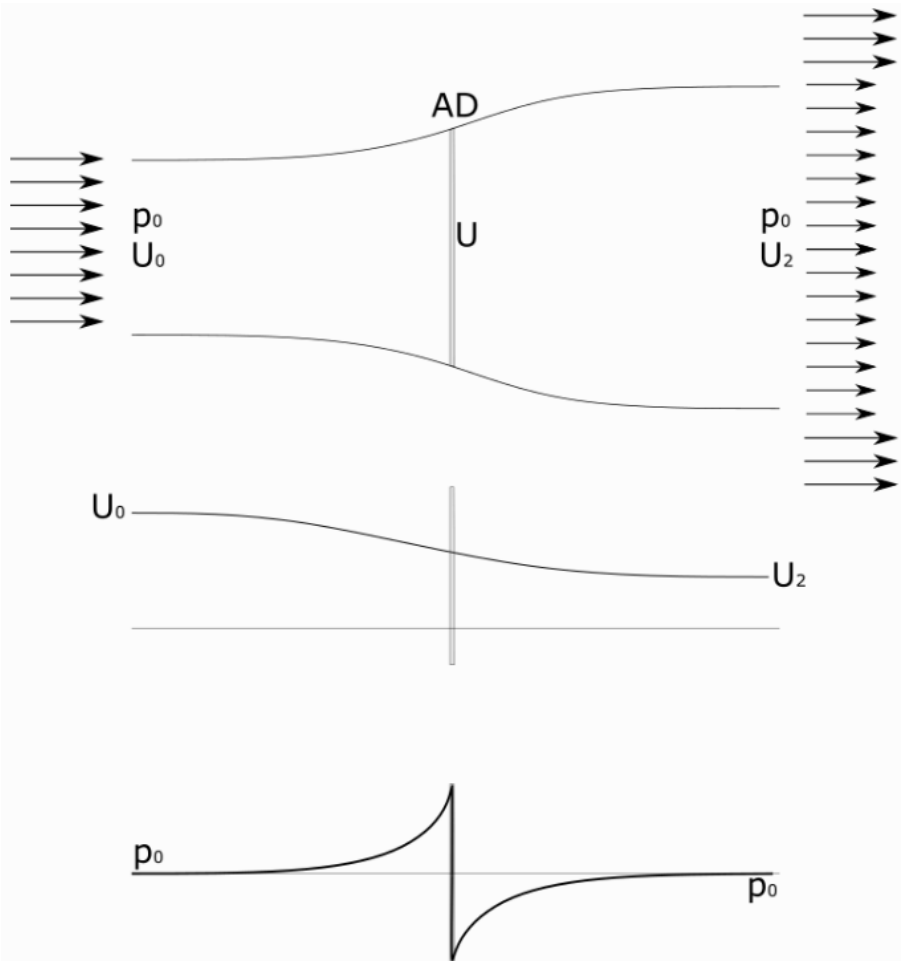

Figure 4.1: 1D momentum theory, pressure and velocity evolution[18]

4.2.2.3 Blade Element Theory

The blade element theory allows for the computation of the loads acting on a rotor based on the geometric and aerodynamic properties of individual spanwise blade sections. The blade is divided into a discrete number of radially distributed sections. The loads on each section are calculated under the assumption that the flow there is locally two-dimensional and in the plane of the airfoil section. This allows for the use of two-dimensional lift, drag and moment coefficients together with the relative flow velocity to determine sectional airfoil forces. [18]

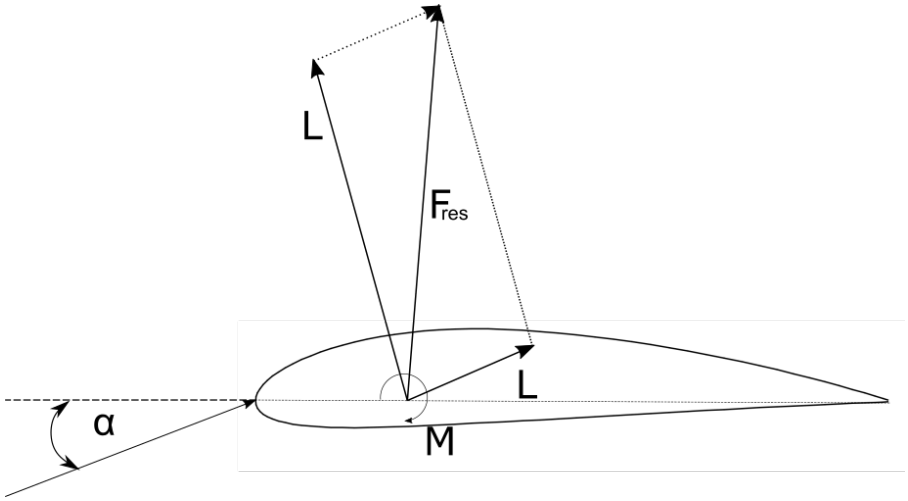

Figure 4.2: 2D forces on an airfoil [18]

4.2.2.4 Classic Blade Element Momemntum Theory

The blade element momentum theory combines the 1D actuator disc theory with the blade element theory. For practical reasons, the stream tube theory is applied to radial annuli that match the discretization of the blade elements. Both theories allow for the expression of the blade forces within an annular segment as a function of streamtube geometric properties and the axial and tangential induction factors a and a', respectively. A solution method is applied which iteratively finds the values of a and a' which satisfy both theories.[18]

4.2.2.5 Corrections

Due to the two dimensional nature of the BEM theory, three dimensional effects are not accounted for by the classical BEM. This leads to large deviations of flow quantities compared with measured turbine data, particularly in regions where strong changes in the blade circulation occur. To improve the accuracy of the BEM results, two correction methods are implemented into QBlade:

- Prandtl Tip Loss Factor (see Glauert[42])
- 3D Correction (see H. Snel, R. Houwink, W. J. Piers[43])

4.2.2.6 Polar Grid

The polar-grid has been developed by (Madsen et al.[44]) to consider azimuthal variations of the axial induction caused by the azimuthal dependence of blade loadings. Within the approach, the annular rings of the actuator disc theory are divided into stationary azimuthal sections. Each point on the azimuthal grid is associated with a local induction factor, based on the local instantaneous velocity. The latter is approximated by the induced velocity of the neighboring two blades and weighted by their azimuthal distance (Behrens de Luna et al.[45]).

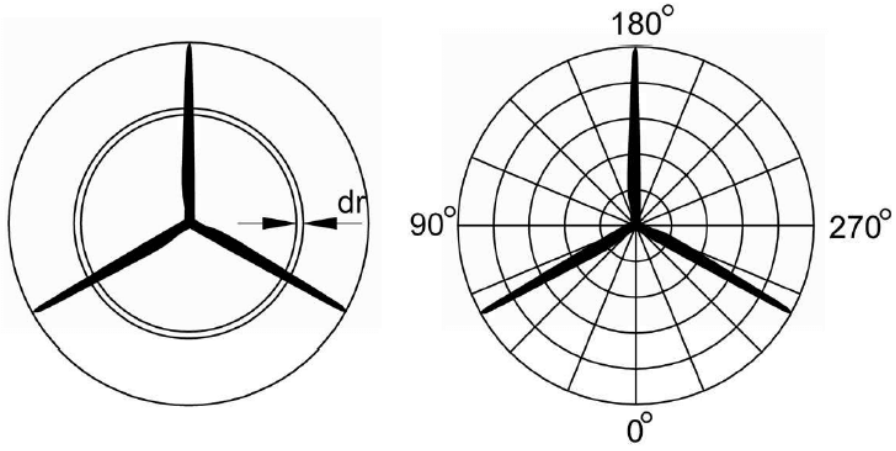

Figure 4.3: Classical BEM approach (left) and polar grid with azimuthal sub elements (right) [18]

4.2.2.7 Lifting Line Free Vortex Wake Method (LLFVW)

In QBlade the aerodynamic forces acting on a rotor can be modeled using the Lifting Line Free Vortex Wake method (LLFVW). Similar to the Blade Element Momentum Method, in the LLFVW model the blade forces are calculated using two dimensional sectional airfoil polar data. The main difference is that the rotor wake, shed from the blades, is explicitly resolved. This is a large improvement over the commonly used Blade Element Momentum Method style approaches, which necessitate the introduction of a large number of empirical corrections into the simulated system. Modeling the wake dynamics explicitly avoids the dependency on such correction models and often leads to more physically sound results. Simulation results are improved especially in cases where the assumptions of the Blade Element Momentum Method are violated. These include unsteady operation, large blade deformations and high tip speed ratios where the turbulent wake state is approached. Such conditions become more and more prevalent with the ongoing trend towards larger rotor sizes and offshore floating wind turbines.[18]

4.2.2.8 Overview of LLFVW Theory

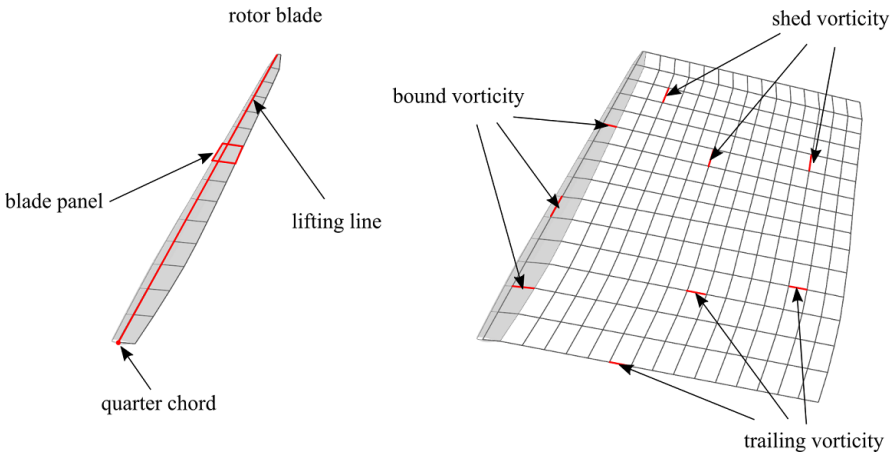

Figure 4.4: Basic elements of the blade and wake model inside the LLFVW algorithm.[18]

The rotor is represented by a lifting line, located at the quarter chord position of the 2D airfoil sections. Each blade panel is represented by a vortex ring which consists of four straight vortex filaments. The circulation of the bound vortex lines, forming the lifting line, is calculated from the relative inflow velocity and the lift and drag coefficients that are obtained from tabulated airfoil data. The sectional circulation $\partial\Gamma$ is calculated according to the Kutta–Joukowski theorem:

$$\partial\vec{F}_L(\alpha) = \rho\vec{V}_{rel} \times \partial\vec{\Gamma}, \tag{4.4}$$

where $\partial\vec{F}_L$ is the sectional lift force and ρ is the fluid density. The relative velocity $\vec{V}_{rel}$ is obtained from a simple vector addition of the free stream velocity $\vec{V}_\infty$, the blade motion $\vec{V}_{mot}$ and the induced velocity $\vec{V}_{ind}$, which is calculated from the contribution of all vortex elements on the blade and in the wake through the Biot–Savart equation:

$$\vec{V}_{ind} = -\frac{1}{4\pi}\int \frac{\vec{\Gamma} \times d\vec{l}}{r^3}. \tag{4.5}$$

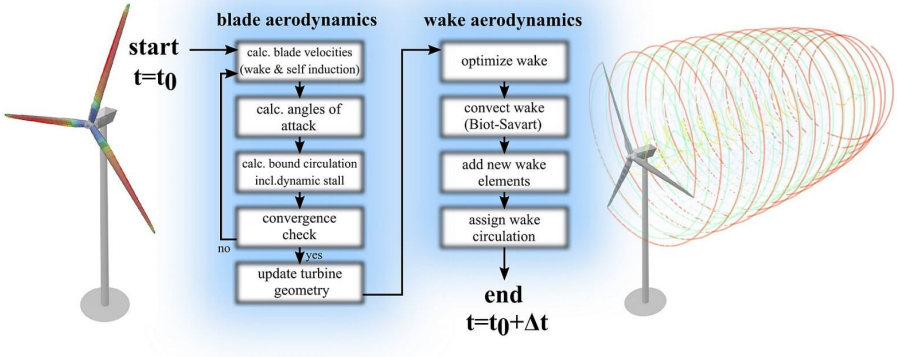

Figure 4.5: Flowchart for a single timestep of the aerodynamic calculations in QBlade[18]

At the beginning of each time step, the circulation distribution along the blade is calculated. This is carried out with an iterative procedure which ensures that the forces predicted by the Kutta–Joukowski theorem and the blade element theorem coincide. During the iteration only the bound vorticity distribution is updated, while the induction of the wake elements on the blade is only evaluated once. After convergence is obtained, the rotor rotation is advanced for a single time step. All free wake vortex elements are convected with the local inflow and local induced velocity. After the wake convection step, new vortex elements are created between the trailing edge of each blade panel and the last row of wake vortices that were convected away from the trailing edge. As a last step, the circulation is computed and assigned to the new released vortex lines through the Kutta condition:

$$\Gamma_{\text{trail}} = \frac{\partial \Gamma_{\text{bound}}}{\partial x} \Delta x \tag{4.6}$$

$$\Gamma_{\text{shed}} = \frac{\partial \Gamma_{\text{bound}}}{\partial t} \Delta t \tag{4.7}$$

4.2.2.9 Wake Lattice and Connectivity

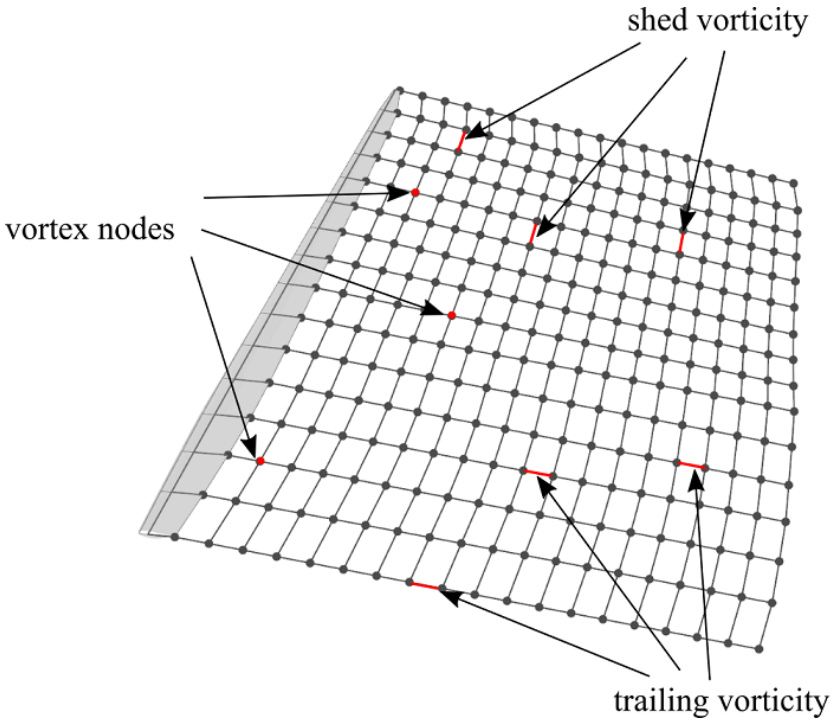

Figure 4.6: Visualization of the wake lattice structure with wake nodes and filaments

This figure above shows the wake lattice structure. Shed- and trailing vortices are interconnected via common vortex nodes. During the free wake convection step the evolution of the wake is evaluated by advancing the positions of the vortex nodes in time. Each newly created vortex node is attached to at least one shed and one trailing vortex filament, thus the total number of vortex nodes is approximately half the number of vortex filaments. Consequently, the Biot-Savart equation has to be evaluated around:

$$N_{\text{nodes}} \cdot N_{\text{vortices}} \approx \frac{N_{\text{vortices}}^2}{2} \tag{4.8}$$

times for a fully populated (assuming that no vortex elements have been removed) infinite wake lattice. Compared to a vortex particle discretization, where no inter-connectivity exists, this means a reduction in computational cost by a factor of 2, due to the inter-connectivity of the wake lattice. To facilitate strategies that reduce the number of free vortices within the wake, a method to remove individual vortices from the wake mesh has been implemented whereby vortex filaments are detached from their corresponding nodes. A check is performed during every step of the simulation that removes isolated vortex nodes which are not attached to any vortex filament. The more vortices have been removed from the wake lattice, the lower the afore mentioned leverage of the interconnections.

4.2.2.10 Vortex Core Desingularization

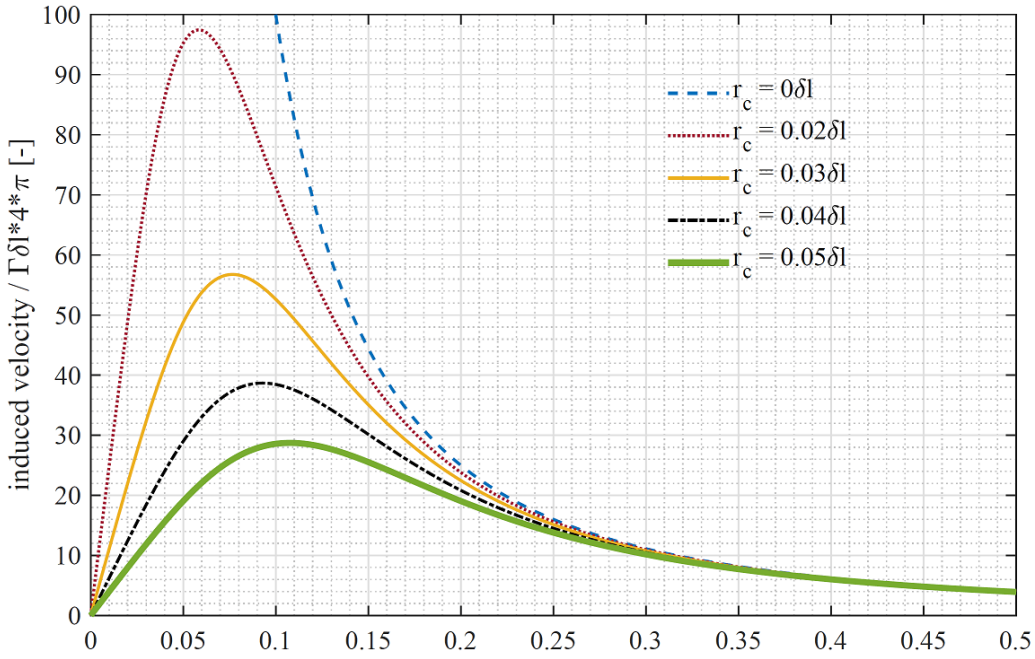

Figure 4.7: Velocity distribution around the vortex core[18]

The Biot–Savart equation exhibits a singularity at the core where $\vec{r} = 0$. To prevent this singularity from affecting the stability of the simulation and also to model the viscous core of the bound and free vortices more accurately, a model for a viscous vortex core was implemented. Many different models that describe the tangential velocity distribution around the core exist, such as the Rankine, Lamb–Oseen or Ramasay and Leishman models (see Hommes[46]). In QBlade, a simple cut-off radius is used, which is added to the denominator of this equation in the form of r_c^2, and ensures that the induced velocity smoothly approaches zero in the vicinity of the core. This is a computationally efficient implementation as the viscous core modeling is directly implemented in the calculation of the induced velocity. For other vortex models, a viscous parameter needs to be evaluated from the relative vortex positions in addition to the Biot–Savart equation. This has a severe effect on the simulation performance, as the evaluation of the viscous parameter is carried $N^2_{\text{vortices}}/2$ times per time step.

When shed from the trailing edge of the blade, a vortex is released with an initial core-size r_c (a value of around 10% of local chord is proposed from experience). The core-size is updated every time step according to:

$$r_c = r_0 + \sqrt{\frac{4a\delta_v \nu \Delta t}{1+\epsilon}}.$$

where $a = 1.25643$ is a constant, δ_v is the turbulent viscosity coefficient (a value depending on rotor size, see Sant[47]), ν is the kinematic viscosity and Δt the time step size. The strain rate of the vortex filament is computed as:

$$\epsilon = \frac{\Delta l}{l}.$$

The desingularized Biot–Savart equation then becomes:

$$V_{ind} = -\frac{1}{4\pi} \int \frac{\Gamma \vec{r} \times d\vec{l}}{r^3 + r_c^2}.$$

4.2.3 Structural Dynamics

4.2.3.1 Multi Body Beam Formulation

The structural model in QBlade is based on the FEA module of the open source multi-physics engine Project Chrono [48]. Project Chrono is based on a platform-independent design (Projectchrono.org[49]), which is developed in the C++ language as an object-oriented library.

For the integration into QBlade, the `Chrono::Engine` module is employed. `Chrono::Engine` is the core module of Project Chrono; it contains functionality for setting up and solving physical systems containing Newtonian dynamics and finite elements. The SparseLU solver of the EIGEN C++ template library Tuxfamily [50] is used as a solver for the finite element problem. A dynamic link library, containing the Chrono module, has been compiled from Project Chrono's GIT repository. The relevant header files of Project Chrono and the EIGEN library are included, and the Chrono DLL is linked to QBlade's source code. This enables the definition of the physical system and the finite elements and grants access to the solver to perform time domain simulation of structural dynamics inside QBlade. [18]

4.2.3.2 Element and Multi-Body Formulation

The structural turbine model in the QBlade-Chrono coupling consists of Euler Bernoulli beams in a co-rotational formulation Negrut [51]. In the co-rotational formulation , a floating coordinate system is attached to each deformable beam element. The overall motion of a beam element is then the addition of the rigid body (translation and rotation) undergone by the floating coordinate system and a smaller strain deformation, expressed in the floating frame of reference. The global tangent stiffness matrix in Project Chrono's implementation is formulated in a way to include terms for geometric stiffness.

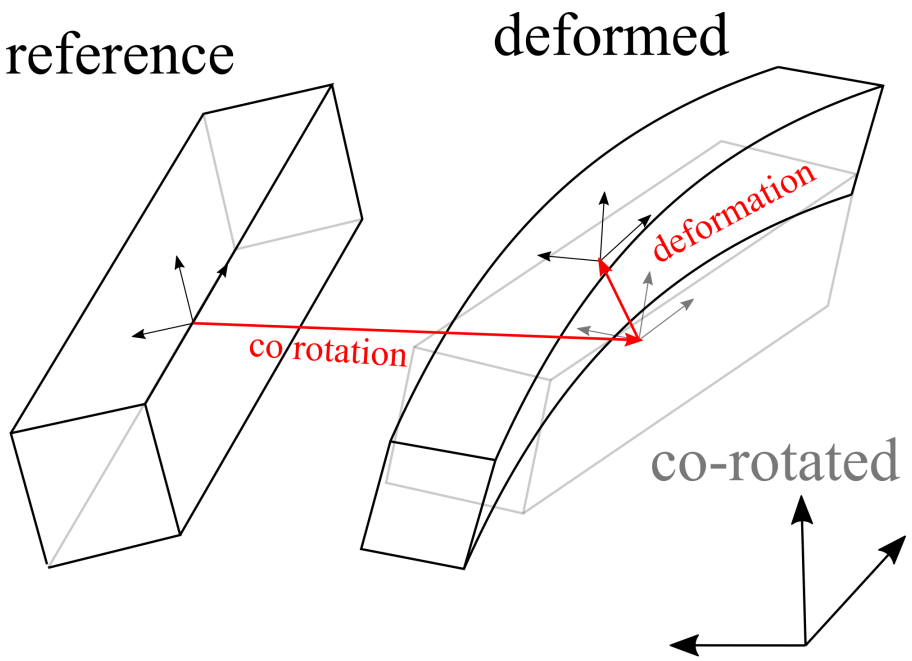

Figure 4.8: Visualization of the co-rotational beam approach. [18]

In QBlade's implementation of the structural model, the complete turbine structure is divided up into body objects. A body object contains an array for its structural nodes, an array for its structural beam elements, a unique identifier and several functions to access forces, torques, positions, velocities, accelerations and deflections. For a common HAWT, one body is created for each blade and one body for the tower.

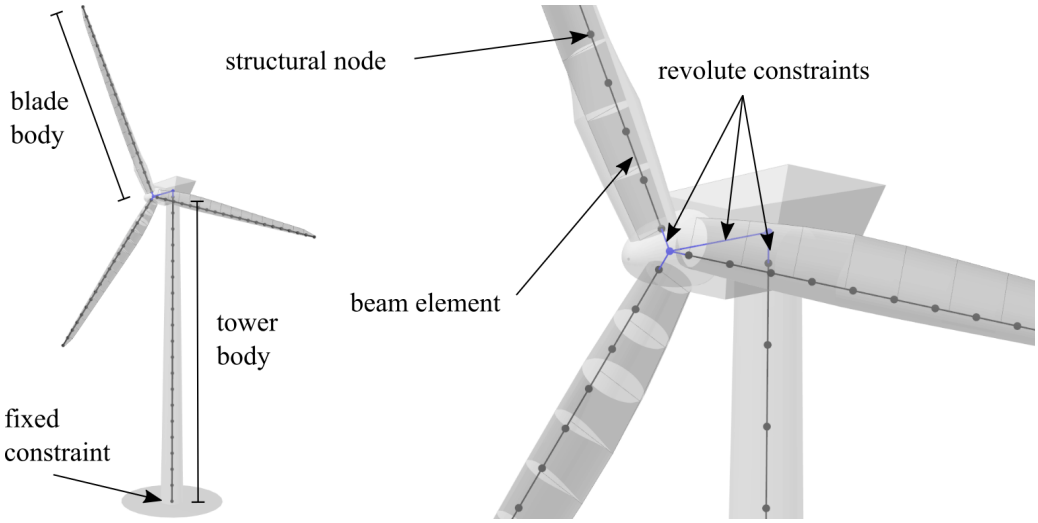

Figure 4.9: Visualization of the co-rotational beam approach.[18]

After the bodies have been created, they are assembled using joints or constraints. The tower is fixed to the ground by constraining all six DoF of the bottom tower node. A spring and damper may be defined at the ground to include foundation and soil dynamics. Using a revolute constraint, a free yaw node is connected to the tower top. Another revolute constraint then connects the hub node to the yaw node. Lastly, the blades are fixed around the hub node with revolute constraints, allowing them to rotate around the pitch axis. After the assembly of the bodies is completed, actuators are added to the revolute constraints. These actuators are used to yaw or pitch the turbine, based on controller signals and to model the generator. Actuators

are implemented as engine type constraints. At these engine type constraints, either a rotational angle, a rotational speed or a torque can be applied. This functionality is used to prescribe pitch angles at the pitch constraints, yaw angles at the yaw constraint and the generator torque at the shaft constraint. Furthermore, if no controller is used within a simulation, a constant rotational speed is prescribed for the main shaft to operate the turbine at a constant rotational speed.[18]

4.2.3.3 Time Integrators and Solver for the Structural Dynamics Simulation

Various factors influence the overall contribution of the structural model to the total computational cost of an aeroelastic simulation. The size of the problem matrix is proportional to the number of degrees of freedom that the system contains. Each main component (blades, struts, tower) of the assembled turbine can be discretized with an arbitrary number of structural nodes, where each node adds 6 degrees of freedom to the system matrix. Clearly, the total contribution of the structural model evaluations to the overall computational cost scales with the time step size of the structural evaluations. Due to the loose coupling method that is being employed in QBlade, the time step size can be set independently of that of the aerodynamic calculations.[18]

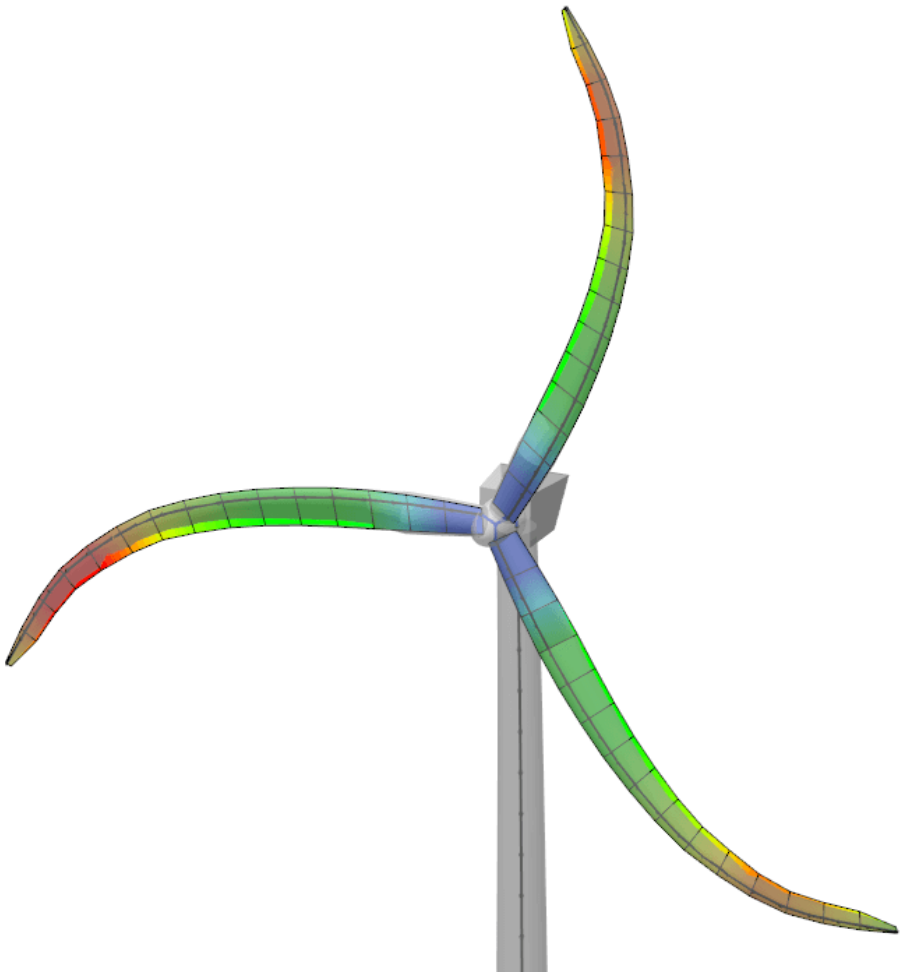

Figure 4.10: Large blade deformations caused by inertial forces during rotor ramp-up.[18]

In the Chrono library, the multi-body FEA problem is formulated as a Differential Variational Inequality (DVI) problem. At each time step of the structural simulation, the DVI problem is solved using the EIGEN SparseLU solver, which is included in the EIGEN C++

template library Tuxfamily[50]. The structural simulation is then advanced using a time integrator of choice. Several different time integrators (Tasora[52]) are available in Chrono. However, only the iterative HHT (Hilber-Hughes-Taylor formulation) has proven its usability within the current integration of Chrono in QBlade. While other, non-iterative, integrators suffer from constraint drifts or require very small timesteps to yield reasonable results, the HHT integrator shows good performance for structural time steps in the range of up to 5 degree azimuthal rotor increments.

4.2.3.4 Aero-elastic Coupling

A loose coupling approach is employed for the aero-elastic co-simulation in QBlade. shows the flowchart for one complete aeroelastic time step:

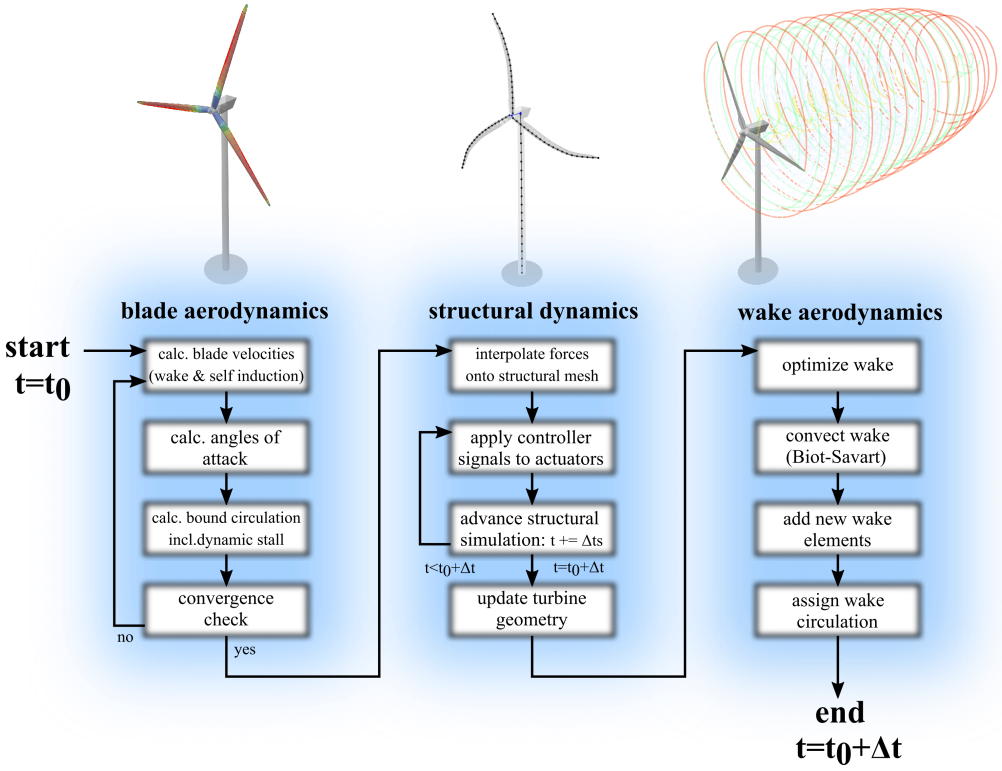

Figure 4.11: Flowchart for one time step of the aeroelastic model in QBlade.[18]

4.3 Simulation of Rotor Blade Using QBlade

4.3.1 Airfoil Design Module

QBlade calculates both local blade values as well as global performance metrics by using local aerodynamic properties of the discrete blade sections (see Blade Design Overview). Prior to designing a blade, these must be defined for each blade section. For this purpose, QBlade has an airfoil module which allows creating or importing airfoil profiles. This module is shown in the main toolbar

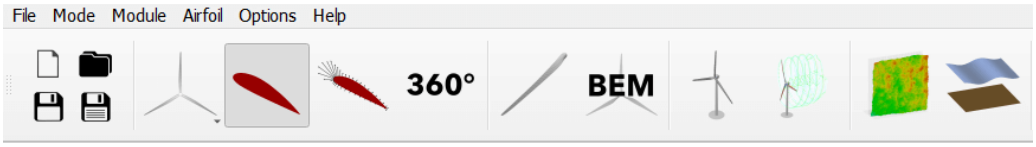

Figure 4.12: The airfoil design module is represented by the foil symbol in the QBlade main tool bar.

4.3.1.1 The selection of Airfoil

The SG6041 airfoil was selected for this study due to its excellent performance at low Reynolds numbers, which are typical in small wind turbine applications. Designed specifically for such conditions, it offers a high lift-to-drag ratio, smooth stall behavior, and strong aerodynamic efficiency, making it ideal for enhancing energy production and stability in low wind speeds. Its proven use in small turbine research and compatibility with tools like XFOIL and QBlade further support its suitability for accurate aerodynamic simulation and blade design.[53]

4.3.1.2 Importing the SG6041 Airfoil

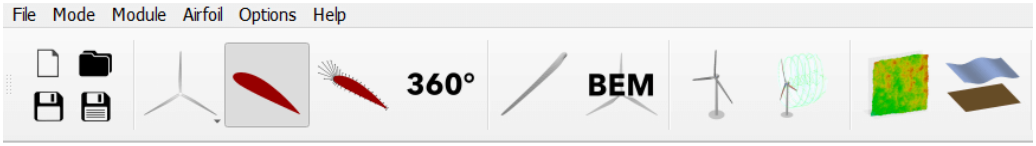

Figure 4.13: The airfoil design module is represented by the foil symbol in the QBlade main tool bar.

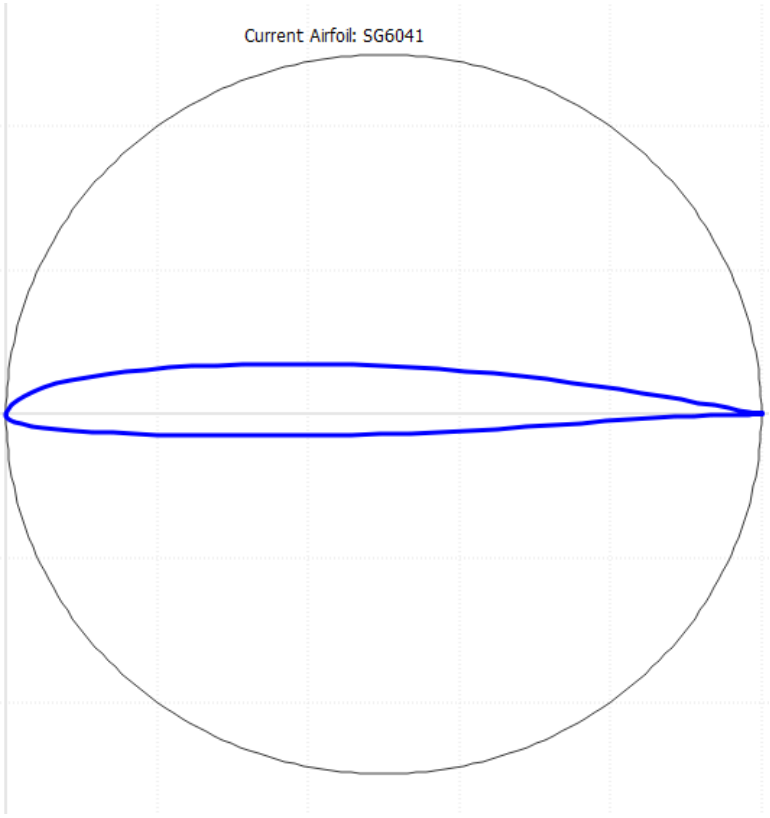

Figure 4.14: The SG6041 Airfoil.

4.3.2 Airfoil Analysis Module

In the Airfoil Analysis module of QBlade, the SG6041 airfoil was analyzed using two Reynolds numbers: 100,000 and 500,000, which are th typical operating conditions of small wind turbines. After importing the airfoil coordinates, polar analyses were conducted over a wide angle of attack range, allowing the computation of lift, drag, and moment coefficients using QBlade's built-in XFOIL interface. For each Reynolds number, a separate polar curve was generated and saved. These polar datasets were then used to enable Reynolds-dependent interpolation during the blade simulation, ensuring accurate aerodynamic modeling across varying wind speeds.

4.3.2.1 Pressure distribution

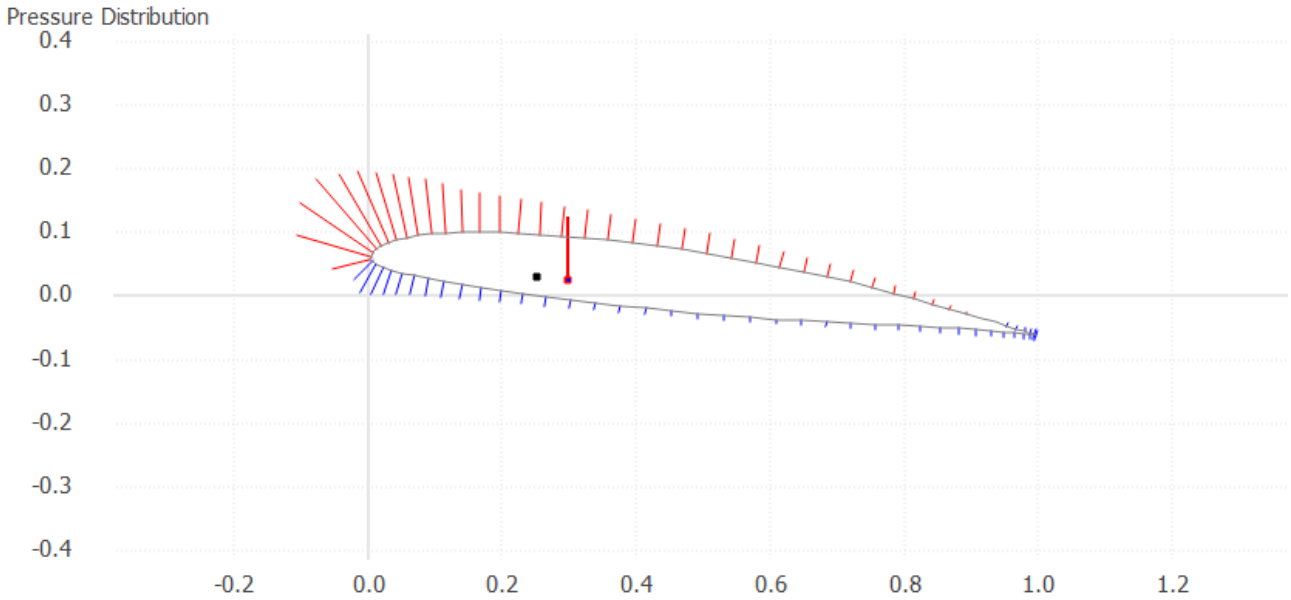

Figure 4.15: Pressure contour

This pressure distribution graph of an airfoil operating at a tip speed ratio (TSR) of 7 reveals efficient aerodynamic performance. The red vectors above the airfoil represent higher pressure, while the blue vectors below indicate lower pressure, creating a significant pressure difference that generates lift. At this high TSR, the airflow remains smooth with a relatively low angle of attack, promoting strong suction on the lower surface and moderate pressure on the upper surface. The resulting lift force, indicated by the red arrow and black dot, is well-centered, ensuring stable aerodynamic loading. Overall, the distribution confirms that the airfoil is functioning optimally, delivering effective lift and aerodynamic efficiency.

4.3.2.2 Lift to Drag ratio

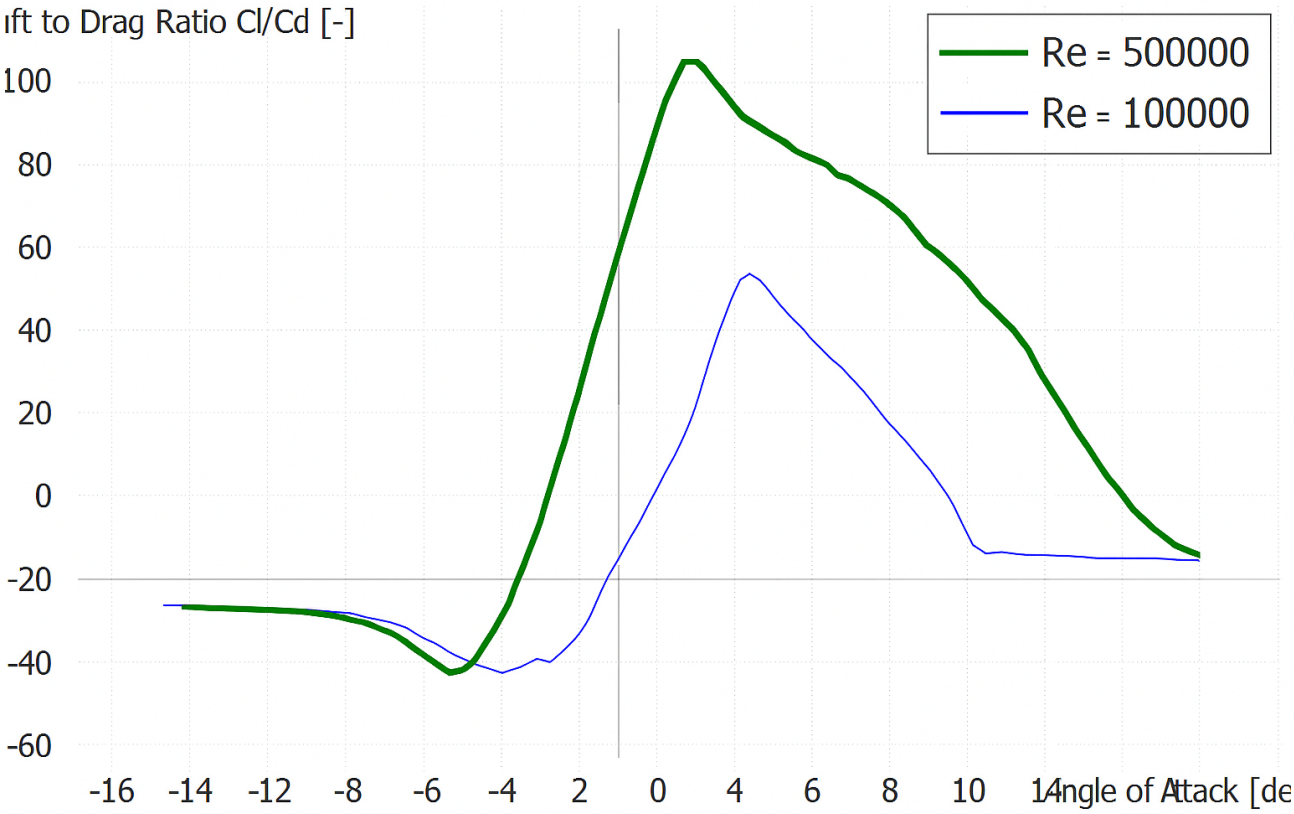

Figure 4.16: Lift to drag ratio

The graph illustrates the lift-to-drag ratio (C_l/C_d) of the SG6041 airfoil across different angles of attack for two Reynolds numbers: 100,000 (blue) and 500,000 (green). At $Re = 500{,}000$, the airfoil exhibits superior aerodynamic efficiency, with a peak C_l/C_d of approximately 90 around 3° angle of attack, compared to a peak of about 55 at 4° for $Re = 100{,}000$. The red curve also maintains higher efficiency over a broader angle range, while the blue curve declines more rapidly, indicating earlier stall and higher drag. This comparison confirms that the SG6041 performs significantly better at higher Reynolds numbers, making it more suitable for small wind turbines operating in conditions that support such flow regimes.

4.3.2.3 HAWT Blade Design

To create the blade geometry in QBlade, go to the Blade Design module and create a new blade. Define multiple sections along the blade span, typically from root to tip, and assign an airfoil to each section using a circular airfoil near the root and the SG6041 airfoil toward the mid and tip regions. For each section, specify the **radial position**, **chord length**, and **twist angle**. Using at least 10 sections ensures a smooth aerodynamic and geometric transition along the blade.

Table 4.1: Distributions of the chord and twist angle for the proposed optimal small wind turbine blade

Radius (m)	**Chord (m)**	**Twist (°)**
0.2	0.255885668	21.65323438
0.254138900	0.247182964	21.41640225
0.308119018	0.240224792	20.9969442
0.361781997	0.234685722	20.43691301
0.41497044	0.230262818	19.77270452
0.467528339	0.226671997	19.03035037
0.51930153	0.223644459	18.22884279
0.570138155	0.22092044	17.38101197
0.619889102	0.218266082	16.49048601
0.668408441	0.215438265	15.57563393
0.715553857	0.212232524	14.62599639
0.761178065	0.208244992	13.64449092
0.805174215	0.203872132	12.64572225
0.847386285	0.198429331	11.63426802
0.887699459	0.192003072	10.58150227
0.925995492	0.185438183	9.532483227
0.962160255	0.176076643	8.43245901
0.996093066	0.166658845	7.444714751
1.027689988	0.156465561	6.27486887
1.05851776	0.145569697	5.44830574
1.083512044	0.134332074	4.510772186
1.10757452	0.123005144	3.633592217
1.12897672	0.111896892	2.832240368
1.14850109	0.101320182	2.110112077
1.163549093	0.091732421	1.48518169
1.176620655	0.083335365	0.960991304
1.187660256	0.07644056	0.544305004
1.19665334	0.071369958	0.243278611
1.198353414	0.068234799	0.061021373
1.2	0.067176588	0

[53]

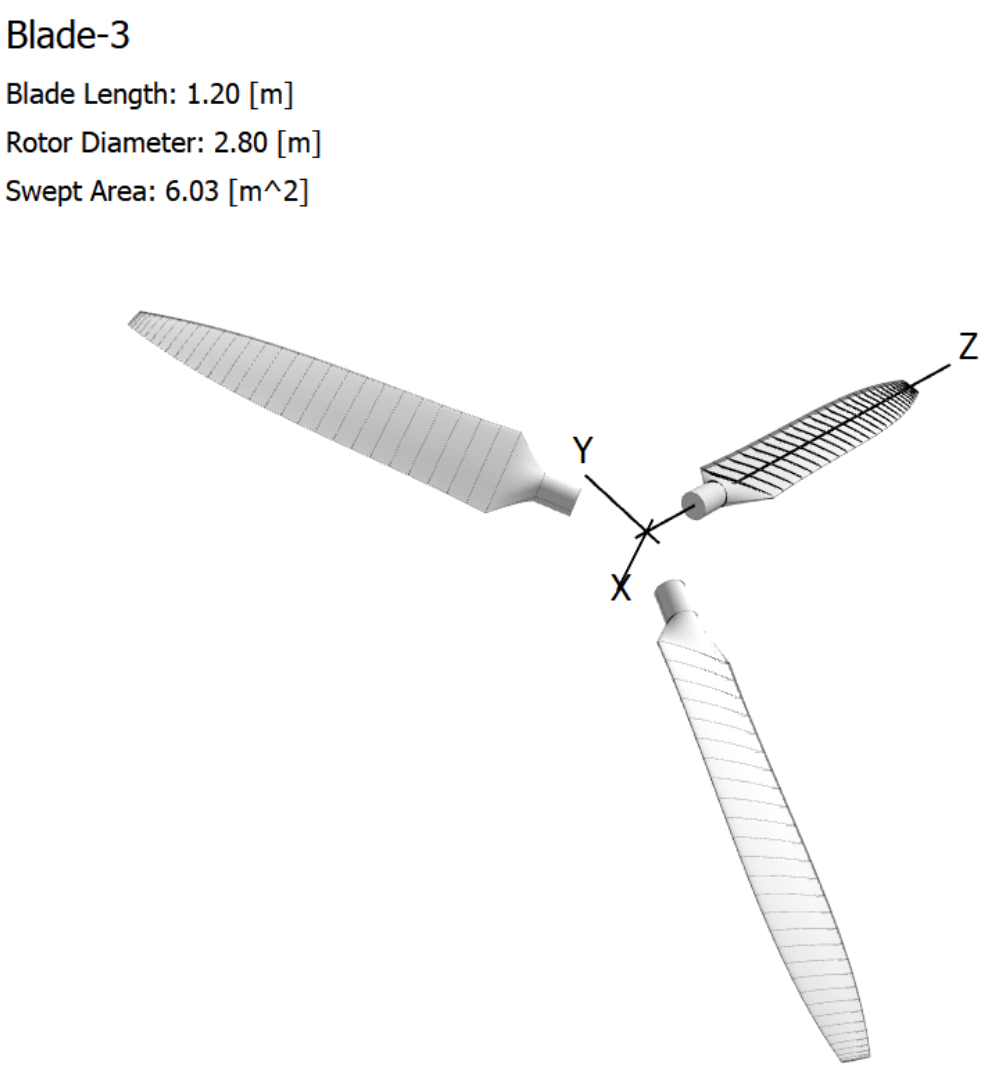

Figure 4.17: Blade Design

Parameter	**Value**
Blade radius, R	1.2 [m]
Number of blades, B	3 [-]
Hub radius, R_{hub}	0.2 [m]
Design tip speed ratio, TSR_{design}	7 [-]
Design wind speed, V_{design}	7 [m/s]

Table 4.2: Design parameters of the HAWT rotor

In this study, an optimal small wind turbine model has been selected based on previous work by Bouhelal et al.[53] . The blade radius ($R = 1.2\,\text{m}$) is chosen to balance efficiency and structural considerations for low to medium wind speeds typical of the region. The number of blades ($B = 3$) is commonly used in small-scale turbines for optimal performance and stability. A hub radius ($R_{hub} = 0.2\,\text{m}$) is chosen to ensure mechanical integrity and effective energy capture while minimizing material usage. The design tip speed ratio ($TSR_{design} = 7$) is set to optimize the aerodynamic performance of the turbine, ensuring efficient energy conversion at the expected wind speeds. Finally, the design wind speed ($V_{design} = 7\,\text{m/s}$) reflects the average wind conditions in Algeria, taking into account safety margins and ensuring the turbine

operates efficiently in local environmental conditions. These parameters collectively ensure that the turbine is both aerodynamically efficient and structurally viable for Algeria's wind energy potential.

4.3.3 Steady BEM Analysis and Aerodynamic results

To perform a steady BEM analysis in QBlade, we must first ensure that airfoils, blade geometry, rotor, and turbine definitions are properly set up. In the BEM Simulation module, a new simulation is created by selecting the turbine and defining a wind speed range . The user sets the pitch angle (typically 0°) and selects a control strategy such as a fixed tip speed ratio **TSR = 7**. Optional settings like tip and root loss corrections can be enabled. Once configured, the simulation is run to compute performance metrics including power, thrust, torque, and aerodynamic loading along the blade. The results can be visualized as performance curves or exported for further analysis.

4.3.3.1 Power Coefficient

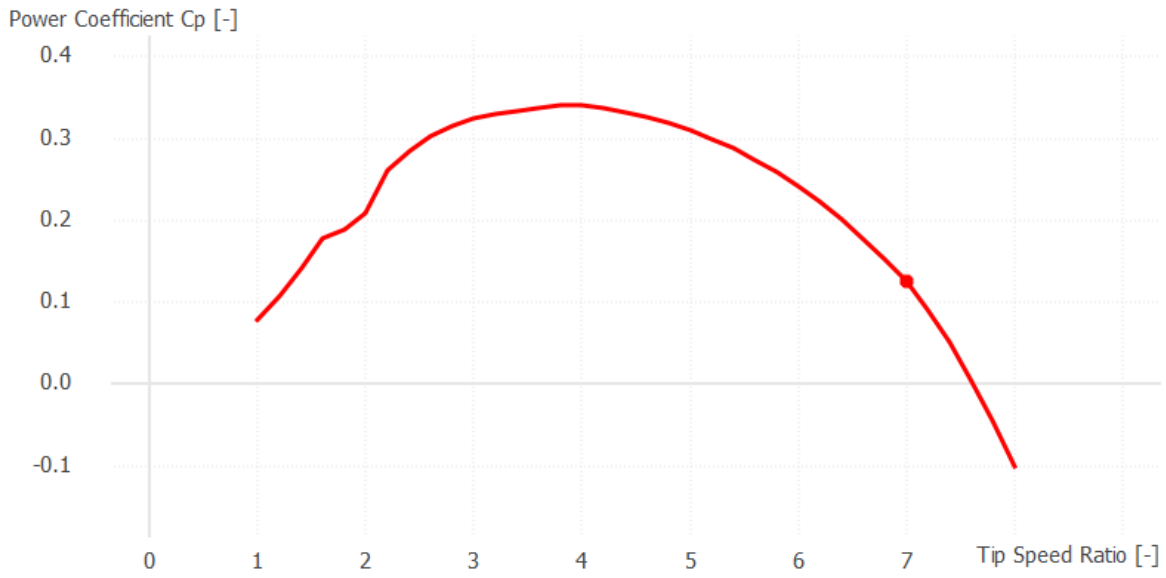

Figure 4.18: Power coefficient in fuction of Tip Speed Ratio

This graph shows the variation of the power coefficient (Cp) of the wind turbine as a function of the tip speed ratio (TSR). From a human perspective, the curve reveals that the turbine becomes increasingly efficient as the TSR increases from 1 to around 4, where the Cp reaches its peak approximately 0.34. This point marks the optimal operating condition of the turbine, where it extracts the maximum possible power from the wind.

Beyond this optimal TSR, the curve starts to decline, indicating that the turbine becomes less efficient at higher rotational speeds. Around a TSR of 7, the efficiency drops significantly, which is also highlighted by the red marker on the curve. Past this point, the turbine begins to lose its ability to effectively convert wind energy into mechanical power and in fact, Cp becomes negative, which may reflect adverse effects such as flow separation or poor angle of attack conditions.

4.3.3.2 Thrust coefficient

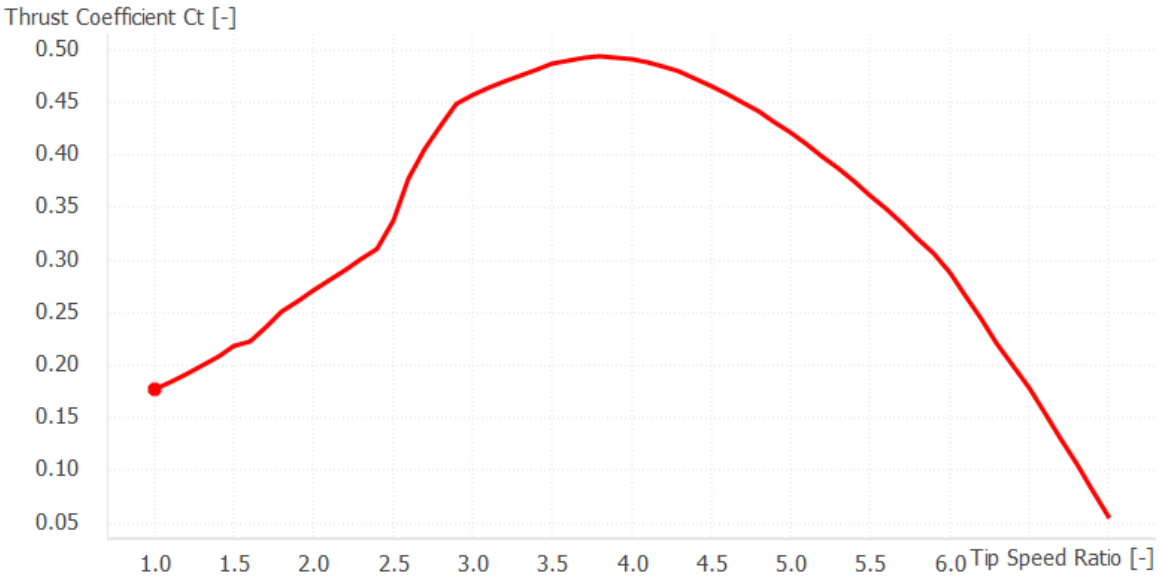

Figure 4.19: Thrust coefficient in function of TSR

This graph illustrates how the thrust coefficient (Ct) varies with the Tip Speed Ratio (TSR). As the TSR increases from around 1.0 to approximately 3.8, the thrust coefficient also increases, reaching a peak value just below 0.50. This indicates that the rotor becomes more effective at generating thrust up to this optimal TSR. Beyond this point, the Ct begins to decline steadily, suggesting that the blades become less effective at producing thrust at higher rotational speeds relative to the wind speed. This behavior is typical in wind turbine performance, where there is a balance between rotor speed and aerodynamic efficiency. Operating near the peak Ct ensures optimal thrust generation, which is essential for maximizing torque and, by extension, power output.

4.3.4 Aeroelastic and structural Analysis

For the structural design and analysis of the blade in QBlade, the process begins by creating a new structural blade model and configuring a modal analysis. The first step involves defining the material properties Young's modulus (E), shear modulus (G), and density ( )—for the blade. In this study, three materials are considered: carbon fiber reinforced polymer and glass fiber reinforced polymer and finaly our composite which PLA reinforced with date palm fibers, allowing for a comparative analysis of their structural performance. Once the materials are defined, the next step is to perform a static blade loading and deflection analysis. This requires importing the aerodynamic loading data normal and tangential forces calculated based on a tip speed ratio (TSR) of 7. With the loads applied, the simulation is run to observe blade deformation and stress response, providing insights into the mechanical behavior of each material under operational conditions.

Property	CFRP	GFRP	PLA Reinforced with Palm Fibers
Young's Modulus (E)	50 GPa	20 GPa	3.2 GPa
Shear Modulus (G)	4 GPa	3 GPa	1.18 GPa
Density (ρ)	1580 kg/m^3	1850 kg/m^3	1220 kg/m^3

Table 4.3: Mechanical properties CFRP, GFRP and PLA Reinforced with Palm fibers[4]

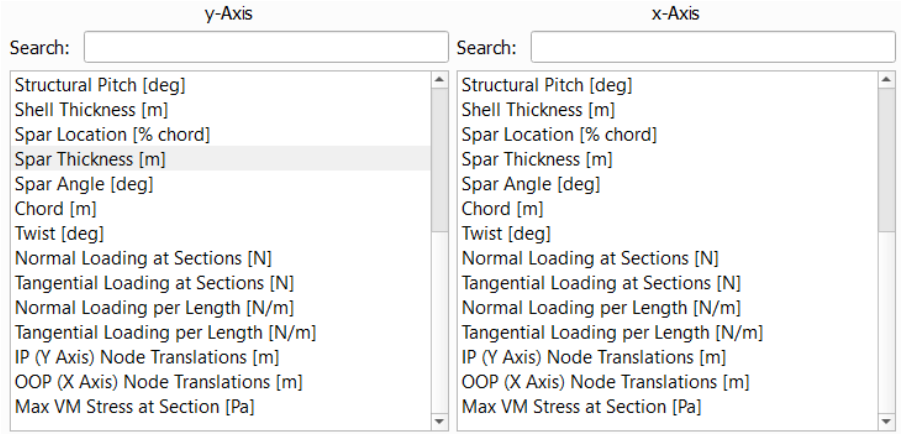

Figure 4.20: Graph Settings

In QBlade, many outputs are available, but we focused on deflection, stiffness, and Von Mises stress because they give us the clearest picture of how the blade behaves under load. Deflection tells us if the blade stays within safe limits, while Von Mises stress helps us check if it might fail. Stiffness, on the other hand, indicates the blade's resistance to deformation under applied loads—higher stiffness means less bending, which directly affects both performance and structural stability. These three outputs were the most relevant for evaluating the structural safety of our PLA–palm fiber blade.

4.3.4.1 Structural Model Results

After introducing the mechanical properties of the three materials we click on import loads of a given TSR (7 as we mentioned before) and Qblade will import the normal and tangential loading calculated before with the BEM method, finally we obtain the following results

Deflection

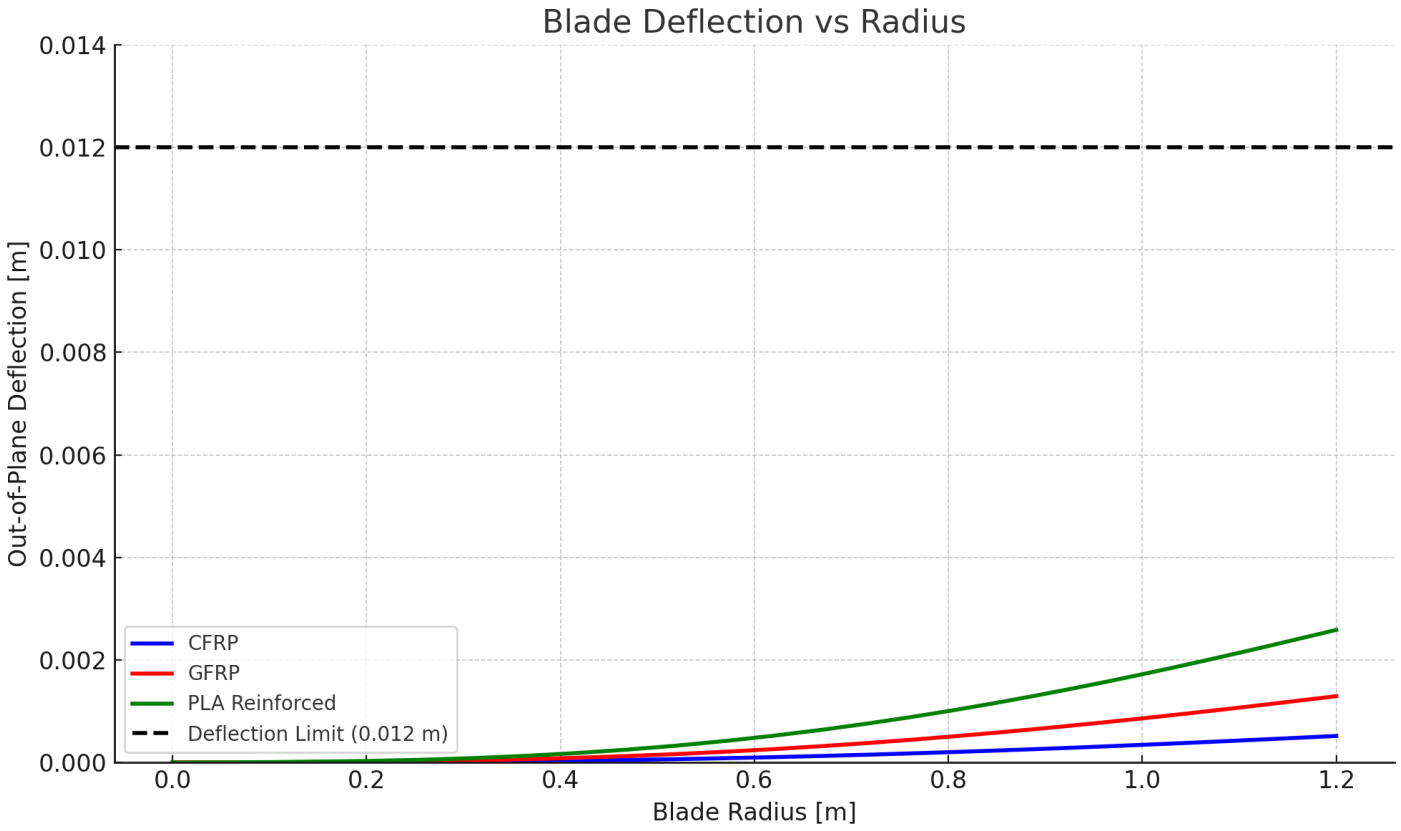

Figure 4.21: Deflection Curves (mm scale)

Figure 4.20 illustrates the out-of-plane deflection behavior of wind turbine blades constructed from three distinct composite materials: carbon fiber reinforced polymer (CFRP), glass fiber reinforced polymer (GFRP), and polylactic acid (PLA) reinforced with palm leaf fibers. The simulation was conducted in QBlade using a tip speed ratio (TSR) of 7, a value representative of typical operational conditions for small-scale horizontal-axis wind turbines. This comparison offers insight into how material stiffness affects structural response under uniform aerodynamic loading. As anticipated, the blade made from CFRP demonstrates the least deflection—approximately 0.5 mm at the tip—owing to its high Young's modulus and superior stiffness-to-weight ratio. GFRP, which has slightly lower mechanical properties than CFRP, exhibits moderate deflection around 1.3 mm. The PLA reinforced with palm fibers, being the most compliant of the three, shows the largest deflection, reaching approximately 2.6 mm at the blade tip.

Despite this increase in flexibility, it is important to note that all three materials remain well below the critical deflection threshold of 1% of the blade length, which corresponds to 12 mm for the 1.2 m blade modeled here[54]. This threshold is commonly accepted in wind turbine design to ensure that excessive deformation does not compromise aerodynamic efficiency or lead to structural instability. The results therefore confirm that, under the specified loading conditions, all three materials provide structurally viable solutions. While CFRP remains the optimal choice in terms of mechanical performance, its high cost and environmental footprint limit its practicality for some applications. GFRP offers a more cost-effective compromise but is still non-biodegradable and reliant on petroleum-based resources.

In contrast, the PLA reinforced with palm fibers—though mechanically less performant—

offers significant advantages in terms of sustainability and material circularity. The palm fibers used are a renewable agricultural by-product, and PLA is a biodegradable polymer derived from starch-based resources, making this composite a strong candidate for eco-friendly wind energy systems. Its mechanical response, while more flexible, remains within safe operating limits, particularly for small or medium-scale turbines in low-wind environments where blade loading is less extreme. Furthermore, the feasibility of processing PLA and palm fibers with accessible manufacturing methods such as compression molding or extrusion broadens its applicability in decentralized or rural settings.

Longitudunal Stiffness

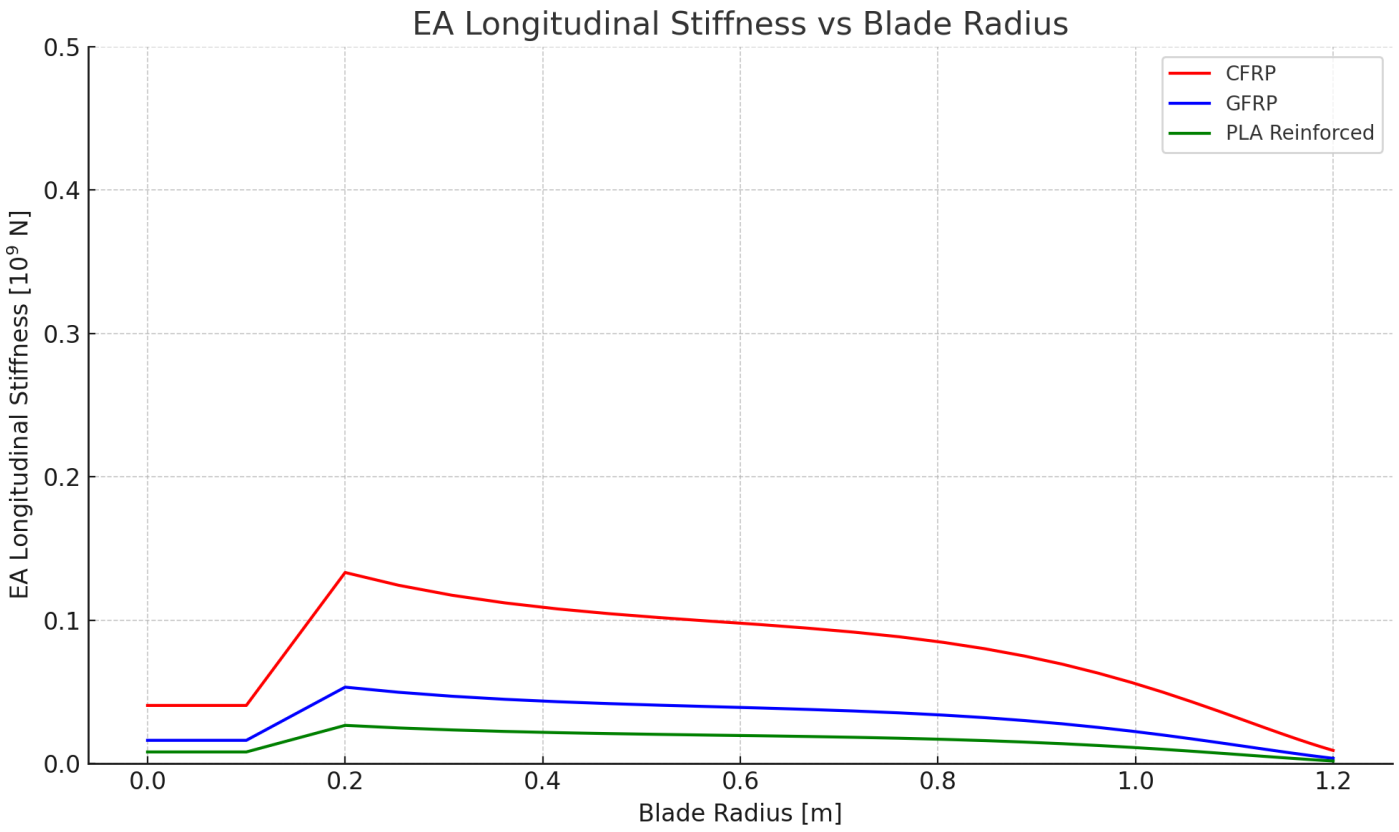

Figure 4.22: Longitudunal stiffness along the blade radius

The chart above illustrates the longitudinal stiffness (EA) variation along the blade radius for three structural blade models: CFRP, GFRP, and PLA-reinforced composite, as simulated using QBlade. While the PLA-reinforced blade exhibits significantly lower stiffness values compared to conventional CFRP and GFRP materials—remaining below 2×10^9 N throughout the radius—it maintains a consistent and coherent mechanical behavior along the span. This level of stiffness remains functionally viable within the context of wind turbine applications. More importantly, the use of PLA reinforced with natural fibers introduces a sustainable, biodegradable alternative that aligns with modern environmental priorities. These results validate the design and methodology developed in our study, demonstrating that such natural composites offer sufficient structural integrity for aerodynamic loads. This positions PLA-reinforced blades as a promising candidate for future eco-conscious developments in the wind energy sector.

Torsional Stiffness

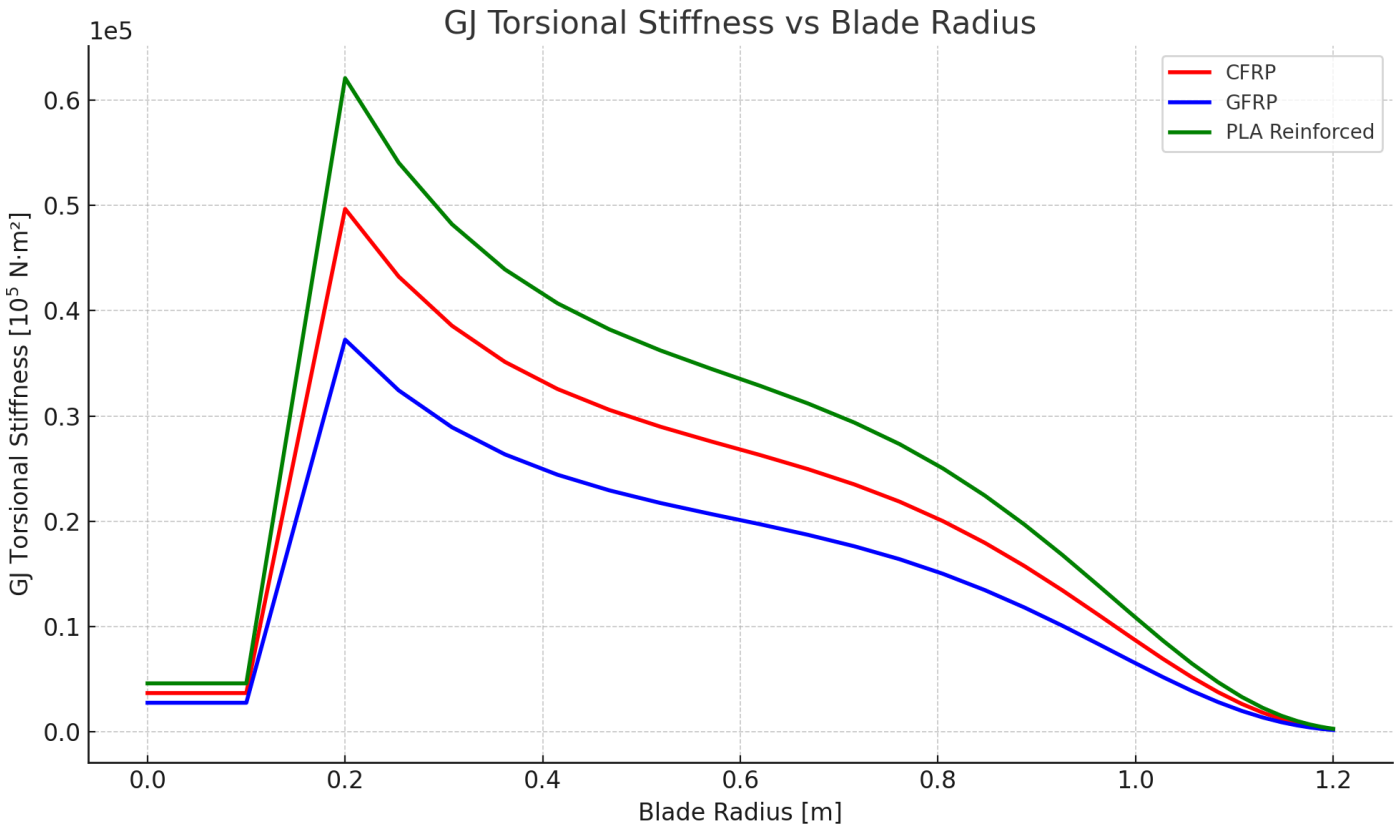

Figure 4.23: Torsional stiffness along the blade radius

This graph highlights that while CFRP and GFRP offer superior mechanical performance, the PLA + palm fiber composite maintains sufficient torsional stiffness for use in small-scale wind turbines. Its compliance may even offer benefits in terms of passive load mitigation. From a mechanical perspective, this result reinforces the feasibility of using biodegradable composites in low-wind applications, particularly where sustainability, local material sourcing, and cost reduction are prioritized over maximum structural rigidity. Nonetheless, to ensure long-term operational reliability, further investigation is warranted into the fatigue resistance and environmental durability of PLA–palm fiber composites, especially under cyclic torsional loads or in harsh climates.

Von Mises Stress

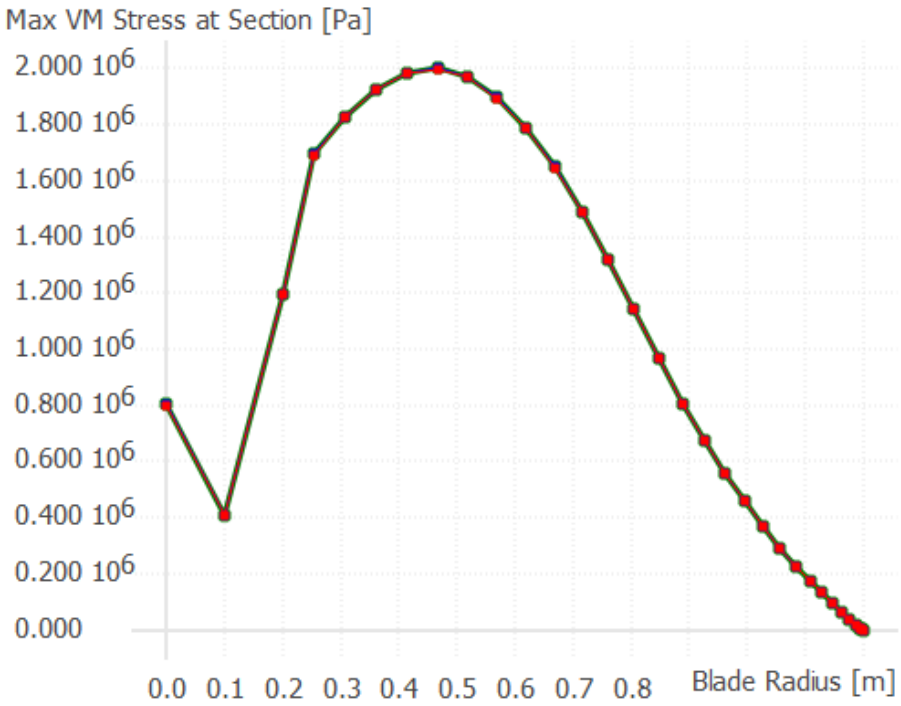

Figure 4.24: Maximum von Mises stress along the wind turbine blade radius

The von Mises stress distribution along the blade radius reveals the critical regions subjected to mechanical loading in the wind turbine blade. As shown in the figure, all three materials exhibit a similar stress profile, with maximum stress occurring approximately between 0.4 m and 0.6 m along the blade span. This mid-span region corresponds to where the combined bending moment and centrifugal forces are most pronounced during operation. The stress values rise sharply up to this peak and then gradually decrease toward the tip of the blade, reflecting the aerodynamic loading distribution. The similarity in the curves suggests that all three materials—CFRP, GFRP, and PLA reinforced with palm fibers—respond in a structurally consistent manner under the same loading conditions. The maximum stress remains well within a range that is structurally acceptable for wind turbine applications. This consistency confirms the reliability of the simulation and supports the use of natural fiber biocomposites like PLA–palm in these applications , which show promising structural behavior in addition to their environmental benefits.

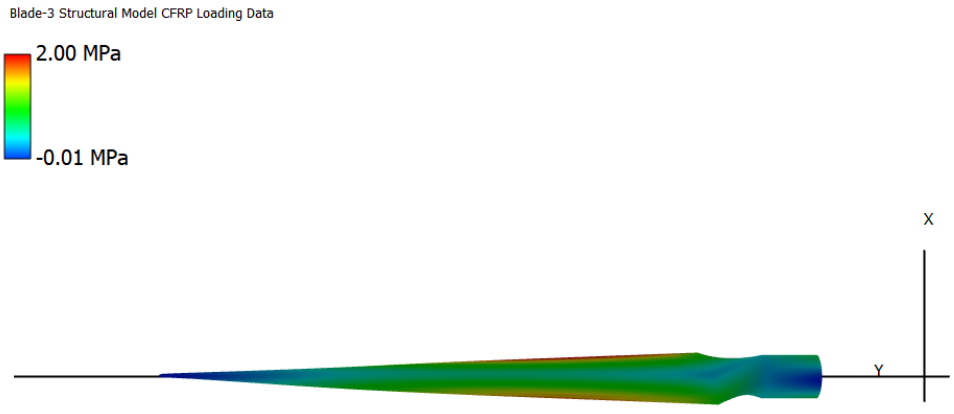

Figure 4.25: CRFP surface contour of normal stress

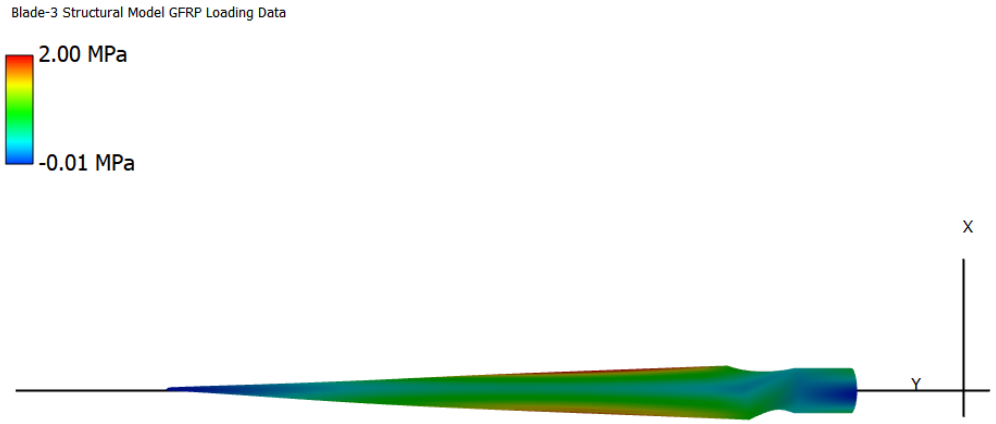

Figure 4.26: GFRP surface contour of normal stress

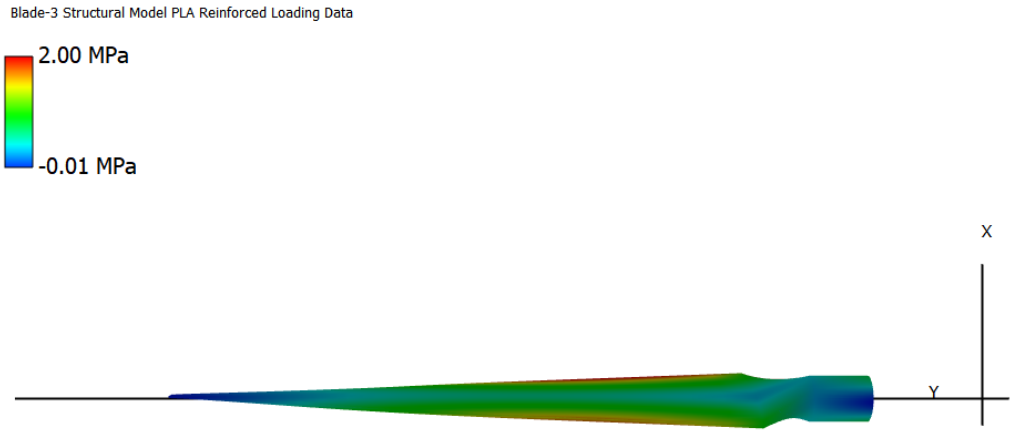

Figure 4.27: PLA reinforced with date palm fibers surface contour of normal stress

Despite its lower stiffness and strength, the PLA + palm fiber blade demonstrates a smooth stress transition from root to tip, indicating efficient load distribution without the presence of sharp stress gradients or concentrations. This behavior suggests improved resistance to localized failure and better adaptability to fluctuating loads, which is advantageous in small wind turbine applications. Furthermore, the reduced stress intensity indicates that the blade undergoes greater elastic deformation, which, while increasing flexibility, helps absorb energy and mitigate peak loads passively. This makes it particularly suitable for installations in low-wind or variable-wind environments where mechanical aggressiveness is limited.

Importantly, the PLA + palm fiber composite stands out for its environmental and economic benefits, making this solution both low-cost and sustainable. The combination not only reduces environmental impact but also opens up opportunities for local manufacturing in regions where access to high-tech materials like CFRP or GFRP is limited. Based on the simulation results, the PLA-based blade operates well within safe stress limits, and although it cannot match the mechanical performance of CFRP or GFRP, its balanced and stable stress behavior confirms its feasibility as a green alternative for small-scale wind turbine blades. Further optimization in fiber orientation or matrix modification could enhance its structural performance while preserving its ecological advantages.

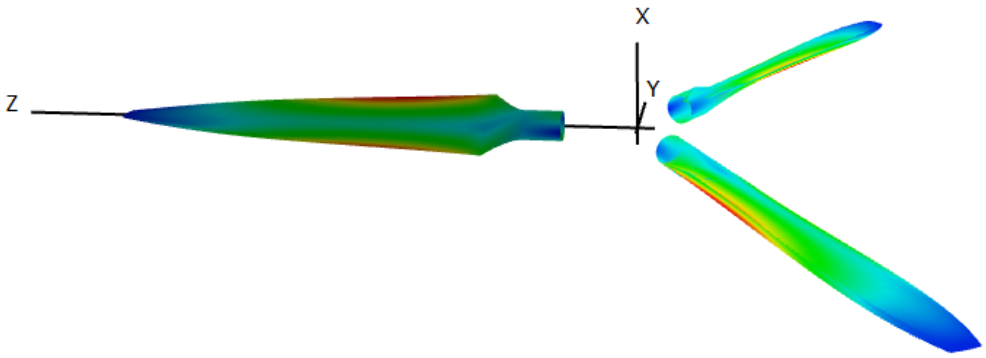

Figure 4.28: 3D view

Table 4.4: Comparative Summary of Blade Material Advantages and Inconvenients

Material	Advantages	Inconvenients
CFRP	- Excellent mechanical properties - High stiffness and strength - Minimal deflection - Long-term durability	- Very high cost, often prohibitive for small-scale use - Energy-intensive and complex production process - Not biodegradable, leading to environmental concerns - Limited accessibility in many regions compared to natural alternatives
GFRP	- Good strength-to-cost ratio - Moderate stiffness - Widely used in wind turbine industry - Good fatigue resistance	- Still reliant on petroleum-based resources - Not biodegradable, creating end-of-life waste issues - Heavier than CFRP and natural composites - Less sustainable and eco-responsible than biocomposites like PLA
PLA+ Palm-Fibers	- Biodegradable and environmentally friendly - Low-cost and renewable - Locally available in many regions - Balanced and stable stress distribution - Adequate structural performance for small wind turbines	- Slightly lower stiffness and strength than CFRP/GFRP, but still within safe operational limits - More flexible under load, which may be beneficial for passive load absorption - Requires further validation for long-term durability — but already shows strong promise for real applications

4.4 Conlusion

In conclusion, the results of the structural simulations conducted in QBlade confirm the technical feasibility of using PLA reinforced with palm leaf fibers as a material for small wind turbine blades. While carbon fiber (CFRP) and glass fiber (GFRP) blades exhibited superior mechanical performance in terms of stiffness and stress resistance, these materials come with significant trade-offs. Their high production costs, energy-intensive manufacturing processes, and environmental drawbacks—including non-biodegradability and reliance on petroleum-based resources—make them less suitable for sustainable or decentralized energy solutions, particularly in regions with limited access to advanced composites.

In contrast, the PLA + palm fiber blade demonstrated balanced mechanical behavior, including acceptable deflection, sufficient torsional stiffness, and a well-distributed stress response, all within the operational safety margins required for small-scale wind energy systems. Moreover, this material combination is biodegradable, low-cost, renewable, and locally accessible, offering a compelling alternative for communities seeking sustainable and affordable energy technologies. While further studies on fatigue behavior and environmental resistance would be beneficial, the simulation results clearly support the use of this natural fiber–reinforced PLA composite as a viable and eco-friendly substitute for traditional fiber-reinforced polymers in wind turbine blade applications.

General conclusion

This thesis has opened new doors of exploration in the development of green energy technologies, particularly in the field of sustainable wind turbine applications. By investigating natural fiber–reinforced biocomposites such as PLA reinforced with palm fibers, the work has not only demonstrated the mechanical feasibility of alternative eco-friendly materials but has also contributed to the broader understanding of how such composites can be integrated into structural components like turbine blades. Moreover, the experimental and simulation-based approach adopted here opens promising prospects for future research into innovative fabrication methods for natural composites—methods that are more accessible, less energy-intensive, and aligned with the principles of circular economy and environmental stewardship.

The first chapter began by establishing the scientific and environmental motivations behind the development of PLA-based composites. Through an extensive review of the literature, the biodegradability, mechanical behavior, and processing methods of PLA and various natural fibers were investigated. Special emphasis was placed on the underutilized potential of palm leaf fibers—an abundant, renewable, and low-cost resource in many regions—as a reinforcing material in polymer composites.

The second chapter was dedicated to the practical development of the composite. This involved several critical steps, including the collection and preparation of date palm fibers, chemical treatment to improve fiber-matrix adhesion, and controlled integration into a PLA matrix. Despite challenges related to mixture uniformity and unsuccessful filament extrusion trials, the fabrication phase yielded molded composite plates suitable for experimental testing, demonstrating the material's processability.

Chapter three focused on the mechanical evaluation of the composite. Through tensile testing and analysis of modulus and strain, the material's structural behavior was thoroughly characterized. The results revealed that a 15% fiber content provided the best balance between stiffness and ductility. While filament extrusion was ultimately unsuccessful due to extrusion machine malfunction or pla grade , the mechanical data obtained served as a robust foundation for the next phase of the study—digital simulation.

The final chapter extended the study into the field of renewable energy by simulating the use of the developed composite in rotor blade applications. Using QBlade software, aerodynamic and aeroelastic analyses were performed on a rotor blade designed with the SG6041 airfoil. The simulation incorporated the experimentally obtained mechanical properties of the composite material. The results from the BEM and structural modules provided insights into the behavior of such a blade under operational conditions. While the simulations suggested that the material could be suitable for mechanical applications especially in wind turbines , because at some point we will all need to use green energy .

Looking ahead, future work could focus on enhancing the filament extrusion process—particularly by experimenting with alternative PLA grades that may offer improved compati-

bility and processability with palm fibers. If successful, such advancements could unlock a wide range of sustainable manufacturing opportunities and enable the broader deployment of natural fiber–reinforced biocomposites in engineering applications. The promising results obtained from the simulations in this thesis reinforce this potential, demonstrating that PLA-palm composites can indeed meet the mechanical performance requirements for wind turbine blades. This not only validates the material's feasibility but also highlights a clear path forward for integrating green materials into renewable energy technologies on a larger scale.

Bibliography

[1] Thando Ncube, Diptiman Das, Elangovan Deenadayalan, and Shalini Singh. Mechanical properties of natural fiber-reinforced composites: A review. *Polymers*, 13(11):1822, 2021.

[2] NatureWorks LLC. Ingeo™ biopolymer 4043d technical data sheet. https://www.natureworksllc.com/~/media/Files/NatureWorks/Technical-Documents/Technical-Data-Sheets/TechnicalDataSheet_4043D_3D-monofilament_pdf.pdf, 2020.

[3] John H. Gosse and Charles E. Harris. A comparison of three popular test methods for measuring the in-plane shear properties of composite materials. Technical Report NASA-TM-104054, NASA Langley Research Center, 1992.

[4] Composite material. Wikipedia, The Free Encyclopedia. Accessed July 2025.

[5] D. S. et al. Trends and challenges in the development of biobased barrier coating materials for paper/cardboard food packaging: a review, 2020.

[6] Pia Skoczinski, Michael Carus, Doris de Guzman, Harald Käb, Raj Chinthapalli, Jan Ravenstijn, Wolfgang Baltus, and Achim Raschka. Bio-based building blocks and polymers – global capacities, production and trends 2020–2025. Technical report, nova-Institute for Ecology and Innovation, January 2021. Short version, published by nova-Institute, Hürth, Germany.

[7] VectorMine. Lactic acid fermentation process scheme, labeled vector illustration diagram. Depositphotos stock vector (ID 333789868), 2020. Licence standard ou étendue, résolution jusqu'à 4000×4000px, 300dpi.

[8] CCELL Marketing. Ccell celebrates earth day with a sustainable solution for disposable vapes—biodegradable and recyclable components, April 2024. Publié sur le site de CCell le 23 avril 2024; communiqué de presse originel du 22 avril 2024 via PR Newswire.

[9] Testbook Editorial. Difference between natural and synthetic fibres. Testbook – plateforme d'apprentissage en ligne, 2025. Consulté le 14 juillet 2025.

[10] Karen Ramírez, Jorge Saldarriaga, Diego Quintero, Fernando Giraldo, John Rojas, and Rafael Cuenca. Chemical, morphological and mechanical characterization of natural fibers from colombian fique and their potential as reinforcement for polymeric materials. *Maderas. Ciencia y tecnología*, 24(1):447–458, 2022.

[11] TPAILE – Une aile plus performante. Les composites. Site Web TPE (lycée) – page explicative sur les matériaux composites, 2025. Consulté le 14 juillet 2025.

[12] Nagappa R. S. Siddgonde. Numerical analysis of low-velocity impact on fibre reinforced laminated composite plates. M.tech. thesis, Indian Institute of Technology, Kharagpur, August 2015. Accédé via ResearchGate – M.Tech. Thesis conseillé par Dr. Shravankumar B Kerur.

[13] Robert M. Jones. *Mechanics of Composite Materials*. CRC Press, 2nd edition, 2018.

[14] Neha Chandarana, Daniel Martinez Sanchez, Constantinos Soutis, and Matthieu Gresil. Early damage detection in composites during fabrication and mechanical testing. *Materials*, 10(7):685, 2017. Special Issue: Structural Health Monitoring for Aerospace Applications 2017.

[15] Ching Hao Lee, Abdan Khalina, and Seng Hua Lee. Importance of interfacial adhesion condition on characterization of plant-fiber-reinforced polymer composites: A review. *Polymers*, 13(3):438, 2021.

[16] S. M. Mirmehdi, F. Zeinaly, and F. Dabbagh. Date palm wood flour as filler of linear low-density polyethylene. *Composites Part B: Engineering*, 56:137–141, 2014.

[17] Tessa Jane Gordelier, Philipp Rudolf Thies, Louis Turner, and Lars Johanning. Optimising the fdm additive manufacturing process to achieve maximum tensile strength: a state-of-the-art review. *Rapid Prototyping Journal*, 25(6):953–971, August 2019.

[18] QBlade Developers. Qblade theory documentation, 2024. Accessed: July 9, 2025.

[19] Michel Vert, Y. Doi, K. Hellwich, M. Hess, P. Hodge, P. Kubisa, E. Rinaudo, and R. G. Schué. Terminology for biorelated polymers and applications (iupac recommendations 2012). *Pure and Applied Chemistry*, 84(2):377–410, 2012.

[20] Renewable Carbon Initiative. For the first time: Growth rate for bio-based polymers with 8% cagr far above overall polymer market growth, 2022.

[21] LXBIO Technology. The production process of pla resin: How pla is made? Online, 2024.

[22] TotalEnergies Corbion. Luminy® pla portfolio, 2024. Accessed July 2025.

[23] K. L. Pickering, M. G. Aruan Efendy, and T. M. Le. A review of recent developments in natural fibre composites and their mechanical performance. *Composites Part A: Applied Science and Manufacturing*, 83:98–112, 2016.

[24] William D. Callister and David G. Rethwisch. *Materials Science and Engineering: An Introduction*. John Wiley & Sons, 10th edition, 2020.

[25] P.K. Mallick. *Fiber-Reinforced Composites: Materials, Manufacturing, and Design*. CRC Press, 3rd edition, 2007.

[26] M. K. Hossain, M. Hasan, and M. Z. Hossain. The effect of alkaline treatment on natural fibers/biopolymer composites. *ResearchGate*, 2022.

[27] L. Wang, W. Ma, R.A. Gross, and S.P. McCarthy. A study of pla and pla/starch composites prepared by solution casting method. *Journal of Applied Polymer Science*, 89(6):1585–1592, 2003.

[28] D. Hull and T. W. Clyne. *An Introduction to Composite Materials*. Cambridge University Press, Cambridge, 2nd edition, 1996.

[29] J. Laukkanen and Others. Effect of mercerization/alkali surface treatment of natural fibres: Enhancing fibre–matrix adhesion in composites. *Materials*, 5(7):175, 2025. Chemical treatment improves adhesion by removing surface impurities and increasing roughness, enhancing mechanical interlocking and composite performance.

[30] Andrzej K. Bledzki and Jürgen Gassan. Composites reinforced with cellulose based fibres. *Progress in Polymer Science*, 24(2):221–274, 1999.

[31] Md M. Kabir, Hai Wang, Kin-tak Lau, and Francisco Cardona. Chemical treatments on plant-based natural fibre reinforced polymer composites: An overview. *Composites Part B: Engineering*, 43(7):2883–2892, 2012.

[32] M. John and S. Thomas. Biofibres and biocomposites. *Carbohydrate Polymers*, 71(3):343–364, 2008.

[33] K. Oksman, M. Skrifvars, and J.F. Selin. Natural fibres as reinforcement in polylactic acid (pla) composites. *Composites Science and Technology*, 63(9):1317–1324, 2003.

[34] Nicole Graupner. Application of lignin as natural adhesion promoter in cotton fibre-reinforced poly(lactic acid) (pla) composites. *Journal of Materials Science*, 44:4447–4451, 2009.

[35] Tech Science Publishing. Mechanical and microstructural properties of flax fiber reinforced pla composites, 2022. Accessed: 2025-07-16.

[36] R. Tokoro, T. Fujimura, M. Tanaka, T. Fujita, K. Hayashi, T. Ito, H. Okubo, and T. Fujii. Interfacial adhesion and mechanical properties of pla composites reinforced by bamboo fiber. *Composites Part A: Applied Science and Manufacturing*, 39(3):393–399, 2008.

[37] Chaitanya V. and Samouh H. Mechanical properties of pla reinforced with treated sisal fibers. *International Journal of Engineering and Technology*, 9(2):120–125, 2020.

[38] Karim Benzarti, Khaoula Khalfaoui, Abir Lajnef, Hatem Kaddami, and Houcem Smaoui. New natural fiber-reinforced composites based on poly(lactic acid) and date palm rachis: Morphology, mechanical and thermo-physical properties. *Polymers*, 13(19):3444, 2021.

[39] Daniel Ferreira, Giulia Gambaro, Davide Forcellese, Francesco Rotatori, Davide Gabrielli, and Mario Bambini. Effects of manufacturing parameters on mechanical performance and dimensional accuracy of fff-printed pla specimens. *Polymers*, 15(7):1651, 2023.

[40] Zhaozhe Yang, Xinhao Feng, Min Xu, and Denis Rodrigue. Properties of poplar fiber/-pla composites: Comparison on the effect of maleic anhydride and kh550 modification. *Polymers*, 2020.

[41] Emmanuel Branlard. *Wind Turbine Aerodynamics and Vorticity-Based Methods*, volume 7. Springer International Publishing, 2017.

[42] H. Glauert. Airplane propellers. In *Aerodynamic Theory*, pages 169–360. Springer Berlin Heidelberg, 1935.

[43] H. Snel, R. Houwink, and W. J. Piers. Sectional prediction of 3d effects for separated flow on rotating blades. In *Proc. European Community Wind Energy Conference*, Lübeck - Travemünde, 1992.

[44] Helge Madsen, Torben Larsen, Georg Pirrung, Ang Li, and Frederik Zahle. Implementation of the blade element momentum model on a polar grid and its aeroelastic load impact. *Wind Energy Science*, 5(1):1–27, 01 2020.

[45] R. Behrens de Luna, D. Marten, T. Barlas, S.G. Horcas, N. Ramos-Garcia, A. Li, and C.O. Paschereit. Comparison of different fidelity aerodynamic solvers on the iea 10mw turbine including novel tip extension geometries. *Journal of Physics: Conference Series*, 2022. [accepted].

[46] T. Hommes, J. Bosschers, and H. W. M. Hoeijmakers. Evaluation of the radial pressure distribution of vortex models and comparison with experimental data. *Journal of Physics: Conference Series*, 656(1):7–11, 2015.

[47] Tonio Sant. *Improving BEM-based Aerodynamic Models in Wind Turbine Design Codes*. TU Delft, 2007.

[48] Alessandro Tasora, Hammad Mazhar, Radu Serban, Arman Pazouki, Daniel Melanz, Jonathan Fleischmann, Michael Taylor, Hiroyuki Sugiyama, and Dan Negrut. Chrono: An open source multi-physics dynamics engine. In *High Performance Computing in Science and Engineering*, pages 19–49. Springer, 2016.

[49] Projectchrono.org. Project chrono - an open-source physics engine, 2019. (visited on 2019-07-12).

[50] Tuxfamily. Eigen - a c++ template library for linear algebra: matrices, vectors, numerical solvers and related algorithms, 2019. (visited on 2019-07-12).

[51] Dan Negrut. Co-rotational formulation in chrono, 2016. Antonio Recuero Chrono, pages 1–10.

[52] Alessandro Tasora. Time integration in chrono::engine, 2017. pages 1–44.

[53] Abdelhamid Bouhelal, Mohammed Nadjib Hamlaoui, Arezki Smaïli, Saïd Rechak, Yacine Belkacemi, Mouna Mahfoud, and Samir Ouchene. Multi-objective optimization and aeroelastic analysis of small wind turbine blades made of date palm fibers. In *Technological and Innovative Progress in Renewable Energy Systems*, Advances in Science, Technology & Innovation, pages 351–355. Springer, Cham, 2025.

[54] Xiaojie Jin, Kevin D'Souza, Kevin Maki, and Steven Ceccio. Numerical and experimental study on an oscillating hydrofoil energy harvester. https://acemrl.engin.umich.edu/wp-content/uploads/sites/412/2019/08/Jin-main_corrected-version.pdf, 2019. Accessed July 16, 2025.